The Cost-Carbon Trade-Off of Green Hydrogen Production

The influence of weather patterns and prioritizing on the design of green hydrogen production chains

Thesis: MSc Sustainable Energy Technology

Klaas Raang (Rolf) Iwema

TU Delft

Royal HaskoningDHV
Enhancing Society Together

The Cost-Carbon Trade-Off of Green Hydrogen Production

The influence of weather patterns and prioritizing on the design of green hydrogen production chains

by

Klaas Raang (Rolf) Iwema

to obtain the degree of Master of Science
at the Delft University of Technology,
to be defended publicly on Friday October 13, 2023 at 13:00 AM.

Student number:	4439139	
Project duration:	February 20, 2023 – October 13, 2023	
Thesis committee:	Prof. dr. ir. E. Goetheer,	TU Delft, supervisor
	Prof. dr. ir. W. de Jong,	TU Delft
	Prof. dr. ir. C.A. Ramirez Ramirez,	TU Delft
Company Supervisor:	MSc. P. Katakwar,	Royal HaskoningDHV

Cover: Kodda/Shutterstock

TU Delft

Royal HaskoningDHV
Enhancing Society Together

Preface

Green hydrogen production is a low-carbon alternative to traditional hydrogen production pathways, but how low is low-carbon? Understanding the implications and effects of the energy system of the future is paramount, as the system of the future will be built in the coming years. This drive for understanding lies at the foundation of this master thesis: ”The Cost-Carbon Trade-Off of Green Hydrogen production: The influence of weather patterns and prioritizing on the design of green hydrogen production chains”. This research has been performed to obtain a masters degree in Sustainable Energy Technology at the Delft University of Technology. The research took place from February to October 2023.

To me the most interesting part of studying Sustainable Energy Technology, was peaking into the future energy system, and its challenge of decarbonisation. This interest pushed me towards this topic. What is the carbon footprint of our decarbonisation method? During this research I expanded my knowledge of sustainable energy technology, economy and ecology and I have strengthened my programming skills. While it wasn’t always smooth sailing, it was during those times that I learned the most. I am proud of the result.

I would like to express my gratitude to my supervisor, Prof. Dr. Ir. Earl Goetheer, for his valuable contributions to this research. His enthusiasm, flexibility, and our discussions provided me with the support I needed for this Thesis. I would also like to extend my thanks to Royal HaskoningDHV for granting me the opportunity to intern and gain practical experience. Writing this thesis wouldn’t have been as much fun without being surrounded by great colleagues. I am particularly grateful to my daily supervisor, MSc. Piyush Katakwar, for his industry insights, guidance, and mentorship. He not only pushed and challenged me when necessary but also reminded me to pause and celebrate milestones.

Finally I want to thank all people near me for all patience, support and above all: gezelligheid.

Klaas Raang (Rolf) Iwema
Amsterdam, October 2023

Summary

Green hydrogen plays a pivotal role in the energy transition as it helps to reduce the carbon footprints of the hard-to-abate sectors. As global hydrogen demand is expected to rise to 100 Mton by 2030, addressing the carbon footprint of hydrogen production is elemental. The conventional hydrogen production method, grey hydrogen, emits 11.24 $kg\ CO_2/kg\ H_2$ and implementing carbon capture and storage, resulting in blue hydrogen, seems to have a limited effect. To accommodate the future hydrogen demand, low-carbon production pathways need to be set-up, that can compete against the low prices of the conventional production method.

The aim of this report is to shed light on the influence of design choices and local weather patterns on the Carbon Footprint (CF) and the Levelised Cost of Hydrogen (LCOH) of green hydrogen production chains.

An optimisation model is developed to map out the effect of weather patterns and the production chain design choices. This optimisation model simulates the hydrogen production chain and optimises its design for a low CF and LCOH, based on location-specific wind and solar data. The research assesses the hydrogen production on a cradle-to-gate basis, taking into account all processes from energy generation up to the compression for delivery. The model is tested for three locations: Duqm, Groningen, and Dakhla. There are three design choices assessed. The first choice is the sizing of the electrolyser, wind and solar plant. The second choice is the selection of PEM or Alkaline electrolysis. The third choice is the selected PV technology, CdTe, CI(G)S or Mono c-Si.

The results show that the different weather patterns of the tested locations have a profound influence on the systems performance. Production in Dakhla is cheapest, due to the presence of consistent high solar and wind energy yields. The production in Groningen has a low CF, due to the abundant available wind, but has a high LCOH due to the lack of consistent sun throughout the year. The situation in Duqm is opposite to Groningen, with a low LCOH, due to the available sun, but a high CF, due to the lack of consistent wind. Consistent and strong winds lead to a lower Carbon Footprint, while consistent and high solar irradiance leads to a lower Levelised Cost of Hydrogen.

Regarding the influence of design choices, it can be concluded that the ratio of solar versus wind energy has the biggest influence of both the LCOH and the CF, with wind in general being more expensive but entailing lower carbon emissions, The selected PV technology also has a clear influence on the LCOH and CF. The CdTe PV technology results in hydrogen with a low CF, but a higher LCOH. CI(G)S is all-round the best performing PV technology in terms of CF and LCOH. The choice of electrolyser shows a clear preference towards alkaline electrolysis, as PEM results in a higher LCOH with barely any influence on the CF.

The research shows that the Carbon Footprint can be influenced significantly through production design choices. The different researched production pathways for green hydrogen result in a range of Carbon Footprints between 0.67-3.64 $kg\,CO_2/kg\,H_2$. The LCOH range found in this report is between 1.67-2.75 $\$/kg\ H_2$, excluding storage and transportation. This is in range with blue hydrogen, while providing the benefit of reducing the Carbon Footprint by more than half. The results show that in most scenarios, a tangible CF reduction can be realised at limited costs.

For future research, storage, transportation and an off-taker must be included in the optimisation model to provide a complete price to benchmark against grey and blue hydrogen. It would also be beneficial to expand the researched impact categories, such as social impact or the impact of critical raw material depletion.

Contents

List of Figures

List of Tables

Nomenclature

Abreviations

AEM	Anion Exchange Membrane
AWE	Alkaline Water Electrolyser
BoP	Balance of Plants
CAPEX	Capital Expenditures
CF	Carbon Footprint
FU	Functional Unit
GHG	Green House Gas
IEA	The International Energy Agency
IRENA	The International Renewable Energy Agency
KPI	Key Performance Indicator
LCA	Life Cycle Assessment
LCOE	Levelised Cost of Electricity
LCOH	Levelised Cost of Hydrogen
LP	Linear Programming
MILP	Mixed Integer Linear Programming
MINLP	Mixed Integer Non-Linear Programming
NLP	Non-Linear Programming
NPC	Net Present Costs
OPEX	Operational Expenditures
PEM	Proton Exchange Membrane
PV	Photovoltaic
RHDHV	Royal HaskoningDHV
SMR	Steam Methane Reforming
SOE	Solid Oxide Electrolyser
TRL	Technology Readiness Level
WGS	Water Gas Shift

Symbols

$\dot{M_{H_2}}$	Annual hydrogen production [$ton/year$]
η_{isen}	Isentropic compression efficiency [%]
C_f	Capacity factor [-]
C_j	Costs in year j [$]
CF_{PV}	Carbon Footprint of solar PV [g/kWh]
CF_{wind}	Carbon Footprint of wind turbines [g/kWh]
H	Hub height [m]
I_mean	The average solar irradiance [kWh/m^2]
m_{H2}	Molar mass of hydrogen [g/mol]
M_{total}	Total hydrogen production [kg]
n	Project lifetime [yrs]
$N_{turbine}$	total number of turbines [-]
P_{comp}	Compressor power [W]
P_{disc}	Pressure at outlet [bar]
P_{rated}	Rated capacity [MW]
P_{suc}	Pressure at inlet [bar]
pc_{elec}	Power consumption electrolyser [MWh/ton]
q_m	Molar flow [mol/s]
SV	Salvage Value [$]
T_{suc}	Temperature at inlet [K]
u_{mean}	Mean wind velocity at 100 m [m/s]
Y_{1MW}	Yield of a 1MW installation [MWh/MW]
k	Ratio of specific heat under constant pressure to specific heat under constant value. [-]
N	Number of compression stages [-]
n	Project lifetime [yrs]
R	Universal gas constant [$J/molK$]
r	Nominal interest rate [-]
w	Weight factor [-]
Z	Compressibility factor [-]

1 Introduction

1.1. Motivation

There is a worldwide call for large-scale green hydrogen production. Hydrogen is widely regarded as a promising alternative to fossil fuels for meeting energy demands in a low-carbon economy. However, the large-scale deployment of green hydrogen and its derivatives as energy carriers, fuel or industrial feedstock requires the development of cost-effective and low-carbon hydrogen production. In Figure 1.1 the projected future demand of hydrogen is displayed. Producing these amounts by conventional methods would have a catastrophic impact on the planet, as 11.24 kg of carbon dioxide is produced for every kg of hydrogen [50]. Following the route of 'blue' hydrogen, by trying to capture and store these emissions, will reduce the overall Carbon Footprint (CF) by just 9 to 12% [22], offering no real solution to the problem. The build-up of green hydrogen production facilities has commenced, with a total of 170-365 GW electrolyser capacity in the pipeline for 2030 [24]. To reach the globally agreed net zero goals however, a total of 550 GW is required. To put this number in perspective, currently there is a total installed capacity of 2.9 GW. With a production facility lifetime of 20 years [31], it is essential to not forget the goal of the net zero targets and to ensure that the build up of the hydrogen economy happens as clean as possible. Research into cost-effective, low-carbon large-scale green hydrogen production is a necessity.

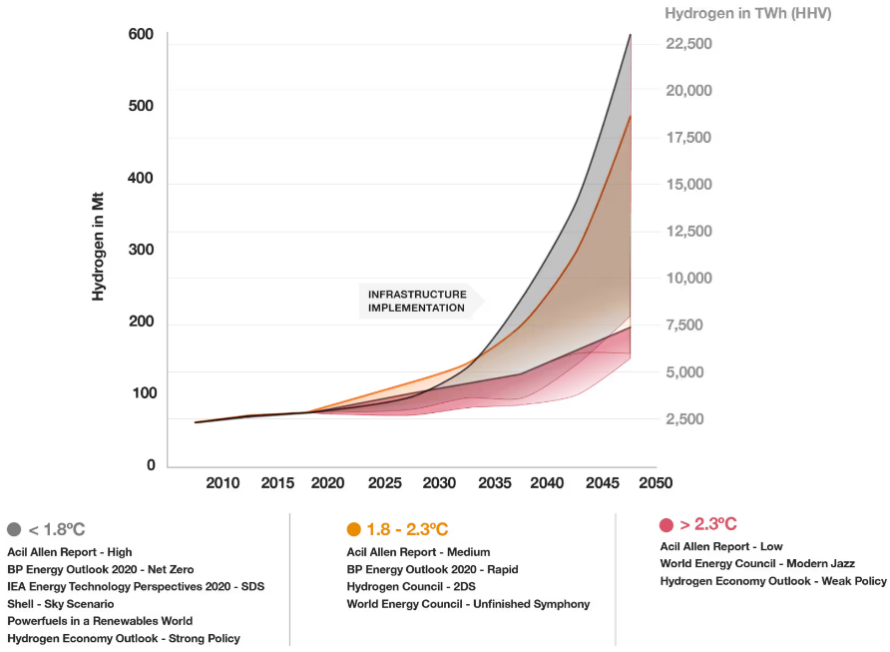

Figure 1.1: Projected hydrogen demand[49].

1.2. Research goal

This thesis aims to address two major challenges of green hydrogen: the cost-competitiveness and carbon footprint of green hydrogen. Interest in green hydrogen is gaining traction, resulting in an increasing amount of research, policy making and large investments. Nonetheless, the economic competitiveness of green hydrogen production remains a critical barrier to its large-scale adoption, as grey hydrogen costs are in the range of 0.9-2.7 $/kg [48] [38] and the costs of blue hydrogen are in the range of 1.9 - 4.7 $/kg [38]. Additionally, the carbon footprint of the produced hydrogen should be kept as low as possible, to maximise the carbon mitigation effect, that is the reason of its production.

With this optimisation framework, the key factors that have the biggest impact on the overall cost and carbon footprint of green hydrogen can be identified by analyzing and comparing different electrolyser technologies, renewable energy resources, and locations. This information can be of great help to policymakers, investors, and industry stakeholders who are seeking to accelerate the deployment of green hydrogen and drive the transition to a low-carbon economy.

An additional goal of this thesis is to develop the optimisation tool such that new production locations can be easily added. This could speed up the process of initial sizing of new projects and thereby increase the potential reach of the project.

1.3. Research gaps

Based on the literature study, summarised in chapter 2, a series of research gaps is identified. Several renewable energy resources and hydrogen production methods were explored, together with the methods to test the costs and carbon footprint of the different production pathways. The identified gaps are presented below, and substantiated in chapter 2, where the necessary background for this thesis is described.

Identified research gaps

- **A wind-solar mix as energy source for hydrogen production :** Despite its utilisation in announced projects, there is little focus in literature on the trade-off between the cost and carbon footprint of hydrogen produced through solar and wind energy. Combining both technologies could limit the effects of intermittency and increase the utilisation factor of the electrolyser.
- **Carbon Footprint optimisation :** Although many studies have been done on the carbon footprint of hydrogen production, no optimisation with the aim to reduce the carbon footprint of hydrogen production has been found in literature. It could be interesting to explore how the design of the production chain is influenced when carbon footprint is prioritised over cost-effectiveness.
- **Regional dependency of costs and carbon footprint:** The yield of solar and wind installations are largely dependant on location, influencing the overall costs and carbon footprint of the produced hydrogen. This dependency is left out in most general papers.

1.4. Research question

Below the research question is formulated, based on the identified research gaps and the goal of this thesis. Three color-coded subquestions are formulated with the aim to substantiate the reasoning behind the answer on the research question.

> *"What is the influence of local weather patterns on the design of large-scale green hydrogen production chains, when optimised for a low 'Levelised Cost of Hydrogen' and 'Carbon Footprint' on a cradle-to-gate basis?"*

Subquestions

- What components of the green hydrogen production chain influence the Levelised Cost of Hydrogen and Carbon Footprint the most?
- What are the most important system design choices that influence the trade-off between Levelised Cost of Hydrogen and Carbon Footprint?
- What influence do weather patterns have on Levelised Cost of Hydrogen and Carbon Footprint?

1.5. Method and scope

To answer the above-mentioned questions, a model is built that simulates the hydrogen production chain and optimises its design for carbon footprint and cost minimisation, based on available wind and solar data. The optimisation is done for three test locations: Duqm, Groningen and Dakhla. In Duqm there is an abundance of solar potential, but a very seasonally dependant wind potential. In Groningen the opposite holds true with a steady year-round wind potential but a lack of solar potential. The final case is Dakhla, where there is both a consistent and high solar and wind potential.

Given the complexity and breadth of the entire green hydrogen production chain, it is important to define the boundaries of the research in order to ensure a meaningful analysis. To this end, the research assesses the hydrogen production on a cradle-to-gate basis for a project executed from 2030, which encompasses all the activities and inputs that are required to produce green hydrogen up to the point of transport. This includes energy generation, hydrogen production, and compressing the hydrogen to delivery pressure. By limiting our scope in this way, the production phase is accurately described, without getting entangled in the complexity of the distribution and use phases.

1.6. Royal HaskoningDHV

This thesis is written in collaboration with Royal HaskoningDHV. Royal HaskoningDHV (RHDHV) is an independent consultancy which integrates 140 years of engineering expertise with digital technologies and software solutions. Backed by the expertise of over 6,000 colleagues working from offices in more than 20 countries across the world, RHDHV aims to help organisations turn local and global issues related to the built environment into opportunities and make the transition to smart and sustainable operations. Through their mission Enhancing Society Together, they take responsibility for having a positive impact on the world.

The Enhancing Society Together framework

As part of RHDHV's strategy, they aim to deliver measurable impact in their projects and their own operations. They focus on five themes where they can have the most influence. The themes form the foundation of their Enhancing Society Together framework and are:

- Climate change (SDG7 and SDG13)
- Biodiversity & natural systems (SDG14 and SDG15)
- Resources & circularity (SDG 6 and SDG12)
- Social value & equality (SDG 4, SDG5, SDG8, SDG9 and SDG11)
- Safety & well-being (SDG3)

This framework guids RHDHV and relates to specific UN Sustainable Development Goals (SDGs) to protect the planet, end poverty, and ensure that by 2030 people everywhere enjoy peace and prosperity. These five themes are relevant to everything RHDHV does. The collaboration with Royal HaskoningDHV offers an opportunity to bring academic research and engineering expertise together, and to

explore the practical implications of the research in real-world contexts. More information regarding Royal HaskoningDHV can be found at their website: www.royalhaskoningdhv.com.

1.7. Structure

The structure of the report is displayed in Figure 1.2. In chapter 2 the research gaps from section 1.3 are substantiated and the necessary background information is provided that forms the foundation for the selection of the method and the understanding of the results, conclusions and recommendations. The background describes the reviewed technologies, how the performance of different scenarios are indicated, and the reasoning behind the selection of the three test cases. In chapter 3 the method for collecting and processing data is described, followed by an explanation of the constructed optimisation model and finally the description of the sensitivity analysis. The results of the research are discussed in chapter 4. The different scenarios flowing from the choice of region, electrolyser and PV module are presented. This chapter is concluded with a sensitivity analysis. Finally in chapter 5 the conclusions of the research are presented, followed by recommendations for future research.

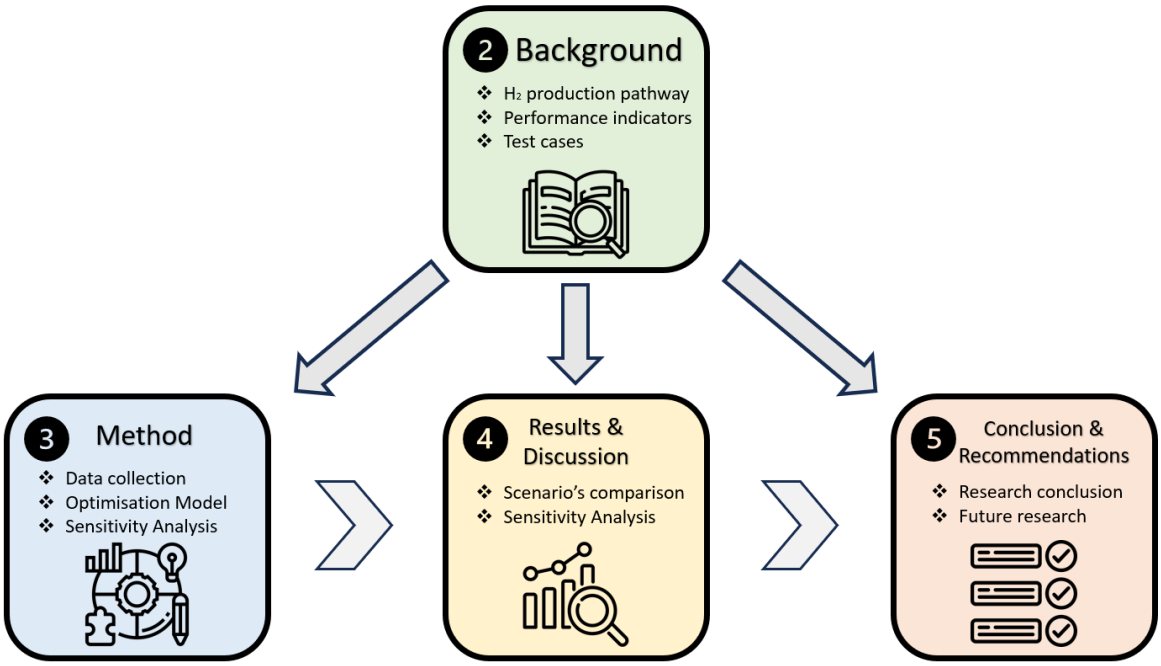

Figure 1.2: Report structure.

2

Background

The goal of this report is to better understand the influence of weather patterns on the costs and carbon footprint of green hydrogen production pathways. The structure of the chapter is displayed in Figure 2.1. First, all components along the hydrogen production chain are explored, starting with the renewable energy resources. This report focuses on solar and wind energy and the inherent intermittency in section 2.1. In section 2.2 the electrolysis process and technology is discussed. The Balance of Plants of a hydrogen production facility are discussed in section 2.3. Section 2.4 describes the necessary project economics to assess the different production scenarios. Economics are required for the feasibility of a project, but the true goal of green hydrogen production is to mitigate the effects of climate change. The environmental impact of different production pathways must be investigated using the Life Cycle Assessment method. The methodology, and a selection of performed Life Cycle Assessments are discussed in section 2.5. The chapter is concluded in section 2.6 with the introduction of the three test cases that will be reviewed in this research.

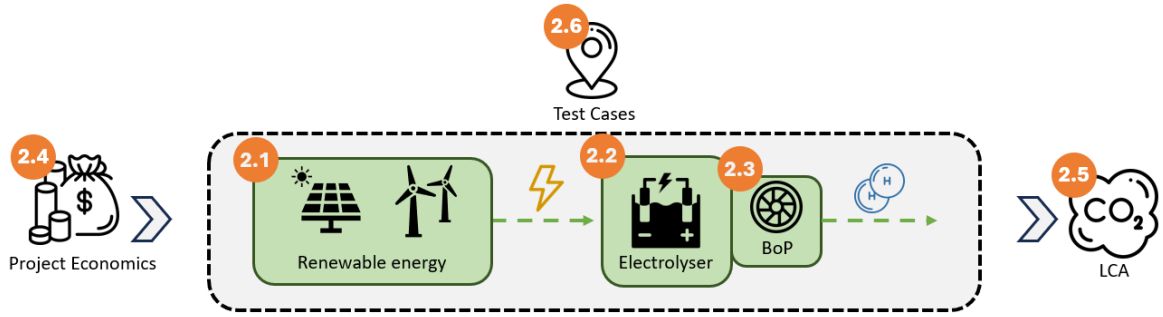

Figure 2.1: Background structure overview.

2.1. Renewable energy resources

The energy source of hydrogen is a determining factor. It defines the sustainability classification of the hydrogen, and it is responsible for the biggest contribution towards the overall costs and Carbon Footprint. Roughly 50 kWh of energy is required for the production of 1 kg of Hydrogen[47]. In order for hydrogen to classify as renewable or 'green', this energy has to come from a renewable source. There are many types of renewable energy sources, but only wind and solar energy will be considered in this report as these technologies are well understood, relatively cheap, and feasible in most locations. The technology, costs developments and Carbon Footprint of solar and wind energy are discussed in subsection 2.1.1 and subsection 2.1.2 respectively. This section is concluded in subsection 2.1.3, where the challenge of intermittency will be explored.

2.1.1. Solar energy

Edmond Becquerel discovered the photovoltaic effect in the 19th century. The photovoltaic effect describes the conversion of light into electrical energy. In the 20th century the technology became commercially available, and today solar Photovoltaïcs (PV) makes up 14.7% of the cumulative installed power capacity, which is projected to be 22.2% by 2027 according to the International Energy Agency (IEA)[25] . The IEA [25] projects that the global installed solar capacity will be 6 TW by 2030. Solar PV will play a big role in the years to come, with the global energy demand more than doubling by 2050 [33]. Another advantage of solar energy, is that it is a decentralised power source, allowing for localised production and consumption even in difficult to reach regions.

One of the most significant developments in solar energy in recent years has been the costs reduction. The levelised Cost of Electricity (LCOE) through solar PV modules has decreased by nearly 90% between 2010 and 2021 [32], driven by improvements in manufacturing processes, economies of scale and increased competition. As a result, solar energy is now cost-competitive with conventional sources of electricity in many regions, and being the cheapest when onshore wind is not available, as illustrated in Figure 2.2.

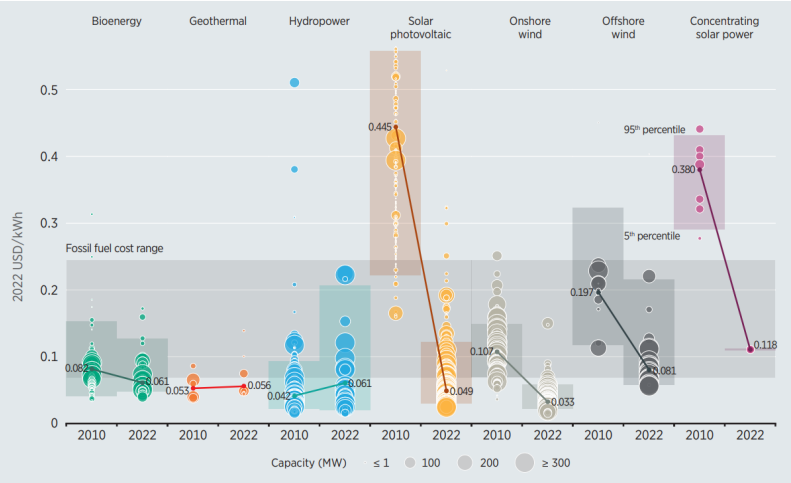

Figure 2.2: Global weighted average LCOEs from newly commissioned, utility-scale renewable power generation technologies, 2010-2021 [32].

There are many different types of PV cells, each with its own characteristics. The first generation of PV cells consists of mono-crystalline Si-based PV cells (Mono c-Si) and poly-crystalline Si-based PV cells (Poly c-Si). These types of modules dominate the market, with a cumulative market share of 90% [25]. Four technologies typically associated with the second generation of PV cells are amorphous Si-based (a-Si), Gallium Arsenide (GaAs), Cadmium Telluride (CdTe) and Copper Indium Gallium Selenide (CI(G)S) PV cells. The second generation PV cells are so-called thin film PV cells, as the light absorbing layer is decreased from 300 µm to only 10 µm [15]. There are also a third and fourth generation, but as these technologies are not ready for utility-scale deployment, they are excluded from this research. Due to Carbon Footprint data availability, for this research only Mono c-Si, CdTe and CI(G)S are taken into account. The prices and efficiencies for these modules can be found in Table 2.1.

Table 2.1: PV module specific characteristics.

	CdTe	CI(G)S	Mono c-Si	unit
Module costs [15]	180	100	150	$/kW
Efficiency [15]	22.1	23.4	23.3	%
Carbon Footprint: β_type [4]	-12.68	-49.43	-48.87	-
Carbon Footprint: β_Y_type [4]	0.006182	0.02451	0.02436	-

Renewable energy sources are often called 'clean' energy, a common misconception is that there are no Green House Gas (GHG) emissions paired with this technology. However there are emissions throughout the lifetime of a panel or turbine, from material mining, to manufacturing, installation, reparation and finally disposal. Therefore the Carbon Footprint of renewable energy sources must be explored further. The Carbon Footprint of energy is typically expressed in [$g\ CO_2/kWh$]. Logically, this number is highly influenced by the energy production location. This becomes clear when thinking of two identical PV panels. The first one is placed somewhere with constant cloud cover, while the second one is placed in an area with constant open skies. The second panel will produce more energy over its lifetime, and can therefore distribute all accumulated lifetime emissions over a larger quantity of energy. This effect is studied for utility-scale PV plants in Bosmans, Dammeier, and Huijbregts [4] and for utility-scale wind farms in Dammeier, Bosmans, and Huijbregts [12]. In both papers a regression analysis is performed as to identify the most influential factors. Using this information a function is constructed that can predict the Carbon Footprint of energy , based upon these identified factors.
For PV power, Bosmans, Dammeier, and Huijbregts [4] have found multiple predictors. With these predictors, two regression models are built that can calculate the Carbon Footprint of solar PV, CF_{PV} in [$g\ CO_2e/kWh$]. The regression model used in this report is the simple variant, being dependant on three main factors. The first predictor is the construction year of the PV panels. Because of electrification and improvement of the production process, a higher construction year results in a lower Carbon Footprint. The input value for $Year$ is the absolute year (e.g. 2023). The second factor is the mean solar irradiance of the location of the solar park, I_{mean} in [kWh/m^2]. The final, and most influential, factor is the module type. The different modules are produced with different materials and different processes, resulting in different Carbon Footprints. The module type is represented by two variables, one fixed, β_{type}, and one that is multiplied by the year, β_{Y-type}. Both beta-factors are dimensionless and the values are presented in Table 2.1. An adaptation of this regression model is shown in Equation 2.1.

$$log\left(CF_{PV}\right) = 64.3 - 0.03088 * Year + \beta_{type} - 0.000232 * I_{mean} + \beta_{Y-type} * Year \tag{2.1}$$

Using this regression model, the Carbon Footprint for different regions can be calculated. The regional variability of the Carbon Footprint is best explained by an example. Mono c-Si pv cells have a Carbon Footprint of 51.61 g/kWh in Dakhla, while in Groningen the emissions rise to 90.15 g/kWh. Overall CdTe is the cleanest cell technology, with a Carbon Footprint ranging from 10.03 to 17.52 g/kWh. All worked out values can be found in Table 3.7 in chapter 3.

2.1.2. Wind energy

Wind energy has been used by humanity for centuries. However, since the late 20th century people began generating electricity from wind. As of today, wind energy is an important part of the global energy mix, at 11.4%. This percentage is projected to grow to 14.4% by 2027 [25] with a total installed capacity of 7.4 TW by 2030 [28].

The classic onshore and offshore wind technologies have serious potential to grow, and even more new technologies are entering the market, such as floating wind [30], increasing this potential further and making wind energy one of the driving factors of the energy transition. In recent years, the cost of wind energy has decreased significantly, driven by improvements in technology and economies of scale. The cost of wind energy has fallen by 60% for offshore wind and by 67% for onshore wind between 2010 and 2021 [32], making it one of the most cost-effective sources of electricity in many regions. As a result, many wind projects are commissioned around the world. This is displayed in Figure 2.2. The price drop can be explained by the rapid growth in capacity, and the scale at which wind parks are deployed today. As of today offshore wind turbines with capacities up to 18 MW are

being produced [46], fulfilling the predictions by The International Renewable Energy Agency (IRENA [30]) as can be seen in Figure 2.3. This figure is adapted from an extensive study of IRENA called 'The Future of Wind'. In this report it is stated that the costs for onshore wind are projected to be between 800-1350 $\$/kw$, and for offshore these costs are projected to be between 1700-3200 $\$/kW$.

The Carbon Footprint of wind energy is typically lower than that of PV modules. This is quantified in the study of Dammeier, Bosmans, and Huijbregts [12]. In this paper many wind farms are analysed and a regression model is constructed, similar to the one for PV. In this model there are five important predictors for Carbon Footprint CF_{wind} in [$g\ CO_2e/kWh$]. The most important predictor of the Carbon Footprint of a wind farm, is the mean wind speed of the wind farm location at 100 m high. The mean wind speed, u_{mean} in [m/s], dictates the energy yield of the wind farm and therefore indicates over how many kWh the production Carbon Footprint is spread out. The Turbine rating, P_{rated} in [MW], is the second predictor. Following the same logic as the wind speed, the turbine rating dictates the amount of energy produced over the lifetime of the wind farm. The third predictor of the CF is the hub height H expressed in[m]. The actual wind velocity received by the turbine is dependant on the height of the hub. The fourth predictor is the number of turbines in a wind farm $N_{turbine}$. This is the least influential predictor of the set. An increase in turbines per wind farm, means an increase in wake effects in the wind farm. The wake effect causes on average a decrease in wind farm performance. The final factor is whether the wind farm is onshore or offshore. This factor O is a categorical variable, 0 for onshore and 1 for offshore. Wind farms that are offshore are more difficult and more polluting to install and maintain, increasing the Carbon Footprint. The regression model can be seen in Equation 2.2.

$$log\,(CF_{wind}) = 2.41 - 0.20 * u_{mean} - 5.9 * 10^{-4} * P_{rated} - 8.3 * 10^{-5} * H + 5.3 * 10^{-3} N_{turbine} + 0.33 * O \quad (2.2)$$

For Duqm and Dakhla onshore 8 MW wind turbines are selected, resulting in a Carbon Footprint of 12.2 $g\ CO_2e/kWh$ and 7.15 $g\ CO_2e/kWh$ respectively. For Groningen offshore 16 MW wind turbines are selected, resulting in a Carbon Footprint of 10.4 g/kWh. Further substantiation of these values can be found in chapter 3.

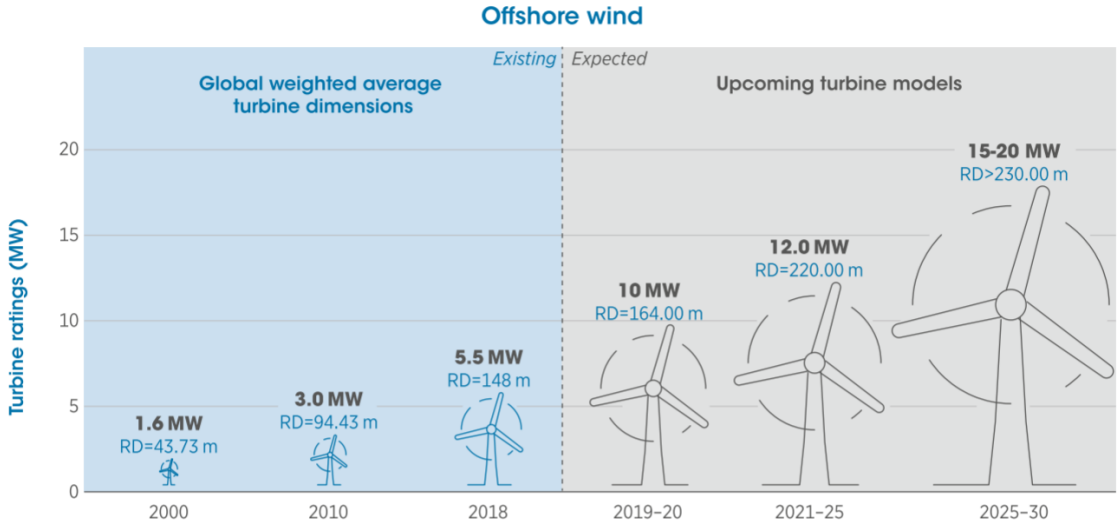

Figure 2.3: Wind turbine capacity prediction [30].

2.1.3. Intermittency

Intermittency is one of the big challenges in the transition towards renewable energy, as the sun does not always shine and the wind does not always blow. This phenomenon is explored in this section.

Insolation (solar radiation power per square meter at the earth's surface) changes daily from 0 to it's local maximum. This maximum depends on the latitude and on the season. On the 52° North line, where The Netherlands is, this maximum changes a factor 6 between mid summer and mid winter [40]. This difference can be explained by a reduction in instantaneous light intensity and the daylight time. In the western Sahara, the 19.5° North line, this variance between winter and summer is a factor 1.5 [40]. Wind resources too express a seasonal and diurnal variance. On Northern latitudes, average wind power can be two times stronger in winter than in summer. On a diurnal scale the wind power is strongest in the afternoon, and has a low point in the early morning, with 12 hours in between [40]. Wind power is heavily influenced by surface temperatures, causing wind power to be strongest when the surface has warmed up after a day of sun. Wind power is thus dependant on the diurnal variance of insolation. Wind velocities can differ between 2 m/s in the morning to 4 m/s in the afternoon. Kinetic energy contained in wind scales with velocity to the third power, causing a variation of factor 2 in wind speed to result in a factor 8 difference in energy output. Although this diurnal variance is due to the heating and cooling of the land, offshore wind parks up to several 100 kilometers of the coast experience this effect [40]. This sea breeze effect largely disappears in winter.

In the upper figure of Figure 2.4 a representation of the approximate insolation per latitude is shown. However the yield of solar panels is also varies due to regional factors, such as desert dust or a lack or surplus of cloud cover. In the bottom part of the figure the seasonal wind variation plus approximation for the US is shown, to give an idea of what such a seasonal pattern looks like. The velocity in this figure is cubed, as wind power relates to the cubed wind speeds.

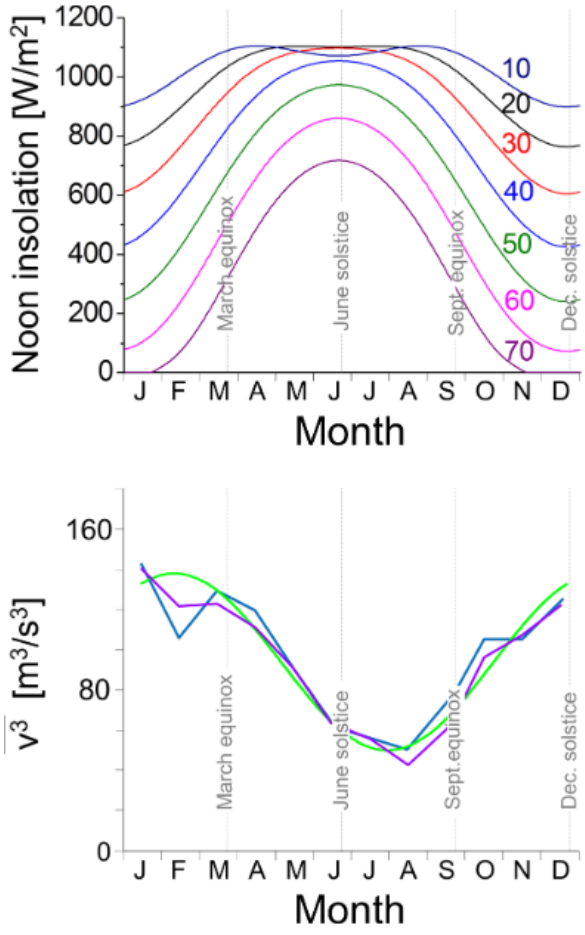

Figure 2.4: Top: Yearly insolation variance approximation for given latitudes. **Bottom:** Yearly cubed wind velocities in the US, onshore (blue), offshore (purple) and sinusoidal approximation (green) [40].

A combination of wind and solar energy sources has the potential of reducing overall intermittency. This is due to the opposite average seasonal variance of wind and solar energy. By appropriately sizing the wind and solar plants, seasonal intermittency can be limited. However, the more pressing challenge is posed by daily energy supply fluctuations. The highs and lows of solar and wind energy patterns do not align seamlessly, and daily variance makes this issue even worse. Some days may experience cloud cover, while others may see a lack of wind. Consequently, a power profile is generated that requires flexibility from the consuming side. The risk of having no power at all, is reduced by installing an energy mix of both solar and wind.

Hydrogen production is often mentioned as solution to the intermittency problem [54][42]. Hydrogen can be produced when there is an excess of energy and be converted back to electricity when there is a shortage. In this report, the production of hydrogen is not a solution to intermittency, but the end product. Therefore intermittency is a challenge to be overcome, as it limits the production capacity of the electrolyser.

Key takeaways Renewable energy resources

- Installed solar PV capacity, is cheaper than installed wind capacity. The actual energy price for wind and solar is location-specific.
- Installed wind capacity, has a lower Carbon Footprint than installed solar PV capacity. The actual Carbon Footprint of energy for wind and solar is location-specific.
- Intermittency can be overcome by combining wind and solar energy.

2.2. Electrolysers

Using the renewable energy from the previous section, green hydrogen can be produced through a process called electrolysis. Water molecules are split using electrons, producing hydrogen and oxygen. The reaction equation is shown in Equation 2.3.

$$H_2O \rightarrow H_2 + \frac{1}{2}O_2 \tag{2.3}$$

The half reactions differ per electrolyser technology, therefore the half reactions are shown in Figures 2.5,2.6.2.7 and 2.8. Electrolysers are a major contributor to the cost of green hydrogen production. It is essential to choose the electrolyser best suited to the situation. First the different types of electrolysers are discussed in subsection 2.2.1. Lastly general dynamic performance is zoomed in on in subsection 2.2.2.

2.2.1. Electrolyser types

Electrolysers can be sorted into four main types, based on operating temperature and electrolyte selection. Because of the difference in cell design, the different types require different materials and Balance of Plant configuration. The Balance of Plant is discussed in section 2.3. Below, the four types of electrolysers will be introduced. First the two most widely used electrolyser technology are discussed: Alkaline electrolysis and Proton Exchange Membrane electrolysis. This is followed by Solid Oxide Electrolysis, an upcoming technology requiring high temperatures. At the end, Anion Exchange Membrane electrolysis will be discussed, the most novel technology.

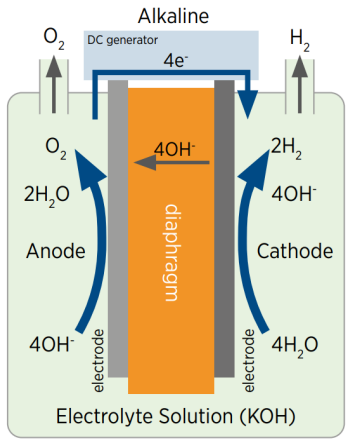

Anode: $4OH^- \leftrightarrow 2H_2O+O_2+4e^-$
Cathode: $4H_2O+4e^- \leftrightarrow 2H_2+4OH^-$

Figure 2.5: AWE cell reactions [31].

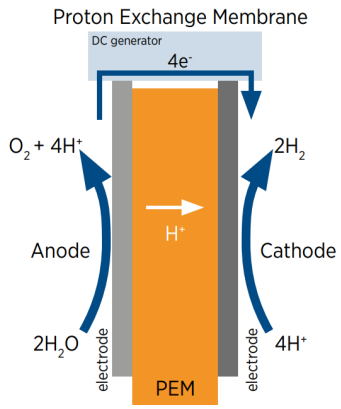

Anode: $2H_2O \leftrightarrow O_2+4H^++4e^-$
Cathode: $4H^++4e^- \leftrightarrow 2H_2$

Figure 2.6: PEM cell reactions [31].

The first type discussed is the Alkaline electrolyser, also called an Alkaline Water Electrolyser (AWE) . This technology was invented at the end of the 19th century and has been in commercially operation since the beginning of the 20th century [31]. The chemical cell reactions and configuration are shown in Figure 2.5. This type of electrolysis uses an alkaline electrolyte, which in most cases is a potassium hydroxide (KOH) solution with a pH of 13 to 14 [57] . A diaphragm is placed between the cathode and the anode. Modern diaphragms are inorganic porous membranes that allow hydroxide anions to pass through, to enable the hydrogen production at the cathode and oxygen production at the anode.

Alkaline electrolysis produces hydrogen at a purity of 99.9-99.9998% [31]. Through hydrogen drying and purification, oxygen impurities can be removed to increase the purity to a desired level. The electrolysis typically takes place at relatively at pressures of 2-30 bar and at a temperature range of 70-90 °C [31]. Hydrogen production through Alkaline Electrolysis has a power consumption of 52 kWh/kg H_2 [31]. Alkaline Electrolysis performs bad in terms of cyclability, referring to its ability to turn on and off quickly. When exposing an Alkaline cell to an intermittent power profile, gas crossover will take place. This means that hydrogen leaks back through the diaphragm to the Anode side. This can be really dangerous as this forms a highly explosive mixture of oxygen and hydrogen. Another problem is

that gas crossover reduces the hydrogen purity. The bad dynamic performance of an electrolyser is a serious disadvantage as intermittent power profiles are inherent to renewable power sources.

The four electrolyser types differ not only in cell design and Balance of Plant, but also in their Technology Readiness Level (TRL) . When a technology is TRL 9, it means that the technology is proven in a commercial and operational environment. Only technologies that are TRL 9 by 2030 will be considered for this research. Alkaline is a very mature and commercially available technology and is therefore TRL 9. The advantages and disadvantages of AWE are summed up in Table 2.2.

Table 2.2: Advantages and disadvantages of an alkaline electrolyser [57].

Advantages	Disadvantages
Mature technology	Low current density
Non-noble electro-catalyst	Corosive Electrolyte
Low capital costs	Gas permeation
High lifetime	Operational Dynamics
High stability	

The next electrolyser type, is PEM or a Proton Exchange Membrane electrolyser. PEM electrolysis was invented in 1966 and commercialised by 1978 [57]. The cell design and reactions can be seen in Figure 2.6. As the name suggests, protons are exchanged through a membrane, commonly a Nafion membrane. Oxide ions are blocked by the membrane and form oxygen on the anode side.

PEM electrolyser systems have a typical power consumption of 51 kWh/kg H_2 [47]. The biggest advantage of PEM are the operational dynamics. PEM electrolysers have the possibility of cycling, enabling it to operate in a irregular production regime more associated with renewable energy grids.

The cell temperature in these cells are typically between 50 to 80 $^\circ$ C and can handle pressures up to 350 bar [31], however due to safety issues flowing from gas crossover, a pressure of 70 bar is considered in this report. High purity hydrogen gas can be produced using PEM technology, with less purification steps than AWE. The membrane blocks all impurities and other gasses, resulting in a hydrogen gas flow that can be used for a variety of high purity use cases, such as sensitive fuel cell operation. This filtering capability is also a drawback however, as the cell needs a very pure water feed in order to prevent membrane and cell degradation, which results in a lower lifetime and performance.

PEM electrolysers have a higher current density than alkaline electrolysers. This can be a big advantage in areas where space is a limiting factor. An electrolyser with a high current density requires less space than an electrolyser with a small current density.

A major drawback of PEM electrolysers are the required metals such as platinum and iridium. These precious metals are required as catalyst and are a major driver of the total investment costs and carbon footprint of this technology [37]. The limited supply of these critical raw materials is an obstacle for the large-scale roll-out PEM electrolysers.

Table 2.3: Advantages and disadvantages of an PEM electrolyser [57].

Advantages	Disadvantages
Compact design	High cost membrane
High current density	Low durability
High purity hydrogen	Acidic medium
Operational Dynamics	Critical raw materials
High operating pressure	

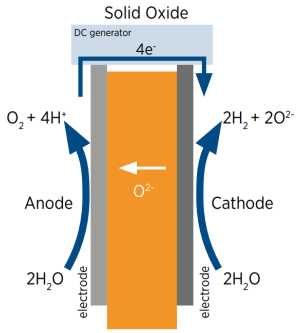

Anode: $2O^{2-} \leftrightarrow O_2 + 4e^-$
Cathode: $2H_2O + 4e^- \leftrightarrow 2H_2 + 2O^{2-}$

Figure 2.7: SOE cell reactions[31].

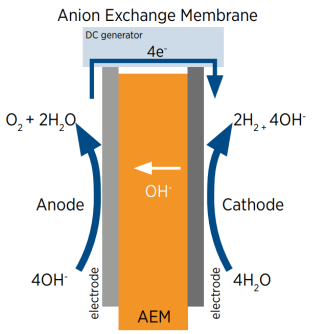

Anode: $4OH^- \leftrightarrow 2H_2O + O_2 + 4e^-$
Cathode: $4H_2O + 4e^- \leftrightarrow 2H_2 + 4OH^-$

Figure 2.8: AEM cell reactions[31].

The next electrolyser type is the Solid Oxide Electrolyser (SOE) . Although SOE is a technology in development, it is assumed to be TRL 9 by 2030, as the Danish company Haldor Topsoe intends to open an annual 500 MW SOE production facility by 2024 [16]. The SOE cell uses a solid electrolyte to transport oxide anions form the cathode to the anode, this is illustrated in Figure 2.7. Special about SOE, is that the cell can be designed to be reversible, enabling the electrolyser to play a balancing role in the grid by supplying electricity when there is a shortage. A major difference between SOE and PEM and AWE electrolysis, is that the SOE process happens at very high temperatures of 800-1000 $^\circ$ C. This has the benefits that less electrical energy is required for the process, high current densities can be achieved and efficiencies are nearing 100%. There are several drawbacks as well, such as safety issues, instability, electrode degradation and the requirement of high temperature steam. Especially the requirement of high temperature steam and the instability under dynamic conditions makes this technology less applicable for the intended purpose of this research, as it is less universally deployable.

Table 2.4: Advantages and disadvantages of a SOE [57].

Advantages	Disadvantages
No precious catalysts	Electrode instability
High current density	Safety issues
Low electricity needs	Improper sealing
High efficiency	Electrode degradation
	Bad dynamic behaviour

The final electrolyser type is the Anion Exchange Membrane Electrolyser (AEM) . AEM can be seen as a combination of the alkaline environment and the simplicity and efficiency of a PEM electrolyser [31]. The cell reactions and design can be seen in Figure 2.8. Titanium-free and non-noble catalysts are used in the design. The membrane also enables a pressure difference between the cathode and anode side, which decreases oxygen cross-over. This results in high purity hydrogen and increased safety. AEM is a new technology, currently at TRL 6: the demonstration phase. The AEM membrane has serious mechanical and chemical stability issues, reducing the lifetime. The performance of the technology is currently subpar due to poor electrode architecture and slow catalyst kinetics [31]. While this technology could be interesting in the future, it is not expected to reach TRL 9 by 2030 and thus is excluded from further review for this research.

Alkaline (AWE) and PEM are selected as technologies of interest for this study, and as the goal of this research is to shed light on the carbon footprint of hydrogen production, the emissions related to these electrolysers must be further investigated. This is done by Lotrič et al. [37]. The complete hydrogen production facility is included in this study, from the electrolyser stacks, to the Balance of Plant. In this study all materials required for the AWE and PEM processes are summed up and translated to several impact categories. For this research the focus is on GHG emissions. The study investigates a container sized electrolyser of 50 kW, which is assumed to be scalable. The resulting carbon equivalent emissions can be found, together with the economic and process related key performance indicators of the electrolysers in Table 2.5. The values of the carbon footprint need further clarification. The

carbon footprint represents the entire hydrogen production facility, including the balance of plant and the housing of the facility. As simplification, the carbon footprint is split according to the mass fractions of these separate components. The used numbers reflect the carbon footprint that is predicted by Lotrič et al. [37] when taking end-of-life processing into account.

Table 2.5: Electrolyser characteristics.

Economics	**Alkaline**	**PEM**	**unit**
Investment costs [31]	900	1400	$\$/kW$
O&M [53]	3	3	% $of\ investment$
Stack investment cost [31]	30	30	% $of\ investment$
Lifetime system [31]	20	20	$years$
Stack lifetime [26]	95000	75000	$hours/stack$
Operation			
Max. pressure [31]	30	70	bar
Operating temperature [31]	80	90	$°C$
Upper load limit [26]	110	160	% $of\ rated\ capacity$
Lower load limit [26]	10	0	% $of\ rated\ capacity$
Power consumption (system) [47]	52	51	MWh/ton
KOH use [18]	0.0037	0	$kg/kg\ H_2$
Environmental			
Carbon Footprint [37]	283	210	$ton\ CO_2/MW$

2.2.2. Dynamic behaviour

Flexibility of operation, or operational dynamics, is an important factor for electrolysers that are coupled to intermittent power sources. The electrolyser must be able to handle the variations that are inherent to these renewable sources. Alkaline electrolysers are able to ramp up and down in a matter of seconds with a ramping rate of 20 $\%/s$ [63]. The systems are operable in a range of 10-100 %. Starting an AWE system up can take 30-60 minutes, as all components must be purged of remaining gasses. When the system is kept at temperature and pressure, a start up takes up to 20 minutes [63]. PEM electrolysers can perform cold start-up in 5 minutes and can shut down in a matter of seconds [61].

Tuinema et al. [61] validate an electrolyser model by comparing it to a real life 1 MW PEM test installation. He found that the installation scaled by 0.2 MW/s at start-up and had an average ramp up rate of 0.5 MW/s and an average ramp down rate of 0.4 MW/s. He further suggests that, as a big facility consists of multiple parallel electrolysers, this rate can be linearly scaled. This would mean a 1 GW plant could ramp with a rate of 0.5 GW/s. Tuinema et al. [61] points to experiments that showed non-linear behaviour in a 40 kW electrolyser. Ramping up or down was generally completed in 0.2 seconds, resulting in an effective ramp rate of 0.1 MW/s. This would suggest a ramping rate of 2.5 GW/s for a 1 GW plant. This would mean that ramping rate of a 1 GW PEM lies between 0.5-2.5 GW/s, or 50-250 $\%/s$. Next to the fact that ramping rates this high can cause safety hazards through gas crossover and faster cell degradation, there is also a practical objection. The bottleneck in the ramping rate of hydrogen production does not lie in the ramping rate of the electrolyser cells themselves, but rather with the ramping rate of the mechanical compressors that are needed to transport the hydrogen [31] and the used converter and controls [61]. A solution to this limitation, is producing the hydrogen at pressure or installing a buffer, to decouple the compressor operating regime from that of the electrolyser.

Key takeaways Renewable Energy Resources

- Only AWE and PEM are suitable technologies for this research.
- AWE is 35.7 % cheaper than PEM per installedMW.
- PEM is 25.8% less polluting than AWE per MW installed.
- PEM needs 2% less energy to produce hydrogen than AWE.
- PEM has a higher current density than AWE
- PEM handles power fluctuations better than AWE

2.3. Balance of Plants

Hydrogen production facilities cannot function without the support of auxilliary systems, also called the Balance of Plants (BoP) . Common components in the BoP are heat exchangers, compressors, gas separators and power electronics. In subsection 2.3.1 the general BoP of alkaline electrolysers is described, followed by the same for PEM in subsection 2.3.2. The characteristics and working principles of compressors are discussed in subsection 2.3.3.

2.3.1. Balance of Plants: Alkaline

A general alkaline system design including the BoP is shown in Figure 2.9. First the feed water is mixed into the KOH cycle. The KOH stream is then fed into the electrolyser. Here the water is split, creating one oxygen-rich and one hydrogen-rich stream. Both streams are fed into the corresponding gas separators. When the gasses are separated from the stream, the KOH solution is cycled back in the KOH cycle. There is a mixing pipe between the anodic and cathodic side, in order to mitigate the imbalance in OH- charges. The difference in charges can't be too large, making it difficult to operate the system at differential pressure.

The resulting oxygen is vented or stored, while the hydrogen stream gets treated. First the hydrogen is transported through a heat exchanger to a deoxo unit. Here the oxygen contents in the hydrogen are reduced, before moving on to the drying process. The hydrogen flow is saturated with water, therefore the hydrogen is purified in the dryer, by removing as much water as possible. The hydrogen stream coming out of the dryer has a purity of 99.9%.

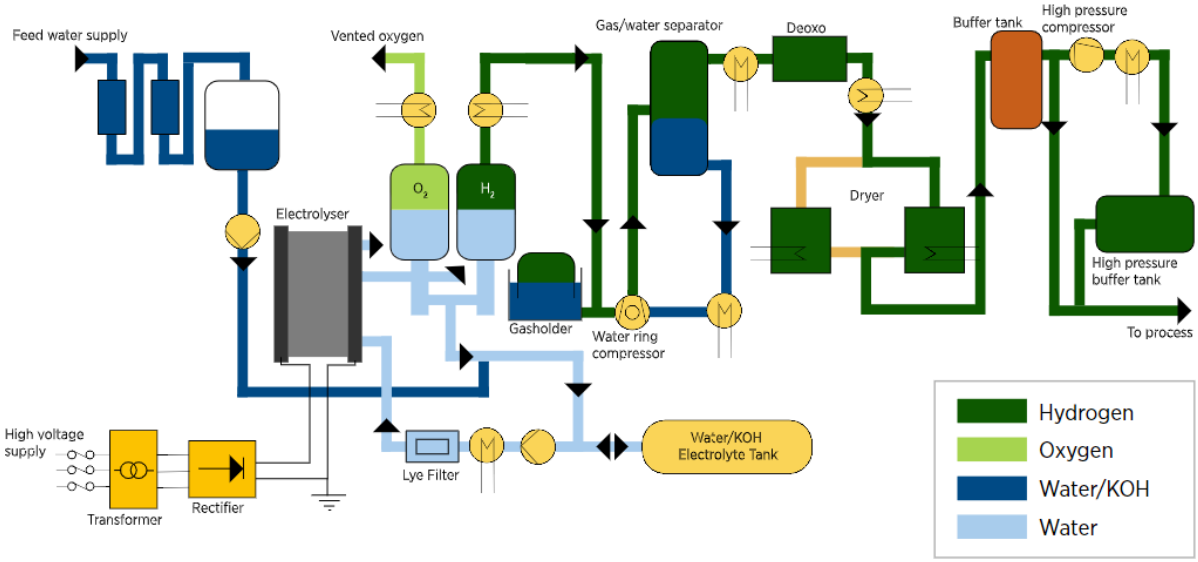

Figure 2.9: Balance of Plant Alkaline [31].

2.3.2. Balance of Plants: PEM

The BoP of a PEM system is less complex than the alkaline system, as illustrated in Figure 2.10. Bareiß et al. [2] gives a careful description of the PEM process. The following is an adaptation from that paper. Deionised water, with a conductivity smaller than 0.1 µS/cm, is pumped to the cell stack. Before the cell stack, the water travels through an ion exchange resin cartridge to maintain the low water conductivity. The water leaves the cell at the anode side mixed with oxygen. Here the oxygen is separated and the water is brought back in the cycle after passing a heat exchanger, to maintain the working temperature in a range of 60-90 °C. At the cathode side a mixture of water and hydrogen is cooled to ambient temperature and is separated. The water is drained to the anodic cycle.The water-saturated hydrogen is fed to a catalytic deoxo purification, lowering the oxygen content to less than 5 ppm. The deoxo unit is typically not included for differential pressure systems. The water concentration is then reduced to less than 5 ppm through an adsorptive dryer. The hydrogen leaves the process typically at 30 bar, while the oxygen is kept at ambient pressure to prevent cross permeation and to simplify the anodic cycle, by removing the need for pressure proof vessels and piping.

The BOP lifetime is assumed to be 20 years. Stack lifetime is 90000h, or roughly 10 years of continuous system operation. The components that are prone to degradation are the Membrane Electrode Assembly and the Porous Transport Layer, both can be substituted in an overhaul process.

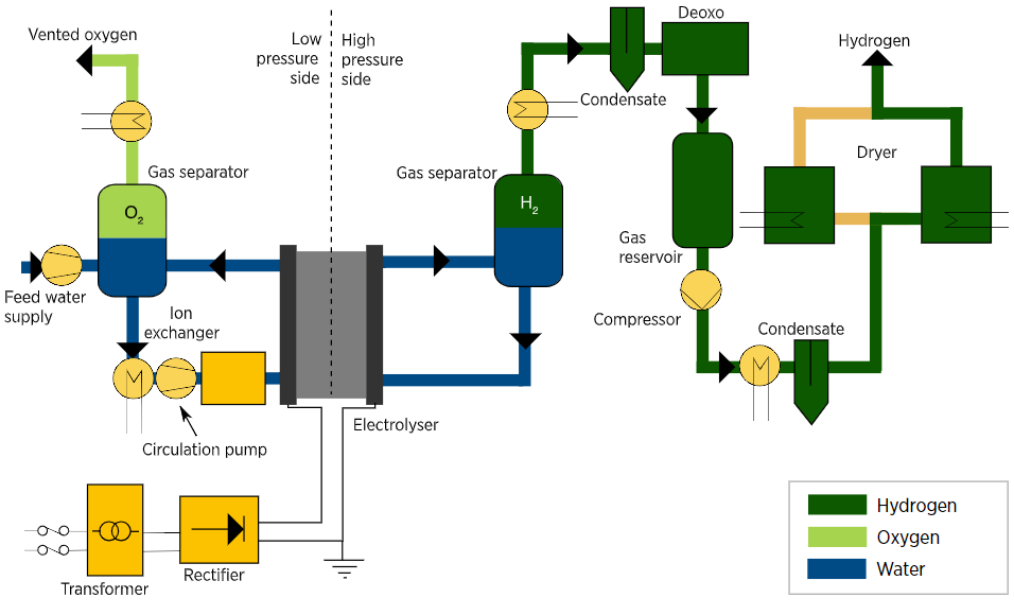

Figure 2.10: Balance of Plant PEM [31].

2.3.3. Compression

Hydrogen compressors are a vital part of hydrogen infrastructure. Hydrogen has a roughly 4 times smaller volumetric energy density when compared to natural gas [59]. At 25° C and 1 bar, one cubic meter of hydrogen contains 12.7 MJ, whereas methane contains 40.0 MJ [5]. In order to transport or store a significant amount of hydrogen, compressors are used to increase the pressure and therefore the volumetric energy density. The typical hydrogen pipeline pressure of 70 bar. This reduces the volume by a factor 65 (due to hydrogen being a non-ideal gas) and thus increasing its volumetric energy density [31].

There are two main options of delivering hydrogen at pressure. Pressurising the produced flow, or pressurising the production process, eliminating the need or lowering the demand for further compression. To pressurise the flow, there are two mechanical compressor types that are able to handle hydrogen flows associated with large-scale hydrogen production: the reciprocating and centrifugal compressors [59][56]. Mechanically compressing hydrogen from 1 to 30 bar has the steepest energy losses, as shown in Figure 2.11. The power required to compress hydrogen P_{comp} is shown in Equation 2.4 [36].

$$P_{comp} = N \left(\frac{k}{k-1} \right) \left(\frac{Z}{\eta_{isen}} \right) T_{suc} * q_m * R \left(\left(\frac{P_{disc}}{P_{suc}} \right)^{\left(\frac{k-1}{Nk} \right)} - 1 \right) \tag{2.4}$$

In this equation, k is the specific heats ratio, for hydrogen equal to 1.4. Z is the compressibility factor, averaged between the suction pressure at the inlet P_{suc} and the discharge pressure at the outlet P_{disc}. R is the gas constant, η_isen is the isentropic efficiency, T_{suc} is the inlet pressure, q_m is the molar flow and N is the number of compression stages. As becomes clear from this equation and Figure 2.11, a lot of energy can be lost when compressing from the atmospheric pressure up to higher delivery pressures, therefore it can be more efficient to pressurise the electrolyser to skip this step.

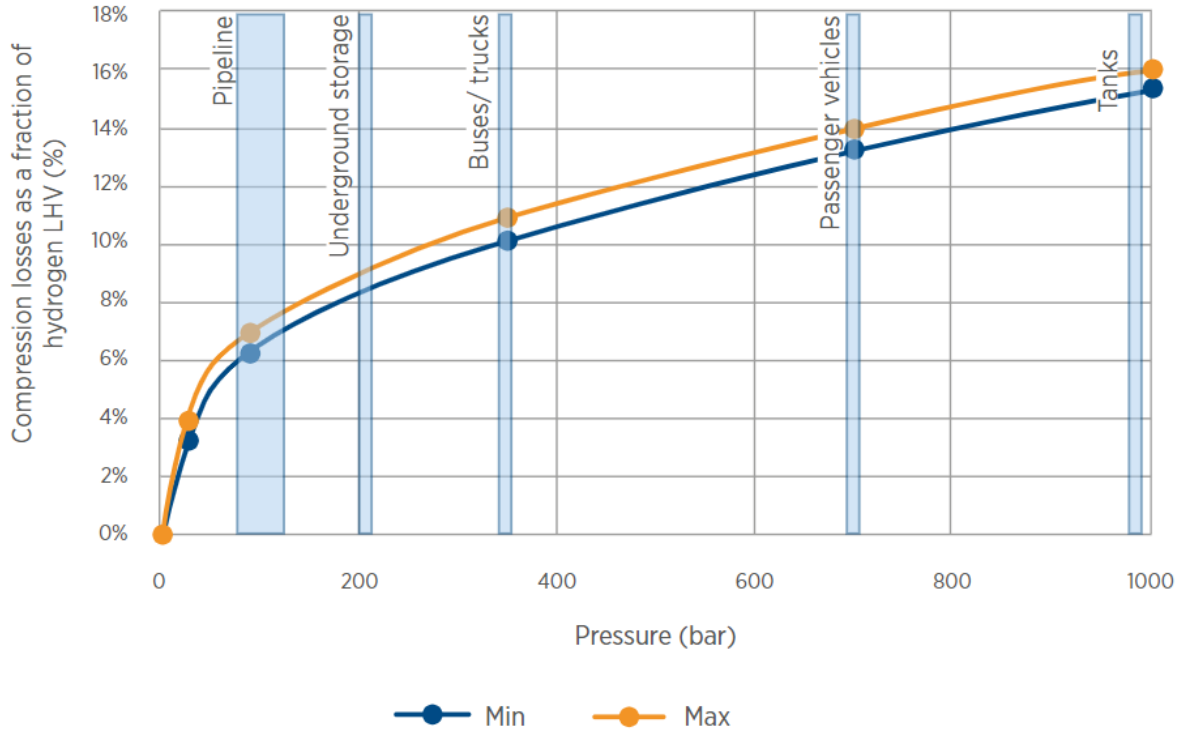

Figure 2.11: Mechanical compression losses [31].

In PEM electrolysers, there are two standard process pressurising methods. balanced and differential. Under balanced pressure, both the anode and cathode side of the electrolyser are pressurised. This enables the use of thin membranes, spacers and porous layers, which increases efficiency as the internal resistance is low. The drawbacks of this methods are an increased safety risk because not only pressurised hydrogen is produced, but also pressurised oxygen. Another drawback is that the equipment is more expensive, as both the anode and cathode side need to be pressure safe. In differential pressurisation, only the cathode side is pressurised. The membranes, spacers and porous layers must be made thicker when compared to balanced pressurisation in order to withstand the pressure difference, which increases internal resistance and thus decreases efficiency. The costs of this type of system is lower however.

For this report a delivery pressure of 30 bar is selected, with an operational pressure of 5 bar for alkaline electrolysis and 30 bar for PEM electrolysis, based on the 1 GW electrolyser plant design from the Hydrohub Innovation Program [47], and the functional unit of the hydrogen certification scheme CertifHy ™, more on this in section 2.5. The selection of a 30 bar delivery pressure eliminates the need for further compression when PEM is used. When alkaline electrolysis is selected, a centrifugal compressor is used, this is substantiated in section A.2.

Key takeaways Balance of Plant

- The Balance of Plant of PEM electrolysers are more compact.
- For this research, only for the AWE electrolyser the hydrogen is further compressed using a centrifufgal compressor.

2.4. Project economics

The previous sections described the technical aspects of the green hydrogen production chain. In this chapter the economical aspect will be discussed. Project economics play a crucial role in the successful roll-out of any major project, including the establishment of a hydrogen economy. Project economics assess the financial feasibility and viability of a project, identifying costs, revenues, risks, and returns. Without a strong business case, it is unlikely that technological feasible projects, such as the development of a hydrogen economy, will be executed. This is because investors and stakeholders require a clear and compelling justification for the risk that they are taking.

In addition to providing a financial framework for decision-making, project economics can also help to identify and mitigate potential risks and challenges. For example, a thorough economic study of the entire production chain can highlight the potential savings. Overall, a robust project economics analysis is essential for the successful roll-out of a hydrogen economy, as it provides the foundation for strategic decision-making, risk management, and stakeholder engagement.

The economic assessment method used for this research, is an adaptation of the economic assessments performed by Sadeghi, Ghandehariun, and Rosen [55] and Gaspars-Wieloch [17]. An important financial indicator in the hydrogen economy, is the Levelised Cost of Hydrogen (LCOH) . This indicator expresses the cost of producing a kg of hydrogen. The equation for the LCOH is shown in Equation 2.5.

$$LCOH = \frac{NPC}{M_{total}} \tag{2.5}$$

NPC stands for the Net Present Costs of the hydrogen production over the lifetime of the project and M_{total} is the total hydrogen production capacity over the lifetime of the project, which is calculated in Equation 2.6.

$$M_{total} = \sum_{j}^{n} M_j \tag{2.6}$$

The total costs over the lifetime of the project, are calculated using the Net Present Costs method. In this method, the cash flows over the lifetime of the project are all scaled to the net present value. The net present value of a future cost, is equal to the amount of money you have to reserve at the start of the project when subjected to the nominal interest rate. This nominal interest rate is the expected interest that can be earned on money when not used for the project. This percentage differs per region and is always an assumption, therefore it is important to test this assumption through a sensitivity analysis. The Net Present Cost formula is shown in Equation 2.7.

$$NPC = \sum_{j=1}^{n} \frac{C_j}{((1+r)^j} \tag{2.7}$$

In this equation n is the lifetime of the project, C_j are the total costs in year j, and r is the nominal interest rate. There are three main cash flows in this research, Capital Expenditures (CAPEX) , Operational Expenditures (OPEX) and the Salvage value. CAPEX are investments that are done once in the lifetime of a project. OPEX are periodic costs over the lifetime of a project, and are often called Operation and Maintenance costs (O&M) referring to the biggest contributing factors. OPEX is typically expressed as an annual costs equal to a set percentage of CAPEX. Salvage value is the remaining economic value of a component at the end of its economic lifetime. This is assumed to be 10% and is subtracted in the final year of the components lifetime. The costs in year j are acquired by summing the CAPEX, OPEX and Salvage Value for year j of all components c

$$C_j = \sum^{c} CAPEX_{j,c} + OPEX_{j,c} - SVj, c \tag{2.8}$$

An economical assessment is important to test the feasibility of a project. However the impact of a project on the world should not be forgotten. A Life Cycle Assessment (LCA) can be performed, to assess the impact of a given project over its life cycle. This is explained in the coming chapter.

2.5. Life Cycle Assessment

A Life Cycle Assessment is performed to assess the impact of a project over its lifetime. This impact can be many things, ranging from human toxicity, to social injustice. In this report the impact on climate change is researched. Assessing the impact on climate change is important in an ethical sense, as the negative influence of a product on the world should be reduced, but it is also important in a project feasibility sense. At request of the European Commission, a hydrogen certification scheme was initiated called CertifHy™ [8]. According to this certification, green hydrogen is defined as hydrogen originating from renewable sources as defined in the Renewable Energy Directive (REDII) with a carbon footprint (CF) smaller than $36.4\ g\ CO_2e/MJ(LHV)$ or $4.4\ kg\ CO_2e/kg\ H_2$. The emissions should consider all production stages required for 99.9% purity and with a delivery pressure of 30 bar. This definition is based on a 60% reduction with respect to the Steam Methane Reforming (SMR) process (section A.1) with a CF of $91\ g\ CO_2e/MJ(LHV)$ or $10.9\ kg\ CO_2e/kg\ H_2$. If you cannot comply to this standard, the product will not be salable and there will be no business case to support the project.

2.5.1. Life Cycle Assessment Standard

The first LCA was performed in 1993 by the Society of Environmental Toxicology and Chemistry [2]. The method has been improved over the years and is now standardised by the International Organisation of Standardisation, under ISO 14040:2006 and 14044:2006. CertifHy ™works with ISO 14076, which is consistent with ISO 14040 and 14044. The LCA process is split up in four phases [39]. In most LCA's there will be multiple iterations on these phases.

Phase 1: Goal and scope definition

In the first phase of an LCA, the goal and scope are defined. This is done such that the choices and assumptions during the process can be understood. An important step is the definition of the Functional Unit (FU). The total emissions of a process are distributed along these functional units, this way it is easy to compare different processes. The FU specified by CertifHy ™is 1kg of hydrogen at 30 bar and at a purity of 99.9%. It is also common practice to define a process flow in the FU. Comparing a process that produces 1 kg of hydrogen vs one that produces 200 kton is of little value. The scope definition must include a description of all processes that transform the inputs of the system, into the outputs. The most common scopes are described below.

- **Cradle-to-grave**: This scope starts at the extraction of raw materials, and follows the product all the way to the disposal of the product.
- **Cradle-to-gate**: For this scope, the product assessment is concluded when it leaves the process step in the life-cycle. By excluding transportation, usage and disposal, the LCA is simplified significantly. This scope provides insights for internal processes of a production facility and will produce results quickly.
- **Gate-to-gate**: When a product undergoes a variety of value-adding steps, it can be helpful to highlight a specific part of the process by assessing one of these value-adding steps in the production chain.
- **Well-to-wheel** : This is a special system boundary specifically for energy carriers in transportation. It includes all processes of extraction of raw materials, until the use as fuel.

The scope should include what region, what time period and what impact categories are assessed. The impact category climate change is typically expressed as the Carbon Footprint in $[kg\ CO_2/kg\ H_2]$. The CF is calculated in Equation 2.9 by dividing the lifetime emissions E_{life} by the lifetime production M_{total} of the process.

$$CF = \frac{E_{life}}{M_{total}} \tag{2.9}$$

Phase 2: Inventory of inputs and outputs

The next phase is the inventory of inputs and outputs. In this phase, the inputs and outputs are mapped out in an environmental sense. Inputs are materials taken from the environment in order to produce the product, and the outputs are all emissions and waste streams. These inputs and outputs are then mapped out by constructing a flow diagram. When all flows are mapped out, data can be collected to

assess the impact of all the inputs and outputs. This data can be collected from LCA databases, past studies or other literature. The inventory phase is typically concluded by a chart, listing all flows and related quantities.

Phase 3: Impact assessment
In the impact assessment phase, the flows of the previous phase are assessed according to the selected impact categories. For a climate change assessment, this means that all flows will be converted to CO_2 equivalence. By presenting the impact of different parts of the process separately, the biggest contributors to the overall impact can be identified, and subsequently be dealt with.

Phase 4: Interpretation of results
In the last phase of the LCA, the results are evaluated. This can range from the selection of the best process, to the identification of the most impactful part of the process. In this phase a sensitivity analysis is often performed to assess the robustness of the results.

Table 2.6: Reviewed LCA's, Carbon Footprint in [$kg\ CO_2e/kg\ H_2$] on a cradle-to-gate basis. The LCA's are differentiated by different production technology, energy source, production location and construction year

Author	Electrolyser	Energy	Region	Project start	Carbon Footprint
Bareiß et al [2]	PEM	Grid	Germany	2050	11.6
Hake et al [20]	AWE	Grid	Gemany	2015	23.7
Hake et al [20]	AWE	Grid	Austria	2015	7.52
CICE [8]	SOE	Grid	Canada	2022	11.9
CICE [8]	PEM	Grid	Canada	2022	15.2
CICE [8]	AWE	Grid	Canada	2022	16.1
Ghandehariun et al [19]	AWE	Wind	Canada	N/S	0.68
Sadehgi et al [55]	AWE	CSP	Iran	N/S	2.45
Sadehgi et al [55]	AWE	PV	Iran	N/S	3
Weidner [66]	N/S	Wind	Global	2035	0.6
Weidner [66]	N/S	Wind	Global	2050	0.4
Weidner [66]	N/S	PV	Global	2035	1.9
Weidner [66]	N/S	PV	Global	2051	1.4

2.5.2. Carbon Footprint of hydrogen

Valente, Iribarren, and Dufour [62] performed a thorough study of 30 LCA's about different hydrogen production pathways, performed between 2004 and 2017. These LCA's are harmonised and compared, resulting in a climate change impact range of 0.51-11.54 $kg\ CO_2e/kg\ H_2$. In Table 2.6 a selection of the LCA's is displayed. All Carbon Footprints in this table are on a cradle-to-gate basis. This selection focuses on papers that consider hydrogen production through electrolysis. This selection is presented because it contains a range of different used electrolyser technologies and energy resources. The regional and the temporal scope are also varied, to give an idea of the effect of the construction year and location.

A clear takeaway from the table is that using the grid as an energy source for hydrogen, performs worse than grey and blue hydrogen. The estimated CF of grey hydrogen is 11.24 $kg\ CO_2e/kg\ H_2$ and of blue hydrogen 6.5 $kg\ CO_2e/kg\ H_2$. The substantiation for the carbon footprints of grey and blue hydrogen can be found in section A.3. If the carbon footprint of a power grid is lowered enough, this should no longer be the case, but even for the future scenario of Germany in 2050, as researched in the LCA of Bareiß et al. [2], the carbon footprint remains above the threshold as defined by CertifHy ™.

A second conclusion from the table, is that hydrogen originating from wind energy results in a lower carbon footprint than hydrogen produced with solar energy, in the present and in the future. In none of these papers a mix between wind and solar energy is reviewed. An energy mix could reduce intermittency and improve the utilisation factor of the electrolyser, possibly decreasing the carbon footprint and the levelised cost of hydrogen. Nearly all papers mention that the energy source is the determining factor for the overall carbon footprint. Ghandehariun and Kumar [19] researched hydrogen originating from wind energy, and they concluded that 65% of the total carbon footprint is due to the construction of the wind energy system.

The LCA of CICE et al. [8] compares different electrolyser technologies. The high efficiency of the SOE becomes clear when comparing it to the CF of PEM and Alkaline. The Carbon Footprint of PEM is approximately 1.8% lower than Alkaline (AWE), which is similar to the difference in power consumption between PEM and Alkaline of 1.9%, as presented in Table 2.5.

Key takeaways Life Cycle Assessment

- The energy source is the defining factor for the Carbon Footprint of hydrogen.
- The production location influences the Carbon Footprint.
- There is a lack of research exploring hydrogen production through a mix of wind and solar.
- Scope definition is very important when discussing the Carbon Footprint.

2.6. Test locations

As explained in section 2.1 the carbon footprint and costs can vary from place to place, mainly due to weather conditions. Three test cases are selected. In the following subsections the test cases will be presented. The three test cases are selected because of the difference in weather patterns.

Duqm - The Sultanate of Oman

The first location of interest is the region around Duqm in the Sultanate of Oman. Multiple large-scale green hydrogen projects in the Duqm region were signed [23] in 2023, signifying the serious interest of the government, and the active role it plays in supporting the build-up of a hydrogen economy. Oman is a very promising location due to the high renewable energy yields that can be achieved. In Figure 2.13 the hourly Capacity factors, C_f for both solar and wind are displayed over a 3 year time-period. A zoomed in version is show in Figure 2.12 to clearly show the day-night fluctuations. The capacity factor for solar is high throughout the year, with a small dip in summer. The wind profile is very low in the majority of the year, with a big peak every summer. This can be used to dampen the dip in the solar profile.

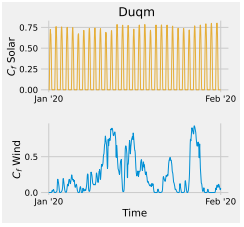

Figure 2.12: Weather profile: zoomed in.

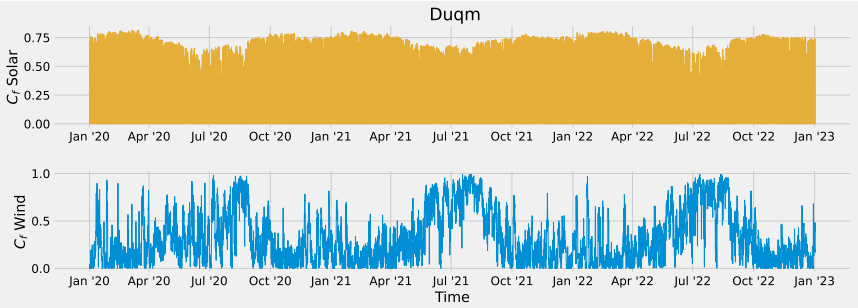

Figure 2.13: Weather profiles: Duqm. The graphs show the capacity factor of solar and wind energy for every hour from January 2020 to January 2023.

Groningen - The Netherlands

A second interesting location is Groningen, the Netherlands. The Groningen region is marked by the European Union as one of the unions Hydrogen Valleys [65]. This means that there is strong motivation, and subsidisation, for setting up large-scale hydrogen production. Groningen is selected because of the present wind farms, and the grid connections to Norway and Denmark, who occasionally spill over their residual green energy to the Netherlands. There is also a large potential for underground hydrogen storage [35]. The solar yield in Groningen is low, especially in winter, but this could be compensated by the high potential of offshore wind as displayed in Figure 2.14.

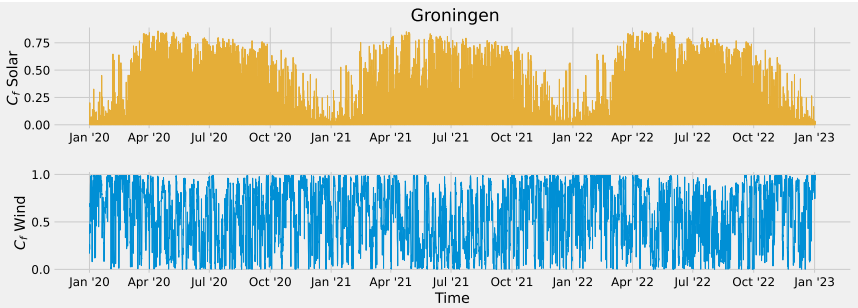

Figure 2.14: Weather profiles: Groningen. The graphs show the capacity factor of solar and wind energy for every hour from January 2020 to January 2023.

Dakhla - Western Sahara

The last area of interest is the area around Dakhla, in Western Sahara. Internationally this area is regarded as one of the cheapest locations to produce hydrogen, with similar reasons as Duqm, abundant space, sun and wind [44]. Morocco, which controls the area, has an ambitious national hydrogen strategy, with the aim on the short tern to reduce production costs, in order to supply countries with ambitious decarbonisation goals [64]. On the long term the aim is global trade and decarbonisation of its own industry, heating and transport. The solar and wind yields can be seen in Figure 2.15. Here you can see that both wind and solar energy produce consistently throughout the year.

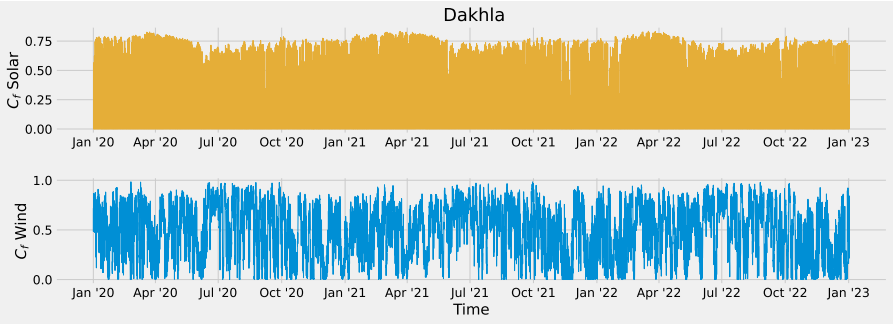

Figure 2.15: Weather profiles: Dakhla. The graphs show the capacity factor of solar and wind energy for every hour from January 2020 to January 2023.

Key takeaways Test Locations

- The solar profile in Duqm displays high potential throughout the year with a small dip in the summer. The wind potential is relatively low, but displays a peak in the summer months.
- The solar profile of Groningen shows low potential in winter, and inconsistent behaviour during the rest of the year. The wind profile is relatively stable and shows high potential.
- Both the wind and solar profiles in Dakhla display high and consistent weather throughout the year.

3

Method

In this chapter the methodology is described that is used to investigate the influence of weather patterns on the design of hydrogen production pathways. First, in section 3.1, the scope of the research is defined, after which two key performance indicators are defined to express the carbon and cost performance of the different configurations. A wide range of scenarios are put together, by combining the three different production locations, with three types of PV modules and two types of electrolysers. To efficiently evaluate these scenarios, an optimisation model is constructed. This model is described step-by-step in section 3.2. Finally, a sensitivity analsysis is performed to test the influence of different defining factors. These factors are presented in section 3.3.

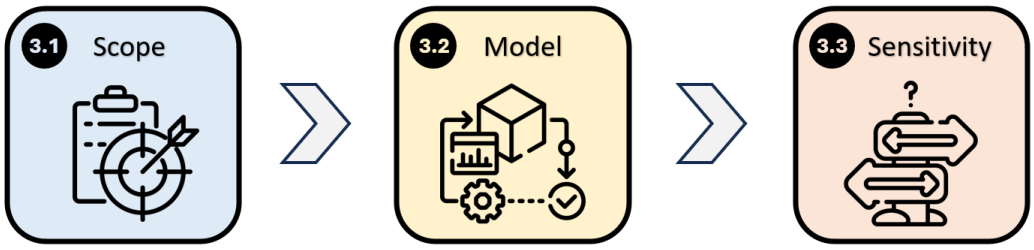

Figure 3.1: Method structure overview.

3.1. Scope definition

The goal of this research is to shed light on the trade-off between the carbon emissions and the costs of different large-scale green hydrogen production pathways. This is done by investigating the hydrogen production pathway in three regions, with two electrolyser technologies and three types of PV modules. For an effective comparison, it is useful to define Key Performance Indicators (KPI'S) . Two KPI's are selected: the Carbon Footprint $[kg\,CO_2/kg\,H_2]$ and the Levelised Cost of Hydrogen $[\$/kg\,H_2]$. Both KPI's relate to the Functional Unit, another method of ensuring fair comparison, as explained in section 2.5. The selected FU is 1 kg of hydrogen, at 70 bar at 99.9% purity. A delivery pressure of 70 bar is chosen as this is a typical pressure for hydrogen pipelines and for industrial processes such as Ammonia production. The purity of 99.9% is a chosen as both PEM and AWE produce hydrogen at this purity or purer. These characteristics defining the functional unit are collected in Table 3.1 together with other assumed project characteristics. Although these values are assumptions, they are carefully chosen. The annual production value of 200 kton is chosen as this is roughly what you can produce with a 1 GW electrolyser at 100% year-round capacity, which is considered in the field as a large-scale

electrolyser [47] The economic lifetime of an electrolyser facility is 20 years, according to IRENA [31], and therefore 20 years is chosen as project lifetime. The chosen values for delivery pressure, carbon price, salvage value and nominal interest rate, are chosen after conversations with experts from RHDHV and TU Delft. A delivery pressure of 30 bar is chosen, as this is the case in the reference system [47]. A salvage value of 10% is chosen in line with the conventions of the H2A project of Energy [14]. The nominal interest rate is chosen separately for every country, in this case 6%, conform models used by RHDHV. Because of the big influence of the interest rate on the resulting LCOH, this value is included in the sensitivity analysis.

Table 3.1: Project characteristics.

	Value	Unit
Project Start	2030	
Project lifetime	20	$years$
Annual production	200	$kton/yr$
Delivery pressure	30	bar
Delivery purity	99.9	%
Salvage Value	10	%
Nominal interest rate	6	$\%p.a.$

The scope and system boundaries of this research are shown in Figure 3.2. This scope applies to both KPI's. The research question defines the scope as cradle-to-gate. This means that everything from the generation of the energy up to the point where hydrogen leaves the production facility is included. As the data that is used for the energy resources does not include the end-of-life emissions, these are placed outside of the scope.

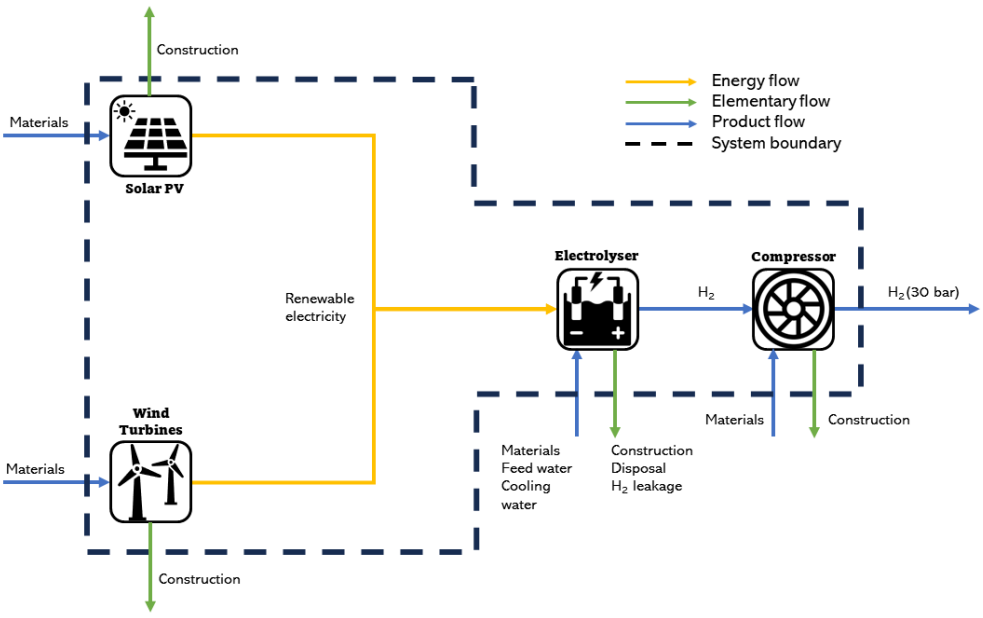

Figure 3.2: System boundaries.

3.2. Optimisation model

The effects of regional weather patterns on the costs and carbon footprint of hydrogen are investigated by constructing a single-objective Linear Programming model. The choice for Linear Programming has been made due to the simplicity of the formulation and the short computation times. In this section, the inner workings of this model are described. The model flow is displayed in Figure 3.3 and this section will be structured in the same way. In subsection 3.2.1, the method for collection the weather data and technical characteristics is described. Before starting the linear programming, the data has to be processed such that the optimisation problem can be correctly formulated, this is shown in subsection 3.2.2. Then in subsection 3.2.3 the optimisation problem is formulated step-by-step. After the optimisation, the last computations are performed to create an honest representation of the system. Why this is required after the optimisation, is substantiated in subsection 3.2.4.

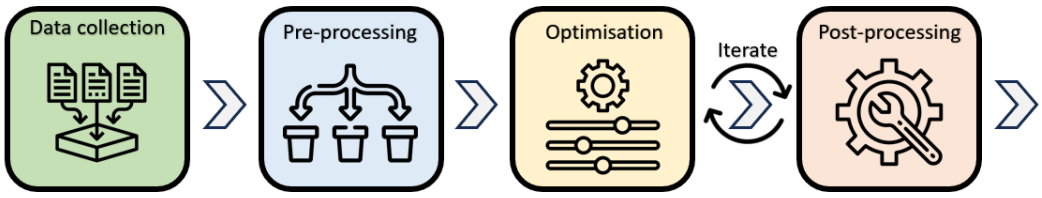

Figure 3.3: optimisation model flow.

3.2.1. Data collection

The most important data for this research, is the regional weather data. The weather data was collected from the website www.renewables.ninja, which is the result of the studies from two co-authored papers by Pfenninger and Staffel [45][58]. Pfenninger and Staffel have built this website using the datasets MERRA-2 [51] and SARAH [41]. The Modern-Era Retrospective analysis for Research and Applications, the full name of MERRA-2, is a data set that is created by NASA's Global Modeling and Assimilation Office (GMAO) and it includes global climate measurements dating back to 1980. SARAH is a dataset produced by the Climate Monitoring Satellite Application Facility using to METEOSAT geostationary satellites that observe solar irradiance of Europe, Africa and Asia. Using this website, data on a range of different weather phenomena can be extracted for specific locations, as well as the yields of potential solar and wind installations. In order calculate optimise the size of solar and wind instalations, the yield of a 1 MW solar array is extracted and the yield of an 8 MW turbine. The choice for an 8 MW turbine is chosen as this is the biggest available turbine in the data-set presented on the website. In addition, the website https://globalwindatlas.info/ was used for collection of mean wind speeds for the carbon footprint calculations, and to find possible test locations. For this research, the weather data from the years 2020, 2021 and 2022 are collected from the website.

Model inputs

Next to the weather data, a whole range of technical, economical and environmental characteristics needed to be collected. Most of this data has already been presented in chapter 2. All this data is collected, together with the wind and solar data, in a single excel file that functions as the input for the python model. In this subsection, all additional information is summarised and substantiated.

In Table 2.1 the PV module specific characteristics are presented that are used to calculate the costs and carbon footprint. The characteristics that apply to all module types are presented in Table 3.2. It is assumed that each module is 33% of the total investment costs [27]. The remaining 66 % represent all remaining cost elements such as the racking, power electronics, and installation. One final variable required for the calculation of the carbon footprint for the different locations is the mean irradiance I_{mean}. This value is calculated with the data from Pfenninger and Staffell [45]

Table 3.2: General PV characteristics.

	value	unit
Module cost [27]	33	% $of\ CAPEX$
O&M [53]	1.5	% $of\ CAPEX$
Lifetime [53]	15	$years$
$I_{mean,Duqm}$	1882	$kWh/m^2/yr$
$I_{mean,Groningen}$	1032	$kWh/m^2/yr$
$I_{mean,Dakhla}$	2076	$kWh/m^2/yr$

All values necessary to calculate the behaviour, carbon footprint and costs of the wind turbines are presented in Table 3.3. The investment costs include all costs from manufacturing the turbine, to civil works, power electronics and project planning [30]. There are also multiple assumptions in this table. In the first place, the rated turbine power. These values are determined after careful consideration and conversations with experts in the field. The hub heights are typical hub heights for turbines of the chosen capacity. The number of turbines plays a role in determining the carbon footprint of the produced wind energy, as can be seen in Equation 2.2. To determine the amount of turbines in a wind farm, the total capacity must be divided by the single turbine capacity. However, this results in the carbon footprint being dependant on the determined required capacity, which is a decision variable of the optimisation problem. This would lead to non-linear behaviour and therefore it would not be viable for Linear Programming. Therefore it is decided to take the carbon footprint of a 1 GW wind farm. This means that the model simulates the wind farms as if they are build in farms of 1 GW each, which is reasonable as wind farms bigger than 1 GW are very scarce globally.

Table 3.3: General wind characteristics, for onshore and offshore wind farms

	Onshore	Offshore	units
Rated turbine power	8	16	MW
Investment costs [30]	1050	2450	$\$/kW$
O&M [53]	2	3	% $of\ Investment$
Lifetime [53]	15	20	$years$
Hub height	105	150	m
Turbines per 1GW farm	125	67	$turbines$
$u_{mean}, Duqm$	8	-	m/s
$u_{mean}, Groningen$	-	10.2	m/s
$u_{mean}, Dakhla$	10.33	-	m/s

In Table 3.4 the necessary components for cost and carbon footprint calculations of the production feed stock are displayed. It is assumed that cooling water and process water are acquired at the same costs. All costs and emissions regarding desalination and water acquisition are included in the values given below. For this research, the feedstock and cooling water consumption are assumed to be the same for both technologies, following the research of Gerloff [18].

Table 3.4: Feedstock characteristics.

	Value	Unit
Water use [18]	8.9	$l/kg\ H_2$
Cooling water [18]	88.1	$l/kg\ H_2$
Price desalinated water [9]	1.65	$\$/m^3$
Carbon Footprint water [11]	0.004	$g\ CO_2e/l$
Carbon Footprint KOH [34]	2.2	$kg\ CO_2/kg\ KOH$

All coefficients related to compressor performance and cost can be found in Table 3.5.

Table 3.5: General Compressor characteristics.

Economics	**Value**	**Unit**
Investment costs [43]	1000	$\$/kW$
O&M [36]	3	% $of\ CAPEX$
Lifetime [36]	20	$year$
Operation [36]		
Efficiency [36]	98	%
H2 leakage [36]	0.2	%
Max inlet pressure [36]	35	bar
Max outlet pressure [36]	88.6	bar
Isentropic efficiency [36]	88	%
Driver efficiency [36]	90	%

3.2.2. Pre-processing

Before the optimisation can start, all necessary constants must be calculated. This is done in the pre-processing phase. First, the required energy is determined, then the cost and carbon footprint components are calculated. The final step is the calculation of the compressor constant.

Energy The total energy required is calculated in Equation 3.1. The annual required hydrogen production in $[ton/year]$ is scaled up to account for hydrogen leakage, and then multiplied by the power consumption of the electrolyser pc_{elec} in $[MWh/ton]$, resulting in E_{req} in $[MWh/year]$.

$$E_{req} = \left(\dot{M_{H_2}}/(1 - leakage_{H_2})\right) * pc_{elec} \tag{3.1}$$

The yield of the solar panels is determined by the dataset from Pfenninger and Staffell [45], This yield is based on CdTe panels. Therefore the CdTe yield $Y_{1MW,CdTe}$ needs to be translated the other PV type yields $Y_{1MW,pv}$, this is done using Equation 3.2 where η_{pv} stands for the efficiency of the other PV modules and η_{CdTe} stands for the efficiency of the Cadmium Telluride modules.

$$Y_{1MW,pv} = Y_{1MW,CdTe} * \frac{\eta_{pv}}{\eta_{CdTe}} \tag{3.2}$$

The wind energy yield can also be calculated using the wind data and the general wind characteristics from Table 3.3. The energy yield for the different energy technologies are presented in Table 3.6.

Table 3.6: Annual energy yield per MW installed capacity in MWh for different technologies.

	Duqm	**Groningen**	**Dakhla**
CdTe	1846	1253	1967
CI(G)S	1954	1327	2083
Mono c-Si	2180	1480	2323
Onshore Wind	2941	-	4488
Offshore Wind	-	5134	-

Costs All cost and carbon footprint values must be calculated on a per-MW-basis. The costs and Carbon Footprint are easily and equally scalable, when presented per MW. Because of this requirement, the Net Present Costs (NPC) are also calculated on a per-MW-basis. The NPC per MW is calculated by looping through the project lifetime n and constructing the NPC year by year. The formula for the NPC_{MW} is shown in Equation 3.3. This equation is an adaptation of the NPC calculation method as presented in section 2.4. An example of a worked out calculation over the lifetime of a project is presented in section B.2

$$NPC_{MW} = \sum_{j=1}^{n} \frac{C_{j,MW}}{((1+r)^j} \tag{3.3}$$

Carbon Footprint The Carbon Footprint per MW, CF_{MW}, for all renewable energy sources is also calculated pre-optimisation. This is done using the methods of Bosmans, Dammeier, and Huijbregts [4][12] as described in section 2.5. Using these equations, the emissions per unit of energy can be found, but for the optimisation, the emissions must be presented per unit of installed capacity. In Equation 3.4 this is done by multiplying the emissions per MWh by the annual yield per 1 MW of installed capacity and the project lifetime.

$$CF_{MW} = CF_{MWh} * Y_{1MW} * n \tag{3.4}$$

In Equation 3.1 the annual produced mass of hydrogen is corrected, because a percentage of the hydrogen leaks away. Hydrogen is no GHG on its own, but through its reaction with radicals in the atmosphere, hindering the breakdown of methane, hydrogen has a global warming potential of 11 [10]. As the leakage percentage is 0.02%, this would result in 0.022 $kgCO_2e$. This is regarded as insignificant in respect to the other contributing components, and is therefore excluded from the research.

The location specific emission factors, and the electrolyser specific emission factors can be found in Table 3.7. In Equations 2.1 and 2.2 the Carbon Footprint of energy in [gCO_2/kWh] is calculated. This value stays constant when expressing it as $kgCO_2/MWh$. By multiplying the results from these equations, by the project lifetime and the location and technology specific energy yield from Table 3.6, the Carbon Footprint per installed MW can be calculated. The calculated values are presented in Table 3.7.

Table 3.7: Calculated Carbon Footprints per technology and region. The Carbon Footprint of the electrolysers is not location specific and is presented at the bottom of the table.

Duqm	CF_{MWh} $kgCO_2/MWh$	CF_{MW} $tonCO_2/MW$
CdTe	11.13	411
CI(G)S	31.79	1243
Mono c-Si	57.25	2496
Onshore	12.16	817
Groningen		
CdTe	17.52	439
CI(G)S	50.06	1328
Mono c-Si	90.15	2668
Offshore	10.37	1334.51
Dakhla		
CdTe	10.03	395
CI(G)S	28.66	1194
Mono c-Si	51.61	2398
Onshore	7.15	816.84
Electrolysers		
AWE [37]	-	283
PEM [37]	-	210

Compressor The final pre-processing step is the calculation of the compressor constants. The equations mentioned in section 2.3 are adapted such that it yields a cost per MW of installed Electrolyser capacity. The compressor must be sized, such that it can handle the largest flow the electrolyser can realize. This is done by making the molar flow dependant on the maximum flow of the electrolyser. In Equation 3.5 this is displayed. The power consumption of the electrolyser pc_{elec} is expressed in [MWh/ton], and the molar mass of hydrogen is $2.016\,g/mol$, this results in a molar flow q_m expressed as $mol/(sMW)$

$$q_{m,MW,E} = \frac{1}{pc_{elec}} * \frac{10^6}{3600} * \frac{1}{m_{H2}} \tag{3.5}$$

$$P_{comp,MW,E} = N\left(\frac{k}{k-1}\right)\left(\frac{Z}{\eta_{isen}}\right) T_{suc} * q_{m,MW,E} * R\left(\left(\frac{P_{disc}}{P_{suc}}\right)^{\left(\frac{k-1}{Nk}\right)} - 1\right) \tag{3.6}$$

$$C_{comp,MW,E} = C_{comp,MW} * P_{comp,MW,E} \tag{3.7}$$

The compressor costs are only present for the AWE scenarios, as the PEM produces hydrogen at the delivery pressure of 30 bar. When performing this calculation, a compressor cost component of 867 $\$/MW_elec$ is found. Being less than 0.1% of the 900 000 $\$/MW$ investment costs of the Alkaline electrolyser [31], this number is insignificant.

3.2.3. Optimisation

All preliminary calculations and data processing steps are covered, the optimisation problem can be formulated. In section B.1, it is explained that an optimisation problem consists of three components, the decision variables, the objective and the constraints. First the variables and the objective will be introduced, followed by the constraints.

Decision variables and objecive

The easiest optimisation algorithm is single objective linear programming, as mentioned in section B.1. This research aim to optimise for both carbon footprint and costs, which is a multi-objective problem. Therefore this multi-objective problem must be phrased such that both objectives can be formulated as one. This is done by normalising the objective constants. Formulating a multi-objective problem as a single-objective problem is prone to subjectivity. To counteract this, a wide range of carbon prices is introduced to translate the carbon footprint to a cost factor. The normalisation and weighting can be seen in Equation 3.9 and 3.8. Through iteration of weight factor w, a front is constructed between the most cost-effective and most carbon-effective design. A weight factor of 0.0 ignores the carbon footprint, and a weight factor of 1.0 ignores cost optimality.

$$CF_w = [CF_{Solar,w}, CF_{Wind,w}, CF_{Electrolyser,w}] = w * \frac{[CF_{Solar}, CF_{Wind}, CF_{Electrolyser}]}{max\left([CF_{Solar}, CF_{Wind}, CF_{Electrolyser}]\right)} \tag{3.8}$$

$$C_w = [C_{Solar,w}, C_{Wind,w}, C_{Electrolyser,w}] = (1-w)\,\frac{[C_{Solar}, C_{Wind}, C_{Electrolyser}]}{max\left([C_{Solar}, C_{Wind}, C_{Electrolyser}]\right)} \tag{3.9}$$

The optimisation problem has two classes of decision variables. The first class consists of three variables: the component size variables $S_{Solar}, S_{Wind}, S_{Electrolyser}$ that represent the capacity in MW of the solar plant, wind farm and electrolyser respectively. The second class consists of as many decision variables as there are time steps in the solar and wind power yield data set, in this research 26280 hours. These variables are denoted as p_t, with t corresponding to the hour. These decision variables describe the power level of the electrolyser in the corresponding hour.

$$S = [S_{Solar}, S_{Wind}, S_{Electrolyser}] \tag{3.10}$$

The objective function is defined in Equation 3.11. The objective is to minimise the sum of the sizes of all components, multiplied with the cost and carbon constants.

$$min. \sum^{c} (S_c * (CF_{w,c} + C_{w,c})) \qquad c \in \{Solar, Wind, Electrolyser\} \tag{3.11}$$

Constraints

The decision space of the optimisation problem is restricted by several constraints. The first constraint, Equation 3.12, guarantees that the electrolyser produces enough hydrogen during the year. It is assumed that the power level of the electrolyser stays constant during that hour, therefore it is possible to sum the power level in MW up to the energy requirements in $[MWh]$, as calculated in Equation 3.1.

$$\sum_{t=1}^{26280} p_t = E_{req} \tag{3.12}$$

The second constraint, Equation 3.13 ensures that the power level p_t of the electrolyser never exceeds the total power produced. $P_{Solar,t}$ and $Pwind, t$ express the power a 1MW installation yields at hour t at the examined location.

$$S_{Solar} * P_{Solar,t} + S_{Wind} * P_{Wind,t} - p_t \geq 0 \quad \forall t \in [1, \ldots, 26280] \tag{3.13}$$

The final constraint, Equation 3.14 has two effect. In the first place, it makes sure that the power level of the electrolyser never exceeds its maximum capacity, $S_{Electrolyser}$. At the same time, the constraints makes sure that the electrolyser is sized such that it can accommodate the highest power level.

$$S_{Electrolyser} - p_t \geq 0 \quad \forall t \in [1, \ldots, 26280] \tag{3.14}$$

Equations 3.11, 3.12, 3.13 and 3.14 form the optimisation problem. This problem is solved in python, using the PuLP module, which in turn uses the CBC solver. This solving algorithm utilises the Branch-and-cut algorithm. Before the results can be presented, first they need some post-processing. This is explained in the next section.

3.2.4. Post processing

There are four post-processing steps in the model. First the electrolyser limits are introduced, then size-independent carbon footprint components are added , and finaly the size-independent cost components are introduced.

A proper simulation of electrolyser operation must include electrolyser limits. While it is possible to include this in the optimisation problem, this would require introducing more constraints and more than double the amount of optimisation variables. All in all, this means a significant increase in computing power and time. When running without these extra constraints and variables, only 0.5 - 1% of the chosen power levels lie lower than 10% the production capacity limit. This only happens for the alkaline electrolyser, as the PEM electrolyser has no lower production limit. Because of the limited effect on results, but large effect upon performance, the electrolyser limits are introduced after the optimisation is solved.

The limits are introduced using the following post-processing steps:

1. Identify power levels p_t, that lie below the 10% production limit of the electrolyser.
2. Redefine all power levels lower than the production limit to 0 $[MW]$.
3. Sum up the new power levels to get the total used energy.
4. Scale up the wind, solar and electrolyser sizes such that the used energy equates to the required energy.

Secondly, the size-independent carbon components are introduced. These components are the carbon footprint associated with the feedstock, KOH, and cooling water. As the feedstock and cooling are related to the total produced amount of hydrogen, and not the component sizing, it is computationally more efficient to introduce them afterwards.

Lastly, the size-independent cost components are introduced. The main component added, are the costs of the stacks. The total stack costs can be calculated separately from the sizing of the electrolyser. This seems counter intuitive, but it holds true. Every stack has a certain lifetime, expressed in full-load hours, after which it must be replaced. As can be seen in Table 2.5, this is 95000 hours per stack for AWE and 75000 hours per stack for PEM. Using Equation 3.15 the total amount of stacks per year can be calculated. The annual hydrogen production $M_{H_2required}$ in $[ton/yr]$ is multiplied by the power consumption of the electrolyser pc_e in $[MWh/ton]$, and this is divided by the electrolyser capacity S_E

in $[[MW]]$. When further dividing this by the lifetime of the stack $[hours/stack]$, you get the amount of stacks per year $N_{stacks,j}$. The costs of one stack is given in Equation 3.16. By combining both equations, the size of the electrolyser can be dropped, resulting in an annual cost contribution of the stacks, as can be seen in Equation 3.17. The final step is calculating the Net Present Cost equivalent of the stack contribution to the total project, this is shown in Equation 3.18.

$$N_{stacks,annual} = \frac{M_{H_2required} * pc_e}{S_E} * \frac{1}{lifetime_{stack}} \tag{3.15}$$

$$C_{stack} = 0.3 * C_{electrolyser,MW} * S_E \tag{3.16}$$

$$C_{stacks,j} = \frac{M_{H_2required} * c_{pc}}{lifetime_{stack}} * 0.3 * C_{electrolyser,MW} \qquad \forall j \in [1, \ldots, n] \tag{3.17}$$

$$NPC_{stacks} = \sum_{j=1}^{n} \frac{C_{stacks,j}}{((1+r)^j} \tag{3.18}$$

After the post-processing step the results are done, the

Key takeaways Optimisation model

- A front between the cost-optimal configuration and the carbon-optimal configuration is constructed, through iteration on the optimisation. During the iteration, the applied weight factor is changed from 0.0 to 1.0.
- Weight factor w = 0.0 results in the configuration being optimised solely based on minimisation of costs.
- Weight factor w = 1.0 results in the configuration being optimised solely based on minimisation of carbon emissions.

3.2.5. Summary of assumptions

All scientific models are simplifications of reality, and therefore contain inherent assumptions. The most important assumptions are displayed below, sorted in three categories: Energy, Operation and Economics & Environment.

Energy

- The only reviewed energy resources are wind and solar energy.
- The number of wind turbines in a wind farm are off influence to the carbon footprint, due to wake effects. To keep the optimisation linear, this number is set to 125 of onshore and 67 for offshore. This number results in a wind farm of 1 GW.
- When there is an abundance of renewable power, more than the electrolyser can use, the excess energy is curtailed and thus does not contribute to the business case.
- The operational profile of the 8MW wind turbine from https://globalwindatlas.info/ is linearly scaled to 16 MW to acquire the 16 MW operational profile.

Operation

- A maximum electrolyser operating capacity of 100% is assumed, even though PEM electrolysers can temporary scale up to 160%. Operating for a long time at this regime results in faster degradation and is therefore excluded.
- Although production limits are regarded, there are no planned down times or other operational limitations.
- Ramp rates of the electrolyser and compressors are not taken into account, as they are below the time step size present in the weather data.
- Performance degradation of the several components are not taken into account.

Economics & Environment

- Salvage value for all components amount to ten percent of initial investment costs, in line with the assumptions of the United States Department of Energy.
- Costs of used area are not included.
- Assets that have not reached the end of their economic life at the end of the project, will be sold at a percentage of the CAPEX, equivalent to the percentage of the economic lifetime that is left.
- Interest rates on possible debt or equity are outside of the economic scope of this research.
- Operation and Maintenance is assumed to be a constant fraction of the total investment.
- The costs and carbon footprint of feed stock and cooling only represent the costs and footprint of the water consumed.
- External costs (financial representation of potential social or climate damage) are not taken into account.
- The costs used for different components is equal for the different locations. In reality these values will differ.

3.3. Sensitivity analysis

In order to further understand the influence of several aspects of the optimisation, a sensitivity analysis is performed. The biggest cost components are varied, as well as the biggest contributors towards the total carbon footprint. The variations are given in Table 3.8. The low and high scenarios for wind, PV and electrolysers are chosen in line with the future forecasts of IRENA. For the costs of solar PV this results in a 40% variation [29]. The sensitivity for wind is based on the spread of potential installation cost per kw as presented in the IRENA future outlook on wind [30]. The cost variation of the electrolysers is based on a similar report, but for hydrogen production[31], in this same report the range for the power consumption can be found. For the Carbon Footprint variation of 20 % is selected. The discount rates are varied in line with sensitivity analyses performed by RHDHV.

Table 3.8: Sensitivity variables.

Solar PV	**low**	**base**	**high**	**unit**
CDTE [29]	327	545	763	$\$/kW$
CI(G)S [29]	180	300	420	$\$/kW$
Mono c-Si [29]	270	450	630	$\$/kW$
Solar CF	80	100	120	%
Wind				
Onshore [30]	800	1075	1350	$\$/kW$
Offshore [30]	1700	2450	3200	$\$/kW$
Wind CF [30]	80	100	120	%
Electrolyser				
AWE costs [31]	540	900	1260	$\$/kW$
PEM costs [31]	840	1400	1960	$\$/kW$
Electrolyser CF	80	100	120	%
AWE Power consumption [31]	50	64	78	$kWh/kg\ H_2$
PEM Power consumption [31]	50	66.5	83	$kWh/kg\ H_2$
General economics				
Discount rate	3	6	9	%

4

Results and Discussion

In this chapter the results will be presented and discussed. First the results of the optimisation are presented in section 4.1, a base case is defined and used to explain the different charts. The base case will act as benchmark to compare all different scenarios to. First the different regions will be discussed, followed by the different electrolyser scenarios. Then the different PV technologies are discussed. The results section is concluded with a discussion about the effects of implementing carbon pricing or tax credits. The chapter is concluded with the discussion of the sensitivity analysis in section 4.4.

4.1. Results: base case

In this first section, a base case is selected to function as a benchmark against the other scenarios that are run on the optimisation model. The base case for this research is hydrogen production through an Alkaline electrolyser (AWE), using Mono-crystalline Silicon PV modules in the region of Duqm in the Sultanate of Oman. Mono c-Si cells are selected, because this PV technology dominates the current global production capacity according to the IEA [25]. Another requirement for good result comparison is a sound understanding of the method and the data visualisation. For every scenario, the optimisation is run 50 times with varying weight factors, as discussed in subsection 3.2.3. Weight factor 0.0, results in a single-objective cost minimisation, whereas at a weight factor of 1.0 the costs are completely ignored in favor of the CF. A weight factor of 0.5 would mean that the Carbon Footprint of the design is just as important as the Levelised Cost of Hydrogen. The weight factor is therefore a representation of a moral incentive to reduce carbon footprint.

The data is visualised through four charts. The first chart is displayed in Figure 4.1 and can be used to compare the CF and LCOH performance of the different weight factors. The second type of chart shows the distribution of the Levelised Cost of Hydrogen as function of the weight factor in the form of a stacked bar chart. The installed capacities of the solar, wind and electrolyser are plotted on top of this, this can be seen in Figure 4.2. The third type of chart, Figure 4.3, is similar to the second type, with the difference that this chart displays the carbon footprint distribution. The charts of Figures 4.2 and 4.3 can be used to inspect the build-up of the LCOH and CF of the different weight factors more detailed. The fourth type of chart is shown in Figure 4.4. It displays the year-round power profile for three different weight factors. In this chart the production regime, the generation and the curtailment of the system can be seen. First the Pareto front will be discussed.

A Pareto-front is a phenomenon in multi-objective optimisation. It is a collection of points that represents the trade-off between the different objectives. Along the front, improvement of one objective, leads to a decreased performance of the other objective. The different points that make up the front in this report, are the results for the different weight factors. The Pareto-front of the base case is displayed in Figure 4.1. The first thing to notice, is that this figure does not conform to the definition of a Pareto-front. The jump at CF=3.5 $kg\ CO_2e/kg\ H_2$ in this graph is a result of the post-processing step. Up to weight-factor 0.02 there is no installed wind capacity, after which the installed wind capacity starts to rise. There is a sharp increase in LCOH, due to the up-scaling of the installed capacities in the post-processing step (subsection 3.2.4), which is necessary to make the optimisation computational lighter. Note that this only happens for AWE scenarios, and is no issue for the further analysis of the results.

The Pareto front can be read as follows. When increasing the weight factor from 0.0 to 1.0, the points move up from the bottom right corner, where the LCOH is low, to the top left, where the CF is low. For the sake of analysing the results, four points are defined, and marked in Figure 4.1.

1. **Cost-optimal point:** This is the solution with the lowest LCOH. This solution is the result of applying w = 0.0.
2. **Carbon-optimal point:** This is the solution with the lowest carbon footprint, following the application of w = 1.0.
3. **Cost-elbow:** This point lies at roughly the same LCOH as the cost-optimal point, but with a reduced carbon footprint. The cost-elbow w = 0.3 where the carbon footprint is equal to 2.6 $kg\ CO_2e/kg\ H_2$. Here the jump at w = 0.02 is ignored.
4. **Carbon-elbow:** This point lies at roughly the same CF as the carbon optimal point, but with a reduced LCOH. This point can be found at w = 0.66 at an LCOH of 2.68 $\$/kg\ H_2$.

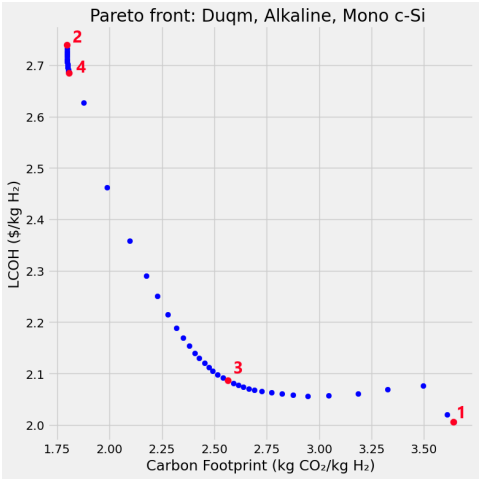

Figure 4.1: Pareto front - Duqm, Alkaline, Mono c-Si. This graph displays the LCOH and CF performance of the scenarios for different weight factors. The numbers correspond to the defined points.

The dense regions of the Pareto front, indicate very little change of KPI's, despite the change of the weight factor. The region between the carbon-elbow and carbon-optimal point are an example of this. The changing weight factor pushes the configuration towards the lowest possible carbon footprint, resulting in an insignificant decrease of carbon (0.01 $kg\ CO_2e/kg\ H_2$) at a relative high cost increase (0.06 $\$/kg\ H_2$) . There is no point in further improving the carbon footprint beyond the carbon-elbow. On the right side of the curve, there is a more effective plateau. Between weight factor 0.04 and 0.3, the LCOH increases by 0.005 $\$/kg\ H_2$, while the Carbon Footprint reduces by 0.9 $kg\ CO_2e/kg\ H_2$. This is a significant decrease of carbon at an insignificant increase of LCOH. This Pareto front shows that good all-round performing configurations are ignored when performing a single-objective optimisation towards either costs or carbon.
The second chart is shown in Figure 4.2, and displays the change in levelised cost and installed capacity as a function of the weight factor. The weight factor is displayed on the x-axis, from no carbon optimisation at the left hand side, towards no cost optimisation at the right hand side. The LCOH is displayed on the primary y-axis. The stacked bar chart corresponds to this axis, displaying the cost contributions of the three main components, the solar, wind and electrolyser systems. In Appendix C the precise distribution per factor can be seen. The PV and Wind costs consist of the CAPEX and O&M costs. The Electrolyser costs consist of the CAPEX, O&M and the stack, compressor, feedstock and cooling costs. On the secondary y-axis the total installed capacity is displayed. The lines in the chart indicate the installed solar, wind and electrolyser capacity for all different weight factors.

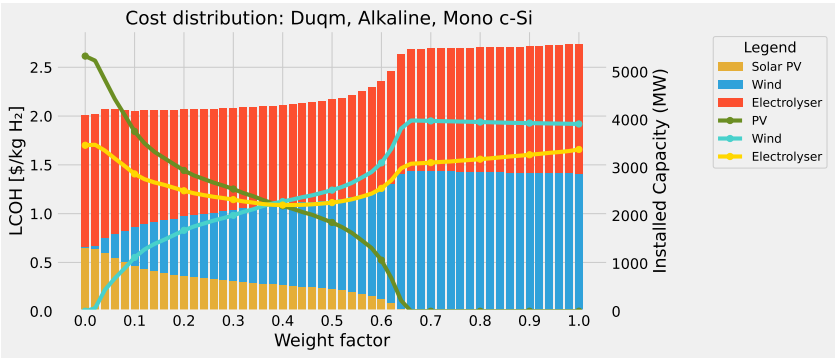

Figure 4.2: Levelised Cost of Hydrogen - Duqm, Alkaline, Mono c-Si. The LCOH (primary y-axis, stacked bar) and installed capacity (secondary y-axis, line graph) plotted against the weight factor.

Figure 4.2 clearly displays the price imbalance between solar and wind energy. At w = 0.4 solar and wind have an equal installed capacity, but the costs of installed wind are double that of the solar capacity. It is good to note that although the capacities are equal, the energy supplied for the production of hydrogen is not equal, as 1 MW of wind capacity annually yields 24% more energy than 1 MW of PV capacity. The electrolyser makes up 67% of the costs at w = 0.0, this is reduced to 48% wat w = 1.0. The absolute contribution is relatively stable, reducing by 3 cents towards the carbon-optimal point at 1.32 $\$/kg\ H_2$. The plateaus between the optimal points and the elbows that were mentioned when discussing the Pareto front, are clearly distinguishable. The difference between the cost and carbon plateau are clear. At the carbon plateau, starting from w = 0.68, the configuration barely changes, resulting in no significant decrease of CF related to an LCOH increase of 0.06 $\$/kg\ H_2$. While at the cost plateau between w = 0.04 and w = 0.3, the configuration of the production chain does change. The effects of these changes become clear when looking at the next chart.

The third chart is shown in Figure 4.3. This chart is similar to the previous chart, except it shows the Carbon Footprint instead of the Levelised Cost of Hydrogen on the primary y-axis. The 0.9 $kg\ CO_2e/kg\ H_2$ CF reduction achieved at the cost plateau between w = 0.04 - 0.3 is clear in this graph. This Figure displays how big the influence of the chosen energy source is on the overall carbon footprint. The Mono c-Si Solar panels are clearly more polluting than the onshore wind turbine. The installed electrolyser, wind and PV capacity are approximately the same at w = 0.4, but PV makes up 57% of the Carbon Footprint, with wind and the electrolyser contributing 37% and 6% respectively. The carbon footprint of the electrolyser and its operation matter little compared to the energy footprint.

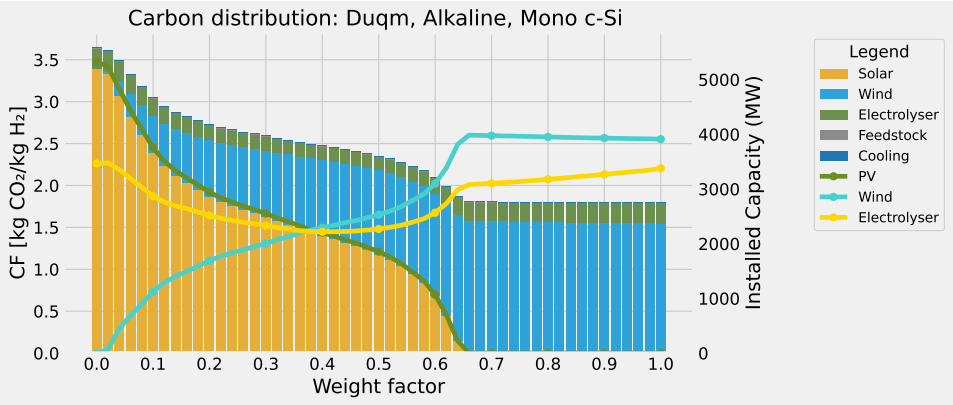

Figure 4.3: Carbon Footprint - Duqm, Alkaline, Mono c-Si. The CF (primary y-axis, stacked bar) and installed capacity (secondary y-axis, line graph) plotted against the weight factor.

Figures 4.2 and 4.3 can be read by following the curve of the yellow line, representing the installed electrolyser capacity. The way the sizing of the components changes with the weight factor follows a standard curve for most scenarios. Four distinct regions in the curve can be identified.

1. w = [0.0, ...,0.2] – The size of the electrolyser reduces, as the capacities of the wind and solar installations are equalised. The electrolyser can be sized down, as the energy mix is diversified and the effect of intermittency is reduced. The CF reduces quickly.
2. w = [0.2, ...,0.54] – The electrolyser capacity remains relatively constant while the solar energy gets gradually exchanged for more wind energy. The CF reduces slowly.
3. w = [0.54, ...,0.66] – The wind capacity is scaled up, while the solar capacity reduction is sped up. The electrolyser capacity experiences a rapid scale up as well. This can be understood when looking at the weather profile of Duqm, presented in Figure 2.13. Wind energy has a lower CF than solar energy, but the potential for wind energy in Duqm lies predominantly in the summer, while being largely inactive during the other seasons. The electrolyser needs to be sized up, as the bulk of the hydrogen has to be produced in a relative short period. The wind capacity is significantly increased to be able to supply enough energy during those producing summer months, and the electrolyser must follow to ensure adequate production. The CF decreases quickly.
4. w = [0.66, ..., 1.0] – The wind capacity is reduced, while the electrolyser is sized up. The CF does not decrease much by this action, but overall less energy gets curtailed. This can be clearly seen in the next chart.

The fourth chart displays the operating regime of the electrolyser, the generated power and the curtailed power. A section of the year can be seen in Figure 4.4. The blue line represents the generated power. This is the sum of solar and wind power that is installed at that specific weight factor. The red line is the power that is being consumed by the electrolyser. The yellow line represents the curtailed power. This is the difference between the blue and the red line. One of the first observations is that as the focus shifts from cost optimisation to carbon footprint optimisation, the curtailment significantly declines. In the most cost optimal solution (w = 0.0) the curtailment is equal to 13.7% of the energy required for hydrogen production. At w = 0.4 this is reduced to 7.5% and at the carbon optimal solution (w = 1.0) it is down to 3.6%. The diurnal pattern of the solar energy is clearly observed in the pattern of the power generation at w = 0.0. This leads to a lot of downtime in the system operations, thereby requiring an over-sizing of the electrolyser and PV capacity in order to harness enough power to produce the required amount of hydrogen. In the middle scenario, with w = 0.4, the electrolyser is smallest, indicated by the maximum height of the electrolyser power. Here it is shown that through the mix of wind and solar, the effects of intermittency are reduced, requiring a lower electrolyser capacity.

Figure 4.4: Production profiles - Duqm, Alkaline, Mono c-Si. The power generation (blue), electrolyser power consumption (red) and curtailed power (yellow) for every hour between March and June are displayed for weight factors 0.0, 0.4 and 1.0.

4.2. Results: regions and electrolysers

In section 4.1 the scenario of Mono c-Si PV, with Alkaline electrolysis in Duqm was explored. In this section, six variations on this scenario will be covered in this chapter. In Figure 4.5 these six variations of the base case are presented. In this figure the Pareto fronts for both PEM and AWE in Duqm (Oman), Groningen (the Netherlands) and Dakhla (Western Sahara) are displayed. First the regional effects will be discussed, followed by the effects of electrolyser choice. The detailed LCOH and CF charts for the different scenarios can be found in Appendix C, but the results will be discussed below.

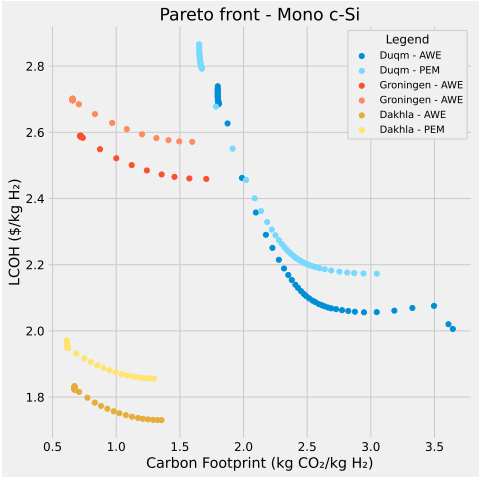

Figure 4.5: Pareto fronts - Mono c-Si with PEM & Alkaline for all regions. This graph displays the LCOH and CF performance of the scenarios for different weight factors.

Of the different regions, production in Dakhla performs best on both Carbon Footprint and Levelised Cost of Hydrogen. The difference between the cost- and carbon-optimal solution is the biggest in the region of Duqm. The main difference between Duqm and the other two regions, is that the wind potential is low for the biggest part of the year. This can be seen in the weather profiles in section 2.6 and the total annual yields per MW in Table 3.6.

Despite the lower wind yield, the production in Duqm also switches completely to wind energy, when applying a high enough weight factor. To harness enough power, 50 and 80% extra wind capacity is required when compared to Dakhla and Groningen respectively. This difference can be observed by comparing the installed wind capacity in Figure 4.3 with the installed capacities for the Dakhla and Groningen scenarios. The Dakhla scenario can be seen in Figure 4.6, the charts displaying the results of Groningen is presented in Figure C.11 in the appendix. For both Groningen and Dakhla the amount of wind energy is already high at w = 0, requiring only a weight factor of 0.2 for Groningen and 0.3 for Dakhla before the entire energy mix is switched to wind. What this implies is that there is less of an incentive required to switch completely over to wind energy.

Judging by Figure 4.5 and Figure 4.6, it can be said that Dakhla is the optimal production location when using Mono c-Si, both in terms of costs and Carbon Footprint. However, this does not disqualify hydrogen production in the other locations. Even the worst solution in terms of Carbon Footprint, the cost-optimal solution in Duqm, is 5 $kg\ CO_2e/kg\ H_2$ lower than the CF of blue hydrogen and 7.6 kg $kg\ CO_2e/kg\ H_2$ lower than the CF of grey hydrogen, at 8.6 and 11.24 $kg\ CO_2e/kg\ H_2$ respectively. A substantiation of the grey and blue carbon footprints is given in section A.3. The overall LCOH of these results is low, being near the global range of grey and blue hydrogen, with an LCOH of 0.98-2.93 $\$/kg\ H_2$ for grey and 1.80-4.68 $\$/kg\ H_2$ for blue hydrogen [38].

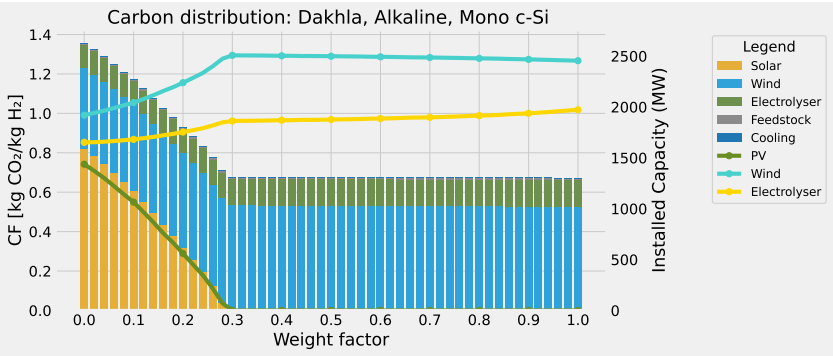

Figure 4.6: Carbon Footprint - Dakhla, Alkaline, Mono c-Si. The CF (primary y-axis, stacked bar) and installed capacity (secondary y-axis, line graph) plotted against the weight factor.

The difference in performance between the two electrolyser types is clear in Figure 4.5, with the scenarios using PEM having a higher LCOH. In Dakhla and Groningen the entire Pareto front moves up without intersecting the AWE scenario. In Duqm there is an intersection, at a high weight factor. The

relative movement of the PEM Pareto fronts is mainly dictated by three effects.

1. **CAPEX:** The CAPEX of the PEM electrolyser is 1400 $\$/kW$, 56% higher than the 900 $\$/kW$ for the AWE electrolyser, which increases the LCOH.
2. **Stacks:** The PEM stack lifetime is 75000 hours per stack, versus the 95000 hours per stack of AWE. This leads to more stack replacements over the project lifetime, contributing towards a higher LCOH.
3. **Power consumption:** The only effect that positively influences the LCOH for PEM, is its lower power consumption. Because the power consumption of PEM is only 2% lower (see Table 2.5), this effect is not enough to negate the previous two effects. This effect does improve the carbon footprint, most notably in Duqm, as this location is more dependant on the more carbon intensive PV energy.

The increased price of the PEM electrolyser, leads in Duqm to the inclusion of wind from the w = 0.0. By comparing Figure 4.7 and Figure 4.2 the difference is clear. The inclusion of wind energy reduces the effect of intermittency and increases electrolyser utilisation, resulting in a smaller electrolyser. The size of the electrolyser can also be lowered due to the lower power consumption. At the lower weight factors the inclusion of wind leads to a higher LCOH, but at the high weight factors, there are PEM configuration that perform better than their AWE counterparts. This happens only in Duqm however at high weight factors.

Overall it can be concluded that production through PEM electrolysis is more expensive most of the time, and offers little Carbon Footprint improvement. PEM offers a better performance in terms of flexibility, but the time resolution used in this research of 1 hour is too low to reflect this. Based on these results, hydrogen production though Alkaline electrolysis should be preferred.

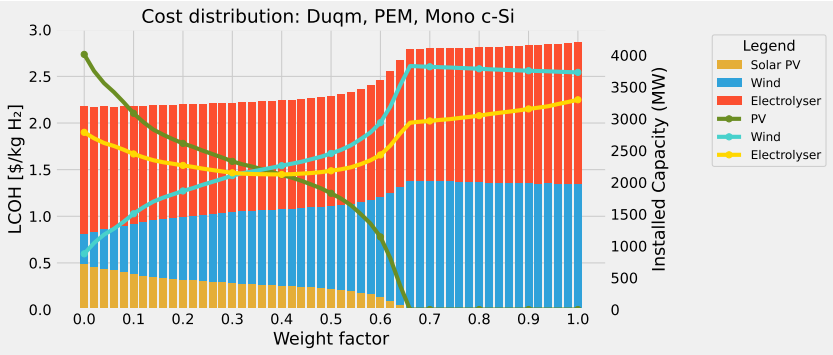

Figure 4.7: Levelised Cost of Hydrogen - Duqm, PEM, Mono c-Si. The LCOH (primary y-axis, stacked bar) and installed capacity (secondary y-axis, line graph) plotted against the weight factor.

4.3. Results: PV modules

In the previous section the performance of PEM and AWE were explored for the different regions. In this section the performance of the different PV types is studied. The Pareto fronts for the different PV types for all regions are plotted in Figure 4.8. Looking at this Figure, it is clear that all Pareto fronts of a country near approximately the same point at w = 1.0. This is because increasing the weight factor up to w = 1.0 results in nearly all configurations relying solely on wind energy. The case that stands out the most, is hydrogen production in Duqm using CdTe PV technology. This scenario does not approach the same LCOH and CF as the other PV technologies in Duqm at higher weight factors. This case is discussed in subsection 4.3.1.

Production in Duqm again displays different behaviour compared to the other regions. Groningen and Dakhla display very similar behaviour, resulting in Pareto fronts with

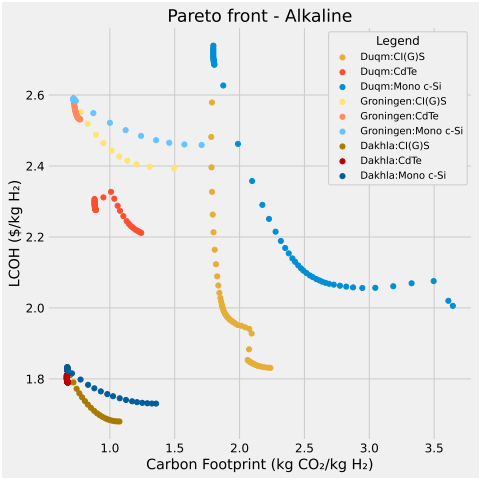

Figure 4.8: Pareto fronts - Alkaline per PV type and region. This graph displays the LCOH and CF performance of the scenarios for different weight factors.

similar shapes for all PV types. There is however, a large difference LCOH. The CdTe technology performs best in terms of carbon footprint. It is good to note that the lower carbon footprint is caused by two characteristics of CdTe technology. The technology has a low carbon footprint per MW installed, but it is also more expensive than other technologies. This gives incentive to install more wind in the w = 0.0 scenario, resulting in a lower Carbon Footprint. The best performing PV technology is CI(G)S. The closer a Pareto front is to the origin of the graph, the better it performs on both KPI's. Therefore it can be said that CI(G)S PV technology delivers the best all round performance.

The scenarios with CI(G)S technology result in a lower LCOH than their counterparts, and a relatively low Carbon Footprint. The CF and LCOH for CI(G)S in Duqm are shown in Figures 4.9 and 4.10 respectively. The way the components change size as a result of the changing weight factor, is similar to that of Mono c-Si. A key difference being that wind only enters the configuration after a weight factor of 0.28 is applied. The incentive to switch to wind is apparently lower. This is can be explained by the fact that the carbon footprint of CI(G)S is only 2 $kg\ CO_2/MWh$ higher than the Carbon Footprint of onshore wind. The LCOE and CF of energy are indicators for the performance of the different scenarios. The CF and LCOE for the different technologies and regions are calculated and presented in Table 4.1.

As mentioned before, the point of the Pareto front that is closest to the origin of the graph, is the best performing scenario. By the same logic it can be said that the instance of a scenario closest to the origin, is the best all-round performing configuration for that scenario. To further inspect these best performers, these configurations are presented in Table 4.2. These points are found by calculating the distance to the origin from every point, and selecting the smallest distance. The weight factor, together with the corresponding LCOH, carbon footprint, percentage of PV with respect to the total capacity, percentage PV to the total generated energy, the percentage of energy that is curtailed and the total contributions of the energy mix towards the LCOH and CF are displayed in the table.

Table 4.1: Levelised Cost of Energy and Carbon Footprint for the different energy resources and locations.

	LCOE	**CF**
Duqm	$\$/MWh$	$kg\ CO_2/MWh$
CdTe	47.12	11.13
CI(G)S	24.72	31.79
Mono c-Si	33.25	57.25
Onshore	78.72	28.79
Groningen		
CdTe	74.57	17.52
CI(G)S	39.13	50.06
Mono c-Si	52.62	90.15
Offshore	38.79	10.37
Dakhla		
CdTe	47.17	10.03
CI(G)S	24.75	28.66
Mono c-Si	33.28	51.61
Onshore	48.14	7.15

The consistent wind profiles of Dakhla and Groningen are reflected by PV energy making up less than 20% of the energy in the system. In Duqm an average of 65% of installed capacity and 61% of the used energy comes from PV. Not only is the percentage of PV higher in the system for Duqm, the total system capacity is also 1.9 times bigger on average. This over-sizing is required because of two reasons. The first reason, is that PV has a lower yield per MW, relative to wind. And second, a system with a high PV percentage must deal with intermittency more. The same amount of energy must be generated in less time.

The PV capacity column of Table 4.2 shows that there is a stronger preference for wind energy when working with Mono c-Si than with other PV technologies. Even in Duqm, where CI(G)S and CdTe are preferred over wind, Mono c-Si makes up only 26 % of the total energy capacity in the all-round performing configuration. This behaviour is logical, as its CF is much higher than that of the other technologies, and at the same time not being cheap.

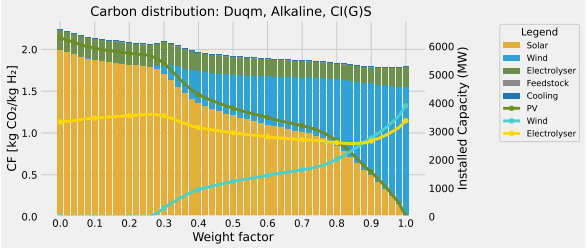

Figure 4.9: Carbon Footprint - Duqm, Alkaline, CI(G)S. The CF (primary y-axis, stacked bar) and installed capacity (secondary y-axis, line graph) plotted against the weight factor.

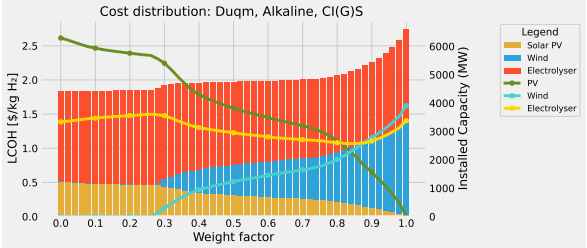

Figure 4.10: Levelised Cost of Hydrogen - Duqm, Alkaline, CI(G)S. The LCOH (primary y-axis, stacked bar) and installed capacity (secondary y-axis, line graph) plotted against the weight factor.

The last two columns of the table show that the energy supply is the biggest influence on the Carbon Footprint of the produced hydrogen, while being on par with the electrolyser towards the build up of the LCOH. Because the energy contributes to half of the LCOH, and contributes the vast majority of the CF, it can be said that the selected energy source is the most influential on the overall performance of the hydrogen production chain.

Table 4.2: Characteristics of the all-round best performing configurations of every scenario.

Duqm	w (-)	CF $kg\ CO_2/kg\ H_2$	LCOH $\$/kg\ H_2$	Total installed capacity (MW)	PV Capacity (%)	PV Energy (%)	Curtailment (%)	Energy (% of LCOH)	Energy (% of CF)
CdTe	0.30	0.89	2.28	5984	100	100	9.2	38.8	70.3
CI(G)S	0.64	1.88	1.99	4905	69	61	6.6	41.8	89.1
Mono c-Si	0.60	2.1	2.36	4166	26	22	6.3	53.1	91.0
Groningen									
CdTe	0.08	0.76	2.53	2848	39	12	4.7	66.8	81.8
CI(G)S	0.12	0.95	2.46	2713	35	11	4.4	63.0	85.4
Mono c-Si	0.24	0.72	2.59	1963	0	0	3.3	63.4	79.4
Dakhla									
CdTe	0.00	0.68	1.79	3121	32	17	7.9	51.2	81.0
CI(G)S	0.26	0.81	1.74	2922	25	13	6.7	49.1	83.6
Mono c-Si	0.30	0.68	1.82	2507	0	0	6	49.7	79.2

4.3.1. CdTe in Duqm

The use of CadmiumTelluride PV modules in Duqm presents a special case, because this is the only scenario where the Carbon Footprint of PV energy is lower than that of wind. Because of this, wind energy is phased out instead of PV, with the increase of the weight factor. By weight factor 0.3, the wind is completely phased out. The CF contributions and component sizing can be observed in Figure 4.12. The LCOH can be found in the Appendix in Figure C.6.

In Figure 4.11 it is evident that the shape of this Pareto-front is different. It can't truly be called a Pareto front, as there are clearly solutions that perform worse on both KPI's than the neighbouring points. Because of the introduction of the electrolyser limits after the optimisation, non-optimal solutions are chosen.

Something that differentiates the CdTe case from the other cases for Duqm, is that the cost-optimal point and carbon-optimal have a very narrow LCOH range of 0.10 $\$/kg\ H_2$. This is due to the quick elimination of wind energy, and the near-stagnation phase after w = 0.3.

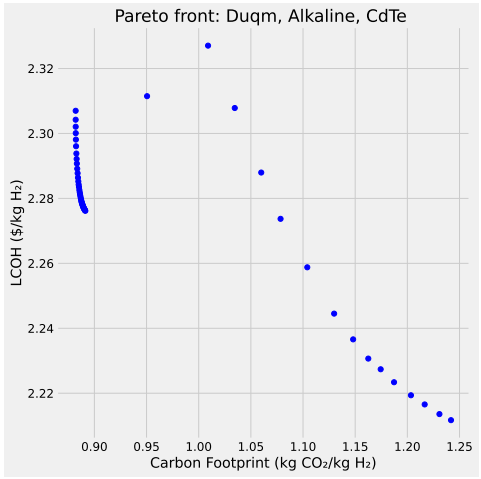

Figure 4.11: Pareto fronts - Duqm, Alkaline, CdTe. This graph displays the LCOH and CF performance of the scenario for different weight factors.

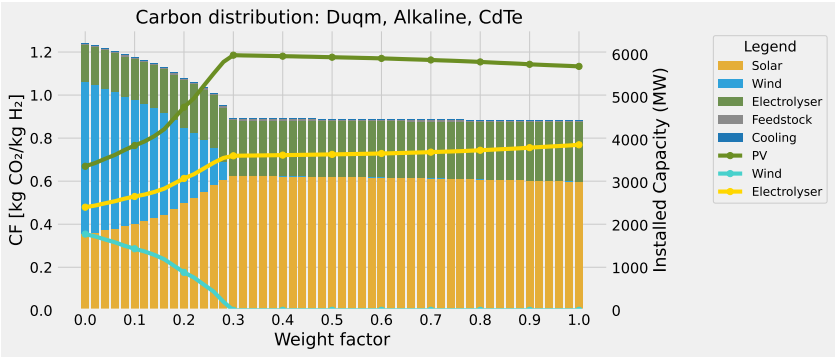

Figure 4.12: Carbon Footprint - Duqm, Alkaline, CdTe. The CF (primary y-axis, stacked bar) and installed capacity (secondary y-axis, line graph) plotted against the weight factor.

4.3.2. Carbon price

Up to this point, a weight factor was introduced to incentivise the model to choose a lower carbon configuration. The weight factor can be seen as a moral or theoretic incentive, showing what production chain designs are possible. In reality, it is unlikely that industry moves towards a more expensive option by itself, just because it would entail less carbon emissions. There needs to be a cost incentive as well. In this subsection the weight factor is removed, and is replaced by cycling from carbon price 0 $\$/ton\ CO_2$, up to 500 $\$/ton\ CO_2$. Note that a carbon price of 500 $\$/ton\ CO_2$ is 555% of the current ETS carbon price, as at time of writing, the price is 90 $\$/ton\ CO_2$ [13]. At the end of the subsection the effects of a tax scheme instead of a carbon price are discussed.

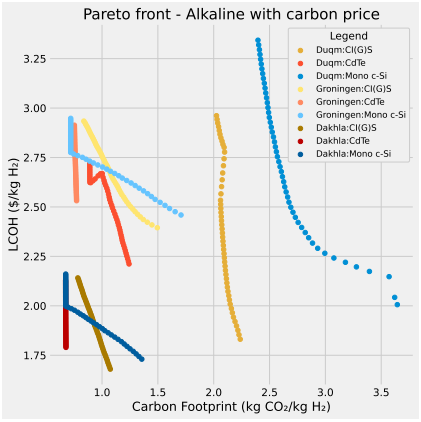

Figure 4.13: Pareto fronts - Alkaline, for all PV types and regions with a carbon price. This graph displays the LCOH and CF performance of the scenarios for different carbon prices.

In Figure 4.13 the effect of the carbon pricing is displayed for all regions and PV types, several aspects change in comparison to the corresponding chart with weight factors (Figure 4.8). In Duqm, the carbon-optimal point of the Pareto front lies at a higher Carbon Footprint, and at the same time has a higher LCOH. The increase in LCOH is due to the inclusion of the carbon price in the LCOH. This price must be included, as a carbon price would be paid by the off taker in the end. Another insight from this chart, is that the theoretical carbon-optimal points illustrated in Figure 4.8 are very unlikely to be constructed when this type of carbon pricing is introduced. Even at a carbon price of 500 $\$/ton\ CO_2$, a price 5.5 times higher than the current carbon price, the theoretical carbon optimal point is not within reach. This is not the case for all scenarios though, as all scenarios that move in a straight line up when approaching the 500 $\$/ton\ CO_2$, have reached the theoretical carbon-optimal point. For the Mono c-Si, Alkaline scenario of Duqm, a carbon price of 500 $\$/ton\ CO_2$ has roughly the same effect on the configuration of the production chain, as a weight factor of 0.45. The sizing of the base case for the different carbon prices is displayed in the Appendix in Figure C.39. The carbon price of 500 $\$/ton\ CO_2$ having the same effect as w = 0.45, means that even when an unrealistic high carbon price is introduced, the carbon footprint is not as important in decision making process as the production costs. Or, to phrase it differently, it is very expensive to decarbonise the production chain in Duqm.

Policies like the EU Hydrogen Bank [6] or the US Inflation Reduction Act (IRA) [21] are other ways to incentivise industry to decarbonise their production chain. Especially the IRA tax credit scheme gives a clear incentive for decarbonising the production chain, as the amount of subsidy is directly related to the lifetime carbon footprint of the produced hydrogen. The IRA works with a tax credit of $3\$/kg\ H_2$. A Carbon Footprint below 0.45 $kg\ CO_2e/kg\ H_2$ receive 100% of the 3 $\$/kg\ H_2$ tax credit, for higher Carbon Footprints the percentages are reduced step-by-step. Even the scenarios in this research with the lowest CF, do not qualify for the highest tax credit. While this credit scheme is only available in the US and thus does not apply to the test cases of this research, the effect of such a scheme is displayed in Figure 4.14. The tax credits are displayed in the graph. Especially for Duqm and Groningen, this particular tax scheme would incentivise industries to reduce their Carbon Footprint.

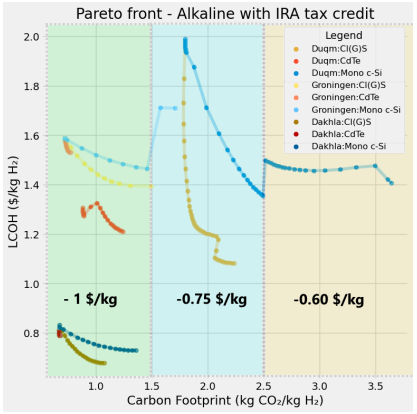

Figure 4.14: Pareto fronts - Alkaline, for all PV types and regions, corrected for IRA tax credit scheme indicated by the colored areas. This graph displays the LCOH and CF performance of the scenarios for different weight factors.

The height of the tax credits might be too high. The cost difference in Groningen and Dakhla between the cost-optimal (w = 0.0) and carbon-optimal (w = 1.0) points is less than 0.20 $\$/kg\ H_2$. A tax credit reflecting this difference should be enough for the purpose of incentivising low-carbon production. This suggests that the tax credit is mainly meant to strengthen its competitive position. To determine what financial tools would work best to incentives clean hydrogen production is a study on its self, and will not be discussed further.

4.4. Sensitivity analysis

The main results of the optimisation have been discussed in this chapter. In this section, the sensitivity analysis is presented. The robustness of the solutions and the influence of the different factors can be better understood when applying a variation. First the general results of the sensitivity are discussed, before moving on to the discussion of the most influential factors.

The values presented in Table 3.8 are applied to the model, the results of which are summarised in Figure 4.15. The left hand side shows the effect on the Carbon Footprint and the right hand side the effect on the Levelised Cost of Hydrogen. For all factors a low scenario and a high scenario are run, representing either a decrease or increase of said variable. The low scenario is illustrated by a blue bar, the high scenario as a red bar. The results for weight factors 0.0 and 1.0 are presented, as these extreme points are affected the most. The 0.0 results are represented by the darker shade bars, the 1.0 scenarios are represented by the lighter shade. Figure 4.15 shows that the variation of the power consumption and the costs have the most influence on the optimisation. This is due to two reasons. First, the applied sensitivity range for these two factors is the biggest. Second, these factors have a big influence on the end result. The sensitivity of the carbon footprint and the interest rate will not be further discussed, because of the relatively small and one-sided effect of the variations on the LCOH and the CF.

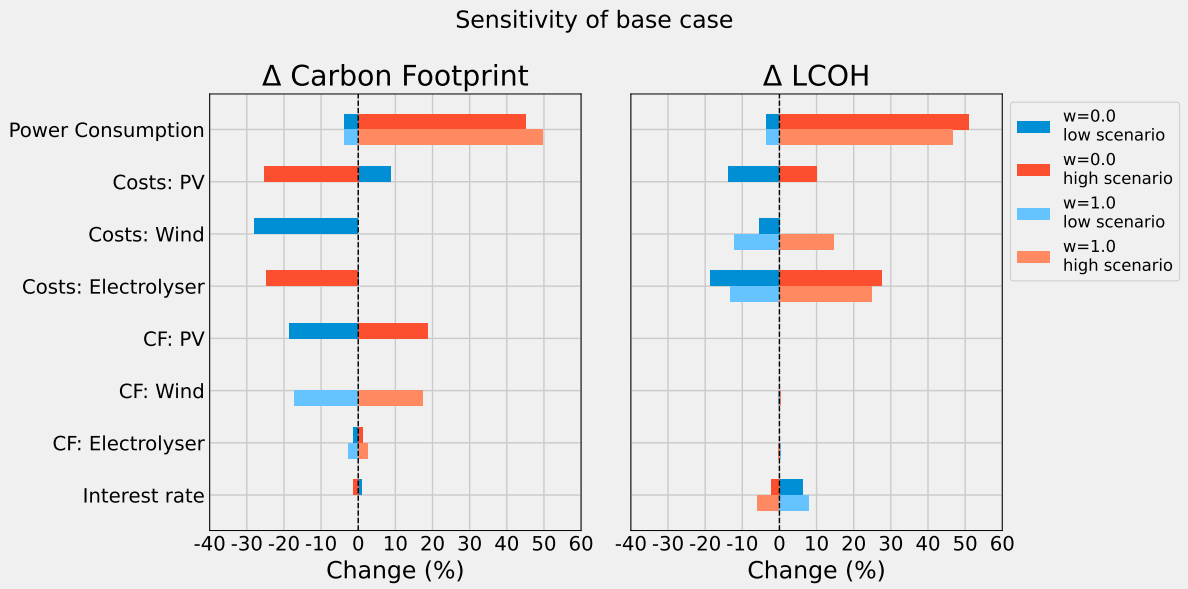

Figure 4.15: Tornado chart - Effect of sensitivity analysis. On the y-axis the sensitivity categories are presented. On the x-axis the effects of the high and low scenarios (red and blue) in percentage change for w = 0.0 and w = 1.0 (dark and light) configurations are plotted. The left pane describes the effect on the Carbon Footprint, the right pane describes the effect on the Levelised Cost of Hydrogen.

First the cost sensitivity will be discussed in section 4.5, followed by the sensitivity of the electrolyser power consumption section 4.6. The different scenarios are coded in sake of brevity. The cost denoted as 'C', followed by the first letter of the effected component and whether it is scaled up (+) or down (-). The low scenario of solar costs is therefore denoted as 'CS-', the high scenario of electrolyser costs is 'CE+'. For the sensitivity of the power consumption of the electrolyser the codes 'PC+' and 'PC-' are used.

4.5. Costs sensitivity

In this subsection the influence of lower and higher investment costs is investigated. The influence of the varied costs is shown for the base case of Duqm with an Alkaline electrolyser and Mono c-Si panels in Figure 4.16. As could be expected, the Carbon Footprint of the w = 1.0 carbon-optimal point is the same for all cases, as the costs don't influence this configuration. The most significant changes, happen in the cost-optimal point.

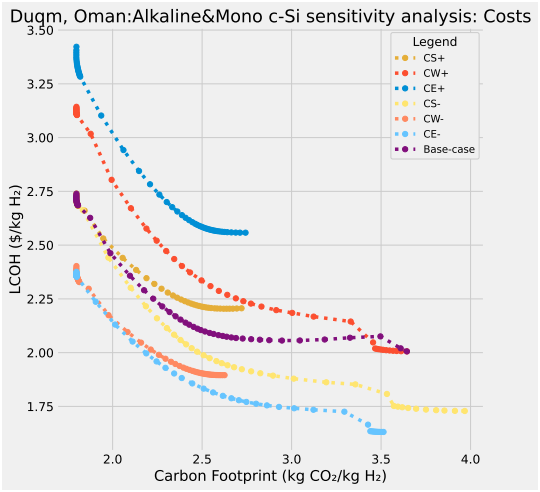

Figure 4.16: Pareto fronts - Duqm, Alkaline, Mono c-Si with costs variations. This graph displays the LCOH and CF performance of the scenarios for different weight factors.

The low solar scenario (CS-) is the only scenario where the carbon performance decreases. A lower solar price means that it becomes cheaper to over-size the energy system. This does not have to mean that a decreasing solar price would actually result in a higher-carbon hydrogen. In Figure 4.16 a plateau is shown at an LCOH of 1.75 $\$/kg\ H_2$, with the end of the plateau having a comparable CF as the base case at w = 0.0. The low wind (CW-) and high electrolyser and solar scenarios (CE+ and CS+) show a significant CF improvement of roughly 30%. This is because of the higher share of wind energy in the initial configuration. For the solar and wind scenarios this is because wind becomes a more attractive options due to the relative cost reduction of wind. In the high electrolyser scenario the need for intermittency mitigation rises, resulting in a higher initial wind capacity.

Inspection of the configuration of the production chains after applying the sensitivity analyses, reveals that the same behavioral pattern of the system can be observed as mentioned at the begin of this chapter in section 4.1. What changes is that the different regions are shifted. Comparing the low wind scenario, in Figure 4.17, to the base case in Figure 4.3, it looks like the sizing curve is moved forwards. Starting half way of phasing out the solar capacity. The phase out is not sped up however, with PV energy being present up to w = 0.66, just like in the base case. This can be expected as the costs are varied in this section, and at w = 0.66 the costs begin to play a smaller role. The LCOH of the low electrolyser scenario is displayed in Figure 4.18. By decreasing the electrolyser price, the standard curve is moved backwards. The weight factor at which wind is introduced, is postponed. The Carbon Footprint is lower than in the base scenario, Figure 4.2, because the initial installed capacity of solar energy is lower. The solar capacity is lower, because it is cheaper to over-size the electrolyser in this case, enabling the configuration to harness more energy from the peak solar yield hours of the year. In the base case the electrolyser makes up 67% of the total LCOH. A reduction of 40% would lead to an overall price decrease of 12%. However, the LCOH actually decreases by 18.5%, due to the described effect of over-sizing.

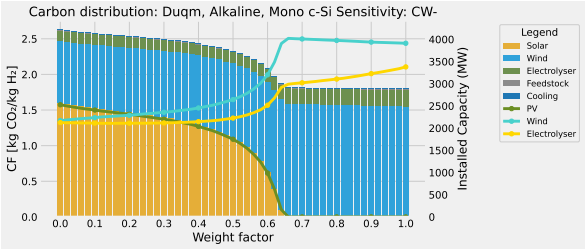

Figure 4.17: Carbon Footprint - Low wind cost scenario for Duqm, Alkaline, Mono c-Si. The CF (primary y-axis, stacked bar) and installed capacity (secondary y-axis, line graph) plotted against the weight factor.

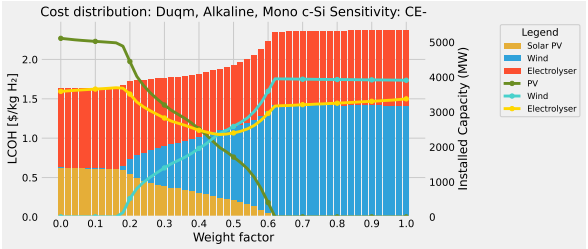

Figure 4.18: Levelised Cost of Hydrogen - Low Electrolyser cost scenario for Duqm, Alkaline, Mono c-Si. The LCOH (primary y-axis, stacked bar) and installed capacity (secondary y-axis, line graph) plotted against the weight factor.

4.6. Power consumption sensitivity

The Pareto fronts for the power consumption sensitivity analysis are illustrated in Figure 4.19. The power consumption has a profound influence on the production chain. As mentioned before, energy is the determining factor in terms of cost and carbon footprint. Reducing the required energy per kg of hydrogen can therefore reduce both cost and carbon emissions. The CF and LCOH reduction as a result of a power consumption decrease is clearly demonstrated in this chart. As mentioned in section 4.3, the closer a front is to the origin, the better it performs. In this chart it can be observed that lowering the power consumption scales the entire front down, moving the fronts towards the origin. Bringing down this power consumption will have a big effect on the feasibility and carbon footprint of hydrogen production. The power consumption values used in this research are taken from the 1 GW facility design presented by Program [47]. Although it is stated in the paper that the power consumption represents the energy use of the entire production facility. Other reports, like the report of IRENA [31] where the sensitivity data originates from, show higher values. The energy use of the entire production facility is an important metric, as it is a major influence on both the LCOH and the CF.

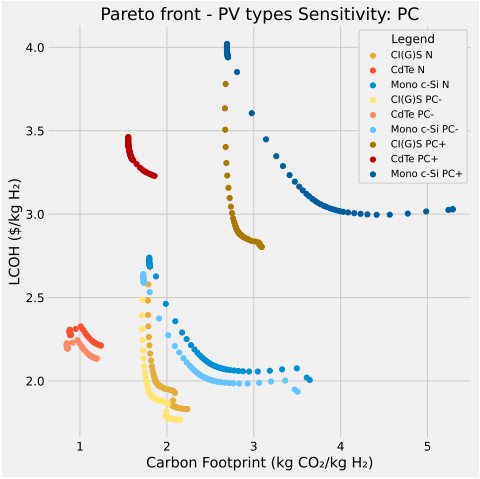

Figure 4.19: Pareto fronts - Duqm, Alkaline, Mono c-Si with variation in power consumption. This graph displays the LCOH and CF performance of the scenarios for different weight factors. The dark shaded represent the high scenarios, the lighter shades represent the low scenarios.

4.7. Summary of results

In this chapter the results of the optimisation model have been discussed. The effects of different design choices and prioritising between LCOH and CF have been explored. The most important findings are summarised in the text box below.

Key takeaways results

- **Regions:** Dakhla is the best performing region on both CF and LCOH. Production in Groningen leads to a lower CF than in Duqm, but has a higher LCOH.
- **Weather:** Consistent wind reduces the CF. Consistent solar PV reduces the LCOH.
- **Electrolysers:** The use of AWE instead of PEM, leads to a lower LCOH. The CF is barely influenced by the choice of electrolyser.
- **PV modules:** The use of CdTe results in the lowest CF, but also in a higher LCOH. CI(G)S is all-round the best choice.
- **Design choice:** The choice for the energy source has the biggest influence on both the LCOH and CF. The energy source contributes on average 53% towards the LCOH, and 82% towards the CF.
- **Impact:** For most scenarios, a tangible carbon reduction can be realised at minor cost increase.
- **Hydrogen alternatives:** Green hydrogen has the potential to become cost-competitive with blue and grey hydrogen. The CF of green hydrogen for all production regions and pathways outperforms that of blue and grey.
- **Financial incentives:** A carbon price provides limited incentive to decarbonise. The IRA tax credits show more potential, and even could be too high.
- **Technical improvement:** A reduction of the power consumption of electrolysers results in LCOH and CF improvement.

5

Conclusions and recommendations

5.1. Conclusions

The aim of this report was to shed light on two major challenges of green hydrogen production: the cost-competitiveness compared to grey an blue hydrogen, and the Carbon Footprint. The research was structured around the following research question:

> "What is the influence of local weather patterns on the design of large-scale green hydrogen production chains, when optimised for a low 'Levelised Cost of Hydrogen' and 'Carbon Footprint' on a cradle-to-gate basis"

To answer this question, it was subdivided into three subquestions, each highlighting a different part of the question. In the following paragraphs these subquestions will be answered.

What components of the green hydrogen production chain influence the Levelised Cost of Hydrogen and Carbon Footprint the most? The most influential factor to both the Carbon Footprint and the Levelised Cost of Hydrogen, is the selected energy source. In Figure 4.8 the performance of the different PV type scenarios are illustrated. The selection of PV type dictates the shape of the Pareto fronts. The difference between the cost-optimal and carbon-optimal points of the Pareto fronts is dictated by the wind-solar ratio of the configuration. Table 4.2 the contribution of the energy resources towards the total LCOH and CF is shown. The contribution of the energy resources is location dependant. In Duqm the energy resources make up 44.6% of the LCOH and 83.5% of the CF, averaged over the different energy scenarios. The energy resources in Groningen contribute on average 64.4% of the LCOH and 82.2% of the Carbon Footprint. In Dakhla the mean contributions are 50% of the LCOH and 81.3% of the Carbon Footprint. The electrolyser has a significant contribution towards the cost, but less so for the Carbon Footprint. This is clearly illustrated in Figure 4.5. The choice of electrolyser has a smaller influence on the overall system performance than the choice of energy source.

What are the most important system design choices that influence the trade-off between Levelised Cost of Hydrogen and Carbon Footprint? The trade-off between producing green hydrogen with a low Levelised Cost of Hydrogen or a low Carbon Footprint is influenced by multiple design choices. The most influential design choice is the constitution of the energy mix. This is best observed when looking at how the CF and LCOH change as the PV slowly gets phased out in favor of wind energy in Figure 4.2 and Figure 4.3. In general, solar energy is cheaper, and wind energy is less polluting. This statement is heavily influenced by the production location however, as both the Levelised Costs and Carbon Footprint are dependant on the yield of the installed energy systems. The associated costs and emissions of the energy sources are a direct influence on the trade-off, but there is also an indirect effect. Through proper energy mix constitution, intermittency can be reduced, resulting in a lower required electrolyser capacity. Depending on the selected energy sources, this can result in a lower overall carbon footprint. The second important design choice, is the selection of the used PV

technology. CdTe PV modules are more expensive than the other considered PV technologies, but the overall lifetime emissions of this technology are significantly smaller, in Duqm being even carbon friendlier than wind energy. The best all-round performance is delivered by scenarios including the CI(G)S PV technology, resulting a lower Levelised Cost than a system with CdTe, but a higher Carbon Footprint. Mono c-Si performs worst, in terms of LCOH and CF. The results of this research, show no tangible trade-off effect, but rather a clear preference coupled to the electrolyser choice. In Figure 4.5 the choice for PEM displays a significant increase of the LCOH, but barely any effect on the CF.

The trade-off effects here are solely based on LCOH and CF. Including other factors, such as critical raw material use, or available global production capacity can also influence the choice a project developer has to make.

What influence do weather patterns have on Levelised Cost of Hydrogen and Carbon Footprint? Weather patterns have a profound influence on both the Levelised Cost of Hydrogen and the Carbon Footprint. The Carbon Footprint of hydrogen is for an average of 80 % dependant on the used renewable energy source. The Carbon Footprint of energy sources is largely dependant on the potential yield of the installations. A side-by-side review of the energy yields per location from Table 3.6, the CF equations 2.1 and 2.2 and the LCOE and CF of energy from Table 4.1 sketches a clear picture. Solar irradiance and wind speeds are an influential indicators for the performance of production locations. Not only is the average wind speed or irradiance of importance, the consistency of this energy supply has a big influence as well. The ideal configuration of the production chain in Dakhla has a significantly smaller total installed capacity than the ideal configuration in Duqm, where there is no consistent wind. Groningen lacks consistent solar yields, but this is compensated by the potential of the wind. The lack of consistent wind speeds also influences the difference in LCOH between the cost-optimal solution and the carbon-optimal solution, as is the case in Duqm. The availability of consistent and strong winds, leads to a lower Carbon Footprint, whereas the availability of consistent and high solar irradiance leads to a lower Levelised Cost of Hydrogen. Dakhla being the prime example where both are the case.

Coming back to the overarching research question, the following can be concluded. Local Weather patterns significantly influence the design of large-scale green hydrogen production chain when optimising for a low Carbon Footprint and a low Levelised Cost of Hydrogen. The local weather patterns, both solar and wind, dictate the Carbon Footprint and LCOE of the renewable energy that is available on-site. This matters, as the renewable energy source is the biggest contributor towards the LCOH and CF of hydrogen. When optimising for a Low Levelised Cost of Hydrogen, abundant sun is required. When optimising for a low Carbon Footprint, abundant wind energy is required. When desiring both a low Levelised Cost of Hydrogen and an low Carbon Footprint, abundant and consistent solar and wind energy is required. The intensity of the available solar and wind makes a project viable, but the consistency of these patterns make a project feasible.

All in all, it is clear that the Carbon Footprint of hydrogen is a very important topic. With annual hydrogen demand ramping up to 100 Mton per year by next decade, shown in Figure 1.1, Carbon Footprints of 3 $kg\ CO_2/kg\ H_2$ will not be good enough. The results of this research show that the Carbon Footprint of hydrogen can be influenced significantly by properly sizing the energy system, and selecting the right PV technology. Government action is required here, as carbon pricing and green subsidies can break the cost-carbon trade-off by providing the financial incentives for industries to design a lower carbon production chain. The topic of the hydrogen Carbon Footprint must be on the agenda of all hydrogen project developers, to reach the global climate goals. *Net zero by 2050*.

5.2. Recommendations for future research

There are many topics that should be researched, that can contribute to the understanding and reduction of the LCOH and CF of hydrogen. In this section a selection of future research recommendations is given.

Include Off-taker in model: This research focuses on the cradle-to-gate LCOH and CF. In reality there are many cost and carbon contributing activities between the production of hydrogen and the actual off-taker. Therefore the optimisation model of this report can be improved by expanding the scope to cradle-to-grave. This includes the hydrogen carrier selection, storage, transportation and end use of the hydrogen. The Levelised Cost of Hydrogen and the Carbon Footprint of a scenario, will be completely different if the hydrogen is used as methanol in Seoul or as ammonia in Rotterdam.

Include Process simulation in the model: Improving the level of detail of the production process modelling will improve the validity of the model. The model in this research is based on the energy balance between generation and consumption. Including process efficiencies, component degradation and bottlenecks of the processes will deliver more realistic results. To correctly model the ramping rate of the electrolyser, a weather data-set with a higher temporal resolution should be used to study the operational dynamics and its effect on the carbon footprint and cost-effectiveness. Using a data-set with a 10 minute interval would be enough to distinguish the dynamics of the PEM and AWE electrolysers.

Improve optimisation model: In this research a simple single-objective Linear Programming model is used. Using a Mixed-Integer Non-Linear Programming optimisation will improve the quality and capabilities of the model. Using this optimisation method will eliminate the need for the post-processing steps and enables the inclusion of power control strategies and financial incentivising tools.

Expand scenarios: To further improve this research, more regions and energy sources can be included in the model. Solar and wind are widely available, but there are plenty of regions where hydro energy, or any other renewable energy source would be a good addition to the energy mix. The inclusion of more energy options will improve the quality of the design choices. The model is built, such that new regions can be included within 10 minutes. The set-up of the model is such that new technologies could be added within a few hours.

Project economics: In this research the Net Present Cost method is chosen to assess the financial aspects of hydrogen production. The NPC represents what funds must be collected and saved up before the start of the project, to accommodate all costs during the project lifetime. This is not the most realistic financial representation. A more elaborate method of project economics can be implemented that includes the effects of equity and debt, future cash flows and loan payments.

More Life Cycle Assessments: More renewable hydrogen LCA's have to be performed in order to understand the carbon footprint of hydrogen better. The focus should be on identifying what components contribute the most, and what areas can be improved. Preferably these LCA's need to be performed for multiple regions and production pathways in order to identify the cleanest path. Current hydrogen production processes must be investigated, as well as the projects that are planned for the coming years.

While the focus of this research was on the carbon footprint of the hydrogen production pathways, this is only one of a wide range of environmental impact categories. An important impact category, is the depletion of critical raw materials, especially for PEM electrolysers. Next to the environmental impact, the social and economic impacts should also be investigated in order to sketch a complete picture.

Study effects carbon pricing or green subsidies: The effectiveness and social fairness of different financial incentivising tools must be researched. The topic of carbon pricing and green tax schemes is briefly mentioned. The results show that a financial regulatory tools are required for industries to choose lower carbon production methods. What tools could be implemented? Can you let industries

pay for embodied carbon emissions? How do you roll out a global carbon pricing system? These and more questions should be answered.

Possible synergies: The best all-round performing configurations resulted in energy curtailments between 3-9%. This is a large quantity of energy that potentially could be used elsewhere. Investigating what can be done with this energy is not only good in terms of the environment, it is also good for the potential business case as it can bring in another cash flow. Possible off-takers could be adjacent industry or desalination plants for drinking water or agriculture.

Sustainable Energy Technology Improvement: Aside from recommendations related to the research performed for this report, there are a few recommendations of a more fundamental technical nature. Further development of the characteristics of the renewable energy sources and the electrolyser will result in lower carbon and cheaper hydrogen. Improvement of these technologies is essential for a future widespread roll-out. Reducing power consumption of the electrolyser and reducing costs and Carbon Footprint of renewable energy should be the focus.

References

[1] A. Ajanovic, M. Sayer, and R. Haas. “The economics and the environmental benignity of different colors of hydrogen”. In: *International Journal of Hydrogen Energy* 47 (57 July 2022), pp. 24136–24154. ISSN: 03603199. DOI: 10.1016/j.ijhydene.2022.02.094.

[2] Kay Bareiß et al. “Life cycle assessment of hydrogen from proton exchange membrane water electrolysis in future energy systems”. In: *Applied Energy* 237 (Mar. 2019), pp. 862–872. ISSN: 03062619. DOI: 10.1016/j.apenergy.2019.01.001.

[3] Christian Bauer et al. “On the climate impacts of blue hydrogen production”. In: *Sustainable Energy and Fuels* 6 (1 Jan. 2022), pp. 66–75. ISSN: 23984902. DOI: 10.1039/d1se01508g.

[4] Joyce H.C. Bosmans, Louise C. Dammeier, and Mark A.J. Huijbregts. “Greenhouse gas footprints of utility-scale photovoltaic facilities at the global scale”. In: *Environmental Research Letters* 16 (9 Sept. 2021). ISSN: 17489326. DOI: 10.1088/1748-9326/ac1df9.

[5] Ulf Bossel and Baldur Eliasson. *Energy Hydrogen Economy*.

[6] CLIMA C2. *Upcoming EU Hydrogen Bank Pilot Auction: European Commission publishes terms amp; conditions*. Aug. 2023. URL: https://climate.ec.europa.eu/news-your-voice/news/upcoming-eu-hydrogen-bank-pilot-auction-european-commission-publishes-terms-conditions-2023-08-30_en (visited on 09/30/2023).

[7] Aruna Chandrasekar and Brittany Westlake. *Modeling the flexible operation of electrolysers for hydrogen production in a low-carbon energy system*. EPRI, 2022. URL: https://us-regen-docs.epri.com..

[8] CICE et al. *Carbon Intensity of Hydrogen Production Methods Supporting the BC Hydrogen Strategy*. 2023.

[9] Rosemary Colciaghi et al. “Levelized cost of water assessment for small-scale desalination plant based on forward osmosis process”. In: *Energy Conversion and Management* 271 (Nov. 2022). ISSN: 01968904. DOI: 10.1016/j.enconman.2022.116336.

[10] Frazer-Nash Consultancy. “fugitive hydrogen emissions future hydrogen economy”. In: ().

[11] Pablo K. Cornejo et al. “Carbon footprint of water reuse and desalination: A review of greenhouse gas emissions and estimation tools”. In: *Journal of Water Reuse and Desalination* 4 (4 2014), pp. 238–252. ISSN: 22201319. DOI: 10.2166/wrd.2014.058.

[12] Louise Christine Dammeier, Joyce H.C. Bosmans, and Mark A.J. Huijbregts. “Variability in greenhouse gas footprints of the global wind farm fleet”. In: *Journal of Industrial Ecology* 27 (1 Feb. 2023), pp. 272–282. ISSN: 15309290. DOI: 10.1111/jiec.13325.

[13] Ember. *Carbon price tracker*. Sept. 2023. URL: https://ember-climate.org/data/data-tools/carbon-price-viewer/ (visited on 09/30/2023).

[14] US Department of Energy. *Assumptions and ground rules*. URL: https://www.hydrogen.energy.gov/h2a_prod_rules.html (visited on 08/23/2023).

[15] M. A. Fazal and Saeed Rubaiee. “Progress of PV cell technology: Feasibility of building materials, cost, performance, and stability”. In: *Solar Energy* 258 (July 2023), pp. 203–219. ISSN: 0038092X. DOI: 10.1016/j.solener.2023.04.066.

[16] Ulrik Frohlke. *TOPSOE to build world’s largest electrolyzer manufacturing facility to accelerate power-to-X capacity*. Feb. 2023. URL: https://www.topsoe.com/press-releases/worlds-largest-electrolyzer-production-facility.

[17] Helena Gaspars-Wieloch. “Project Net Present Value estimation under uncertainty”. In: *Central European Journal of Operations Research* 27 (1 Mar. 2019), pp. 179–197. ISSN: 16139178. DOI: 10.1007/s10100-017-0500-0.

[18] Niklas Gerloff. “Comparative Life-Cycle-Assessment analysis of three major water electrolysis technologies while applying various energy scenarios for a greener hydrogen production”. In: *Journal of Energy Storage* 43 (Nov. 2021). ISSN: 2352152X. DOI: 10.1016/j.est.2021.102759.

[19] Samane Ghandehariun and Amit Kumar. “Life cycle assessment of wind-based hydrogen production in Western Canada”. In: *International Journal of Hydrogen Energy* 41 (22 June 2016), pp. 9696–9704. ISSN: 03603199. DOI: 10.1016/j.ijhydene.2016.04.077.

[20] Jürgen Friedrich Hake et al. “Towards a Life Cycle Sustainability Assessment of Alkaline Water Electrolysis”. In: *Energy Procedia* 105 (2017), pp. 3403–3410. ISSN: 18766102. DOI: 10.1016/j.egypro.2017.03.779.

[21] Siri Hedreen. *Ira at 1: Hydrogen developers hold off construction, ramp up lobbying*. Aug. 2023. URL: https://www.spglobal.com/marketintelligence/en/news-insights/latest-news-headlines/ira-at-1-hydrogen-developers-hold-off-construction-ramp-up-lobbying-76810758 (visited on 09/30/2023).

[22] Robert W. Howarth and Mark Z. Jacobson. “How green is blue hydrogen?” In: *Energy Science & Engineering* 9.10 (2021), pp. 1676–1687. DOI: https://doi.org/10.1002/ese3.956. eprint: https://onlinelibrary.wiley.com/doi/pdf/10.1002/ese3.956. URL: https://onlinelibrary.wiley.com/doi/abs/10.1002/ese3.956.

[23] Hydrom. URL: https://hydrom.om/AboutAuctions.aspx?cms=iQRpheuphYtJ6pyXUGiNqgnTvLaOi%2FEP (visited on 08/23/2023).

[24] IEA. *Electrolysers - Tracking*. URL: https://www.iea.org/energy-system/low-emission-fuels/electrolysers#tracking (visited on 08/23/2023).

[25] IEA. *Solar tracking*. URL: https://www.iea.org/energy-system/renewables/solar-pv (visited on 08/23/2023).

[26] IEA. *The Future of Hydrogen*. URL: https://iea.blob.core.windows.net/assets/9e3a3493-b9a6-4b7d-b499-7ca48e357561/The_Future_of_Hydrogen.pdf.

[27] IEA. *Utility-scale PV investment cost structure by component and by commodity breakdown*. URL: https://www.iea.org/data-and-statistics/charts/utility-scale-pv-investment-cost-structure-by-%20component-and-by-commodity-breakdown (visited on 08/23/2023).

[28] IEA. *Wind*. URL: https://www.iea.org/energy-system/renewables/wind#tracking (visited on 08/23/2023).

[29] The International Renewable Energy Agency IRENA. *Future of solar photovoltaic : deployment, investment, technology, grid integration and socio-economic aspects*, p. 72. ISBN: 9789292601560.

[30] The International Renewable Energy Agency IRENA. *Future of wind : deployment, investment, technology, grid integration and socio-economic aspects*. 2019, p. 87. ISBN: 9789292601553.

[31] The International Renewable Energy Agency IRENA. *Green Hydrogen Cost Reduction - Scaling up hydrogen to meet the 1.5 ° C Climate Goal*. 2020. ISBN: 9789292602956. URL: www.irena.org/publications.

[32] The International Renewable Energy Agency IRENA. *Renewable power generation costs in 2021*. 2022. ISBN: 978-92-9260-452-3. URL: www.irena.org.

[33] The International Renewable Energy Agency IRENA. *World Energy Transitions Outlook 2023: 1.5°C Pathway; Preview*. 2023. ISBN: 9789292605278. URL: www.irena.org.

[34] Melinda MJ de Jonge et al. *Life cycle carbon efficiency of Direct Air Capture systems with strong hydroxide sorbents*, pp. 1–17.

[35] Joaquim Juez-Larré et al. “A detailed comparative performance study of underground storage of natural gas and hydrogen in the Netherlands”. In: *International Journal of Hydrogen Energy* (2023). ISSN: 03603199. DOI: 10.1016/j.ijhydene.2023.03.347.

[36] M A Khan et al. “The Techno-Economics of Hydrogen Compression”. In: *TRANSITION ACCELERATOR TECHNICAL BRIEFS* 1 (2021), pp. 1–36. ISSN: 2564-1379. URL: www.transitionaccelerator.ca.

[37] Andrej Lotrič et al. “Life-cycle assessment of hydrogen technologies with the focus on EU critical raw materials and end-of-life strategies”. In: *International Journal of Hydrogen Energy* 46 (16 Mar. 2021), pp. 10143–10160. ISSN: 03603199. DOI: 10.1016/j.ijhydene.2020.06.190.

[38] Polly Martin. *Blue hydrogen cheaper than Green H2 in all markets except China amid falling gas prices: BNEF*. July 2023. URL: https://www.hydrogeninsight.com/production/blue-hydrogen-cheaper-than-green-h2-in-all-markets-except-china-amid-falling-gas-prices-bnef/2-1-1486049 (visited on 08/25/2023).

[39] H. Scott Matthews, Chris T. Hendrickson, and H. Deanna Matthews. *Life Cycle Assessment: Quantitative Approaches for Decisions That Matter-lcatextbook.com 2*. 2014. URL: https://www.lcatextbook.com/.

[40] F M Mulder. “Implications of diurnal and seasonal variations in renewable energy generation for large scale energy storage”. In: *J. Renewable Sustainable Energy* 6 (2014), p. 33105. DOI: 10.1063/1.4874845. URL: http://dx.doi.org/10.1063/1.4874845].

[41] Richard Müller et al. *Surface Solar Radiation Data Set - Heliosat (SARAH) - Edition 1*. 2015. DOI: 10.5676/EUM_SAF_CM/SARAH/V001. URL: http://wui.cmsaf.eu/safira/action/viewDoiDetails?acronym=SARAH_V001.

[42] Nick Ni and Xu Liu. *Hydrogen storage solution for an intermittent energy source: Solar*. May 2020. URL: https://energydigital.com/smart-energy/hydrogen-storage-solution-intermittent-energy-source-solar.

[43] Florian Nigbur, Martin Robinius, and Patrick Wienert. *Levelised cost of hydrogen Making the application of the LCOH concept more consistent and more useful*. AGORA energiewende, July 2023. URL: www.agora-industry.org.

[44] Ilham Ourya et al. “Assessment of green hydrogen production in Morocco, using hybrid renewable sources (PV and wind)”. In: *International Journal of Hydrogen Energy* (2023). ISSN: 03603199. DOI: 10.1016/j.ijhydene.2022.12.362.

[45] Stefan Pfenninger and Iain Staffell. “Long-term patterns of European PV output using 30 years of validated hourly reanalysis and satellite data”. In: *Energy* 114 (Nov. 2016), pp. 1251–1265. ISSN: 03605442. DOI: 10.1016/j.energy.2016.08.060.

[46] Darre; Proctor. “GE Developing 18-MW Offshore Wind Turbine”. In: *Power magazine* (Mar. 2023). URL: https://www.powermag.com/ge-developing-18-mw-offshore-wind-turbine/ (visited on 08/23/2023).

[47] Hydrohub Innovation Program. *Gigawatt green hydrogen plant*. 2020. URL: https://ec.europa.eu/commission/presscorner/detail/en/ip_20_1259.

[48] PWC. *Analysing the future cost of Green Hydrogen*. URL: https://www.pwc.com/gx/en/issues/esg/the-energy-transition/analysing-future-cost-of-green-hydrogen.html (visited on 08/25/2023).

[49] PWC. *Green hydrogen economy - predicted development of tomorrow: PwC*. URL: https://www.pwc.com/gx/en/industries/energy-utilities-resources/future-energy/green-hydrogen-cost.html (visited on 08/23/2023).

[50] Amjad Al-Qahtani et al. “Uncovering the true cost of hydrogen production routes using life cycle monetisation”. In: *Applied Energy* 281 (Jan. 2021). ISSN: 03062619. DOI: 10.1016/j.apenergy.2020.115958.

[51] Michele M. Rienecker et al. “MERRA: NASA’s modern-era retrospective analysis for research and applications”. In: *Journal of Climate* 24 (14 July 2011), pp. 3624–3648. ISSN: 08948755. DOI: 10.1175/JCLI-D-11-00015.1.

[52] Jefferson A. Riera, Ricardo M. Lima, and Omar M. Knio. “A review of hydrogen production and supply chain modeling and optimization”. In: *International Journal of Hydrogen Energy* (2023). ISSN: 03603199. DOI: 10.1016/J.IJHYDENE.2022.12.242.

[53] John Kerkhovem Rob Terwell. *HyChain 2 - Cost implications of importing renewable electricity, hydrogen and hydrogen carriers into the Netherlands from a 2050 perspective*. 2019. URL: www.ispt.eu/projects/hychain..

[54] Martin Rothbart et al. *Hydrogen to deal with intermittency of renewable electricity generation*. 2020, pp. 239–251. DOI: 10.1007/978-3-658-30500-0_16.

[55] Shayan Sadeghi, Samane Ghandehariun, and Marc A. Rosen. "Comparative economic and life cycle assessment of solar-based hydrogen production for oil and gas industries". In: *Energy* 208 (Oct. 2020). ISSN: 03605442. DOI: 10.1016/j.energy.2020.118347.

[56] G. Sdanghi et al. "Review of the current technologies and performances of hydrogen compression for stationary and automotive applications". In: *Renewable and Sustainable Energy Reviews* 102 (Mar. 2019), pp. 150–170. ISSN: 18790690. DOI: 10.1016/J.RSER.2018.11.028.

[57] Seddiq Sebbahi et al. "Assessment of the three most developed water electrolysis technologies: Alkaline Water Electrolysis, Proton Exchange Membrane and Solid-Oxide Electrolysis". In: *Materials Today: Proceedings* 66 (Jan. 2022), pp. 140–145. ISSN: 2214-7853. DOI: 10.1016/J.MATPR.2022.04.264.

[58] Iain Staffell and Stefan Pfenninger. "Using bias-corrected reanalysis to simulate current and future wind power output". In: *Energy* 114 (Nov. 2016), pp. 1224–1239. ISSN: 03605442. DOI: 10.1016/j.energy.2016.08.068.

[59] Mohammad Reza Tahan. "Recent advances in hydrogen compressors for use in large-scale renewable energy integration". In: *International Journal of Hydrogen Energy* 47 (83 Oct. 2022), pp. 35275–35292. ISSN: 03603199. DOI: 10.1016/J.IJHYDENE.2022.08.128.

[60] The Piping Talk. Feb. 2021. URL: https://thepipingtalk.com/centrifugal-compressor-parts-their-function/ (visited on 08/23/2023).

[61] Bart W. Tuinema et al. "Modelling of large-sized electrolysers for realtime simulation and study of the possibility of frequency support by electrolysers". In: *IET Generation, Transmission and Distribution* 14 (10 May 2020), pp. 1985–1992. ISSN: 17518687. DOI: 10.1049/iet-gtd.2019.1364.

[62] Antonio Valente, Diego Iribarren, and Javier Dufour. "Harmonised life-cycle global warming impact of renewable hydrogen". In: *Journal of Cleaner Production* 149 (Apr. 2017), pp. 762–772. ISSN: 09596526. DOI: 10.1016/j.jclepro.2017.02.163.

[63] Christopher Varela, Mahmoud Mostafa, and Edwin Zondervan. "Modeling alkaline water electrolysis for power-to-x applications: A scheduling approach". In: *International Journal of Hydrogen Energy* 46 (14 Feb. 2021), pp. 9303–9313. ISSN: 03603199. DOI: 10.1016/j.ijhydene.2020.12.111.

[64] *Vecteur de Transition Énergétique et de Croissance Durable (National Hydrogen Strategy Morocco)*. URL: https://www.mem.gov.ma/Lists/Lst_rapports/Attachments/36/Feuille%20de%20route%20de%20hydrog%C3%A8ne%20vert.pdf.

[65] Francisco Vigalondo et al. "Position paper Hydrogen Valleys 2023". In: (). URL: https://heavenn.org/wp-content/uploads/2023/03/Position-paper-Hydrogen-Valleys-2023.pdf.

[66] Till Weidner, Victor Tulus, and Gonzalo Guillén-Gosálbez. "Environmental sustainability assessment of large-scale hydrogen production using prospective life cycle analysis". In: *International Journal of Hydrogen Energy* 48 (22 Mar. 2023), pp. 8310–8327. ISSN: 03603199. DOI: 10.1016/j.ijhydene.2022.11.044.

[67] Andrzej Witkowski et al. "Comprehensive analysis of hydrogen compression and pipeline transportation from thermodynamics and safety aspects". In: *Energy* 141 (Dec. 2017), pp. 2508–2518. ISSN: 03605442. DOI: 10.1016/j.energy.2017.05.141.

A

Complementary Literature

A.1. Hydrogen

Hydrogen, a colorless, odorless, and highly flammable gas has great potential as an energy carrier in the transition towards a more sustainable energy future. The use of hydrogen as an energy carrier has gained attention in recent years due to its ability to produce it from renewable sources, its potential to reduce greenhouse gas emissions and its high energy density [31]. Currently there is an annual pure hydrogen demand of 70 Mton, mainly for industry [26]. Nearly all this hydrogen is 'grey', meaning that it is produced using fossil fuels, mostly produced through a process called Steam Methane Reforming (Equation A.1) and the subsequent Water Gas Shift (WGS) reaction (Equation A.2) . The problem is that this process releases 11.89 $kg\ CO_2e/kg\ H_2$ [19].

$$CH_4 + H_2O \rightleftharpoons CO + 3H_2 \tag{A.1}$$

$$CO + H_2O \rightleftharpoons CO_2 + H_2 \tag{A.2}$$

The hydrogen that gets attention in the last years, is called 'green' hydrogen or renewable hydrogen, which is produced through water electrolysis using renewable energy resources. This reaction can be seen in Equation A.3. In this process no CO_2 or other green house gasses are emitted.

$$H_2O \rightarrow H_2 + \frac{1}{2}O_2 \tag{A.3}$$

Green Hydrogen has a big role to play in the energy system of the future, as not all current energy demand can be fulfilled by electricity. Hydrogen will play a role in energy storage, transportation, and in industrial processes such as steel and cement making [31]. There are some challenges regarding the large-scale adoption of green hydrogen, namely production costs, transport and storage. This research will focus on the emissions and on the costs.

A.2. Reciprocating vs centrifugal compressors

As mentioned before, there are two compressor types able to handle large-scale hydrogen flows. First the reciprocating compressor will be discussed and then the centrifugal compressor. Afterwards the characteristics are compared.

The reciprocating compressor, or piston-type compressor, is the most widely used compressor type. The volume is displaced in phases by the linear movement of a piston. Reciprocating compressors can be classified by different categories, dependant on the design specifications, the different types can be found in the paper of Tahan [59], here the most relevant compressor type is discussed.

Multistage double acting multiplex horizontal type reciprocating compressors are the most commonly used reciprocating compressors for large-scale application as mentioned by Tahan [59]. The compression happens in multiple stages as the compression ratio of a single compressor is limited due to an increase in temperature. The compressor being multiplex ensures a more continuous flow. The

orientation is horizontal for industrial purposes as the vertical orientation compressors are limited at 300 kW.

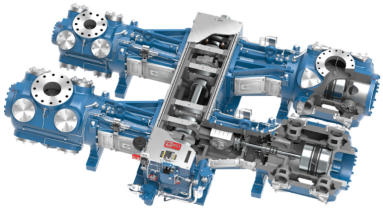

Figure A.1: large size horizontal-type reciprocating compressor [59].

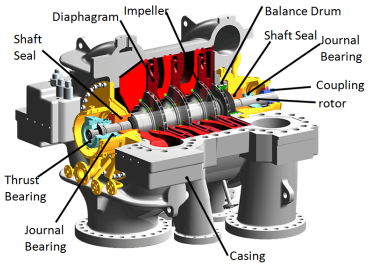

Figure A.2: Centrifugal compressor [60].

The second most used compressor is the centrifugal compressor. Pressure is built by the transfer of energy of moving impellers to the gas in the form of velocity and pressure. This energy transfer is hindered by the molecular weight of hydrogen, which is no issue for the volume displacing reciprocating compressor. For hydrogen compression barrel-type double flow compressors are best suited. This type prevents leakage when handling low molecular weight, while the double flow configuration ensures high flow rates.

Two important characteristics are the capacity and the compression rate that compressors can handle. Reciprocating compressors typically can handle flows up to $4800 Nm^3/h$, where centrifugal compressors can handle flow up to $50000 Nm^3/h$. Although the flow rate is higher, centrifugal compressor need more stages to get to high pressures as the compression ratio is limited. An advantage of centrifugal compressors over reciprocating compressors is the issue of lubrication. Lubrication with oil is not possible with hydrogen compression, because the oil would react with the hydrogen, fouling the stream. Oil-free reciprocating compressors exist, however the piston rings need frequent replacement. This is because the lack of oil causes a non-uniformity in pressure, increasing the wear and tear. Centrifugal compressors are typically oil free. A study from Witkowski et al. [67] concludes that the choice for compressor type in industry is mainly based on the capacity it must handle. For low flows of 0.2-0.5 kg/s reciprocating compressors are used. For flows of 1-2 kg/s a combination of centrifugal and reciprocating compressors are used, and for high flows of 2.8 kg/s complex eight-stage centrifugal compressors are used. Centrifugal compressor have several operational advantages over reciprocating compressors, as explained by Witkowski et al. [67]. The centrifugal compressor causes less fouling, requires less maintenance, has less leakage and needs less compressors in total as a single compressor can handle higher flow rates, reducing the overall operation costs further. A major downside is that it is not clear if the technology is ready for deployment by 2030.

Key takeaways Compressors

- Centrifugal compressors are able to handle higher flows.
- Operation costs are lower for Centrifugal Compressors.
- Reciprocating compressors are better understood and already in operation.
- This report looks at hydrogen production by 2030, and therefore centrifugal compression is selected.

A.3. Carbon Footprint hydrogen production

The carbon footprint of hydrogen depends on the production pathway. The promise of 'green' hydrogen is that it has a lower carbon footprint than 'grey' and 'blue' hydrogen. The exact carbon footprints of these production pathways are subject of debate however. In this section, several studies on the carbon footprint of the different hydrogen colors will be presented with the goal to highlight why different studies work with different values for carbon footprints.

In Figure A.3 the carbon footprint for 4 different production pathways is displayed. Yellow hydrogen is the production of hydrogen through grid electricity, in this case the average EU carbon footprint of

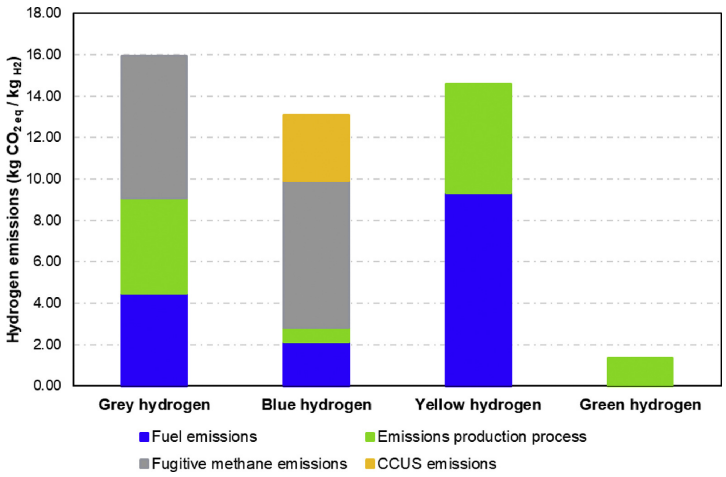

Figure A.3: Hydrogen Carbon Footprint for different production pathways[1].

electricity of 0.354 kg CO_2e per kWh is used. The emissions of blue hydrogen production are reduced by 18-25% with respect to grey hydrogen. If the hydrogen is used for the purpose of heat production, this results in 20% higher emissions than when the gas or coal would be used directly. The biggest contributor to the emissions of grey and blue hydrogen are the fugitive natural gas emissions. In this study, a relatively high carbon footprint for grey and blue hydrogen is displayed, especially compared to the green hydrogen, which has a low carbon footprint compared to other studies. This is because a relatively high methane leakage percentage of 2.54% is assumed. The actual leakage percentage varies per producing party and production location. This is further investigated by Bauer et al. [3], the results of this study are presented in Figure A.4.

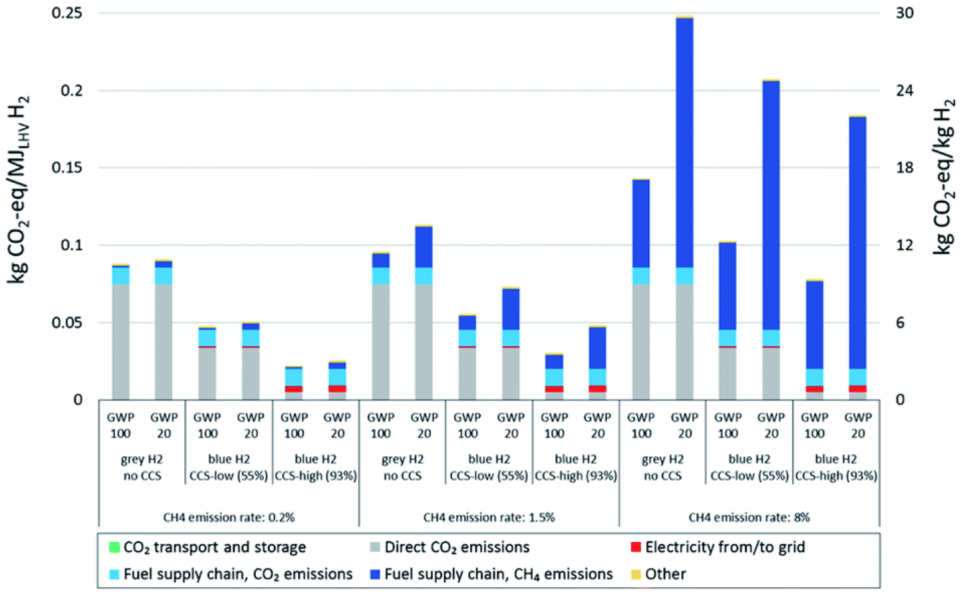

Figure A.4: Emissions associated with grey and blue hydrogen, for different CCUS capture, CH_4 emission rates and time horizons [3].

In Figure A.4 a realistic range is presented. The CO_2 capture rate of CCS is also varied between low and high capture rate scenarios, where the low scenario represents the capture rate of existing plants and the high capture rate represents possible future plants. The final variation in scenarios is the chosen time horizon, as the GWP of methane is heavily dependant on this horizon due to its short atmospheric lifetime of roughly 12 years. The carbon footprint of blue hydrogen is only in the most optimistic scenario nearing the carbon footprint of green hydrogen.

The selected project start year is also influences the overall carbon footprint. As supply chains

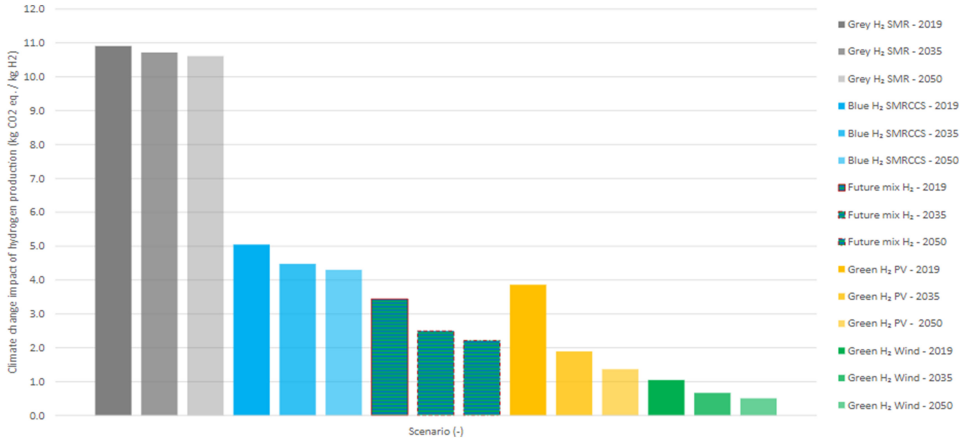

Figure A.5: Carbon footprint different production pathways at a combined capture rate of 70% over a 100-year time horizon. [66].

decarbonise through electrification and implementation of renewable power sources, the embodied emissions resulting from the production of building materials and technologies comes down. This can be seen in Figure A.5. The CH_4 leakage rate is not specified for this research, but comparing it to Figure A.4 would place it around the 1.5%.

As it is useful to compare the resulting carbon footprint of different hydrogen production pathways, for this research a carbon footprint of 11.24 $kg\ CO_2e/kg\ H_2$ is used, inline with Al-Qahtani et al. [50] and approximately the GWP 100 values of the 1.5% leakage scenario of Figure A.4. For blue hydrogen, a 55% CCS capture rate is assumed, resulting in a carbon footprint of 6.5 $kg\ CO_2e/kg\ H_2$.

Key takeaways Carbon Footprint Hydrogen production

- The scope and assumptions of an LCA heavily influence the resulting carbon footprint.
- Fugitive methane emissions are very poluting and should not be excluded when reviewing the total carbon footprint.
- Blue hydrogen is only in the most optimistic scenarios in the same carbon footprint range as green hydrogen.
- Blue hydrogen is more polluting when utilised for heat delivery than methane.
- For this report: Grey Hydrogen has a carbon footprint of **11.24** $kg\ CO_2e/kg\ H_2$, and Blue hydrogen has a carbon footprint of **6.5** $kg\ CO_2e/kg\ H_2$.

B

Methodology

B.1. Production chain modeling

Constructing the entire production chain for hydrogen requires significant investment and generates a substantial amount of carbon emissions. As a result, it is crucial to carefully consider and select the most efficient design and setup that minimises both costs and emissions. However, due to the numerous trade-offs and various factors influencing the KPI's, this can be a challenging task. This is where optimisation models can be of great use.

Optimisation models are mathematical tools that can find the optimal solution for a given problem. The problem is presented by a set of equations and constraints. In the context of hydrogen production, optimisation models can be used to identify the optimal configuration and design of a hydrogen production pathway that minimises both the cost and the carbon footprint. By using optimisation models, it is possible to evaluate the impact of different design choices, such as the selection of technologies or the sizing of energy resources, on the cost and carbon footprint of the hydrogen production pathway.

In this section, the optimisation and modeling of the green hydrogen production chain are discussed. First, in section B.1 different ways of representing a physical production chain as a computer model are presented. This subsection is followed by section B.1 where different optimisation methods are discussed. Each method has pro's and con's and these will be reviewed.

Physics modelling

There are several different approaches when modeling a hydrogen production chain. The choice for the best approach largely depends on the goal of the model. When researching electrolyser cell behaviour, a detailed electro-chemical equation might be the best option, while for a techno-economic review a simple equation converting power to kilograms of hydrogen might suffice. in this section the different approached will be highlighted in order to choose the best method for the purpose of this report.

The paper of Chandrasekar and Westlake [7] addresses what model design choices there are, when building an electrolyser model. The first choice is what processes to include in the model. Typical physiscs modeling domains are power, electrical, thermal, electrochemical, fluidic or thermochemical. What domains to include in the model depends on the level of detail that is required for the purpose of the model and the computational capacity that is available. In order to make a model that runs smoothly, some simplifications can be made that enable excluding some domains. For the purpose of this research, the process can be simplified to a power balance, equating the generated energy to the power requirements of the electrolyser.

The type of model is the next choice in model design.Chandrasekar and Westlake [7] identifies three different model types.

- **Empirical or semi-empirical models:** This type of model uses parametric equations that are fitted on experimental data. These models are relatively simple, but do not necessarily represent mathematical or physical reality. The equations are highly dependant on the setting of the performed experiment. Semi-emperical models include some physical models to improve performance. Empirical and semi-empirical models do not allow scaling.

- **Analytical models:** These models are built using physical law equations. These models are a simplified theorethical representation of reality.
- **Mechanistic models:** These models use physical law equations and electrochemistry. These models are computational heavier but give a more detailed description of reality.

As the aim of this report is investigating large-scale hydrogen production in multiple scenarios, the choice for an analytical model is best, as it offers scalability, without becoming computationally too heavy for running a lot of different experiments.

Optimisation methods

Optimisation can mean a wide range of things. It can be the maximisation of something positive, like the profitability, or the minimisation of something negative, like the carbon footprint. But more often, it means finding the optimal trade-off between multiple of these objectives. Optimisation can be very subjective. Subjectivity can come to play in the form of weighting different objectives, but it can also come to play in the definition of one of these objectives. For impartial research it is important to clearly state the assumptions and choices made during the process as to limit the subjectivity and to make any remaining subjectivity identifiable by third parties. There is a multitude of different optimisation methods. To clearly explain this, it is best to start with the defining optimisation problems. An optimisation problem contains three main components.

- **Objective function:** This is the goal of the optimisation, formulated as a function. This can be a linear or non-linear function.
- **Decision variables:** These are the degrees of freedom of the model, and can also be seen as the decisions that the model makes.
- **Constraints:** These contain the conditions the solution has to satisfy.

The most simple optimisation method is Linear Programming (LP) . In this method, the objective function and the constraints are all linear and the variables are continuous. When the objective function or the constraints are non linear, the optimisation is called Non-Linear Programming (NLP) . The next alteration includes integer decision variables. This results in Mixed Integer (Non-)Linear Porgramming (MILP/MINLP). A reason to include integer decision variables, is when there are components in a system that can be tuned on or off, or when the solution should tell whether components should be in- or excluded in a production chain.

The most common method for optimising a hydrogen production chain is MILP, as can be seen in the hydrogen optimisation review report of Riera, Lima, and Knio [52]. This is due to the limited computational capacity requirements of linear programming and due to the fact that making binary choices requires the use of integer decision variables. There are several examples of papers that use MINLP as well. Although this is computational more heavy. Linear Programming is selected as the optimisation method of choice. The trade-off for choosing the optimisation method is between a rough estimation of reality that requires little computing power, or a detailed representation of reality that is computational heavy. This research focuses on the rough estimations of costs and carbon footprint of a hydrogen production chain, and therefore needs not to be a detailed description of reality. Furthermore the selected method requires many optimisations in sequence, making the choice for a computational light modelling method best suited. That is why Linear Programming will be used for this research.

Key takeaways Production Chain Modelling

- Physics modelling can be done through various methods, ranging from computationally heavy to very light. In combination with an optimisation the choice is made for a computational light option: an energy balance.
- Single-Objective Linear Programming is selected as optimisation method due to the low computational costs.

B.2. Project economics example

In order to understand the Net Present Cost calculation method used in this report, it can be helpful to look at Table B.1. Here the NPC calculation for an onshore wind farm is displayed. It is assumed that at the end of a components lifetime, 10% of its original value is subtracted from the new investment. This is the salvage value as can be seen in Table 3.1. At the end of the project, if an asset has not reached the end of its economic lifetime, it is assumed that it is sold at a percentage of the remaining lifetime, times the CAPEX. This assumption is made due to the fact that the assets are very valuable and therefore it is reasonable that they will be reused in another business case.

Table B.1: NPC example: onshore wind farm.

year	OPEX$[k\$/MW]$	CAPEX$[k\$/MW]$	Total$[k\$/MW]$
1	21.0	1050.0	1071.0
2	18.7	0.0	18.7
3	17.6	0.0	17.6
4	16.6	0.0	16.6
5	15.7	0.0	15.7
6	14.8	0.0	14.8
7	14.0	0.0	14.0
8	13.2	0.0	13.2
9	12.4	0.0	12.4
10	11.7	0.0	11.7
11	11.1	0.0	11.1
12	10.4	0.0	10.4
13	9.8	0.0	9.8
14	9.3	0.0	9.3
15	8.8	438.1	446.9
16	8.3	0.0	8.3
17	7.8	0.0	7.8
18	7.4	0.0	7.4
19	6.9	0.0	6.9
20	6.5	-218.3	-211.7
Total	**242.1**	**1269.9**	**1511.9**

B.3. Optimisation model

Good research is replicable. That is why the model, created for this research, is uploaded to the following website: https://github.com/RolfIwema/LCOH_CF_Optimisation.

On this website the model and the accompanying files can be downloaded. Make sure to read the README file, as it highlights how to run the model and the additional files. In the README there is a section explaining how to include new regions, new technologies and how to visualise the results.

In the textbox below the required software is listed.

Required Software

- **Python 3.10:** The version of the software languaga, used when creating the model.
- **Microsoft Excel:** Used as input for the Python model.
- **PuLP:** a Linear Programming modelling Python package.
- **Numpy:** a general-purpose array-processing Python package.
- **Pandas:** a data manipulation and analysis Python package.
- **Scipy:** a scientific computing and technical computing Python package.
- **Matplotlib:** a data visualisation Python package.
- **Os:** an operating system interaction Python package.
- **Time:** a time tracking Python package.

C

Complementary Results

C.1. Complementary results

In this section, all graphs from the different scenarios are presented. In the first three subsections, all different PV types are presented with alkaline electrolysis. In the fourth subsection, the PEM electrolyser with Mono c-Si PV modules are displayed for all regions.

C.1.1. Duqm - Alkaline

Mono-crystalline Silicon

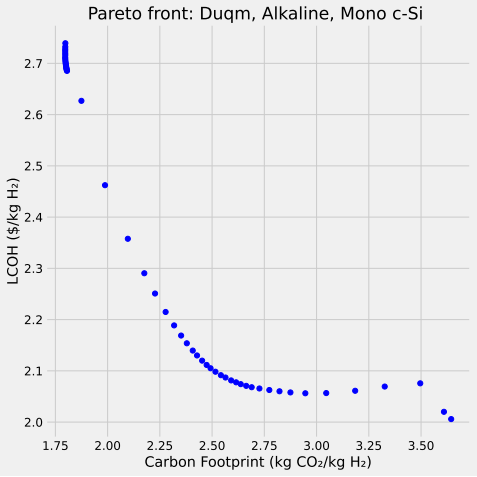

Figure C.1: Pareto front - Duqm, Alkaline, Mono c-Si. This graph displays the LCOH and CF performance of the scenario for different weight factors.

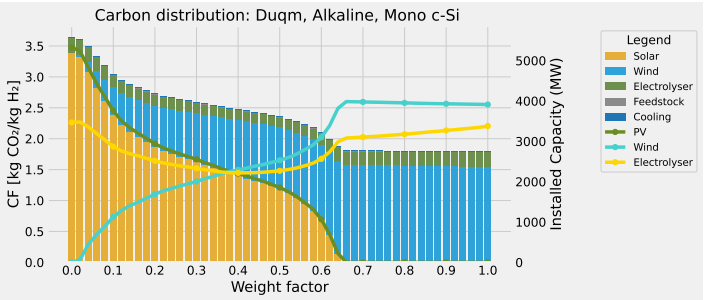

Figure C.2: Carbon Footprint - Duqm, Alkaline, Mono c-Si. The CF (primary y-axis, stacked bar) and installed capacity (secondary y-axis, line graph) plotted against the weight factor.

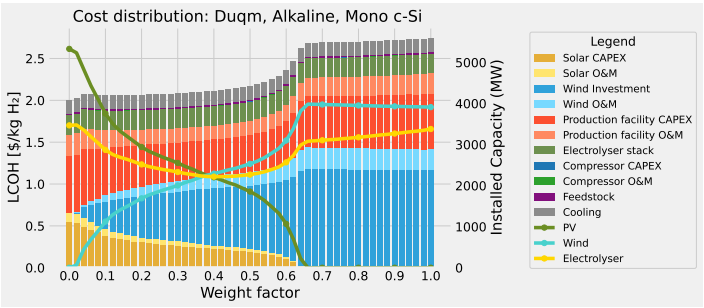

Figure C.3: Levelised Cost of Hydrogen - Duqm, Alkaline, Mono c-Si. The LCOH (primary y-axis, stacked bar) and installed capacity (secondary y-axis, line graph) plotted against the weight factor.

Cadmium Telluride

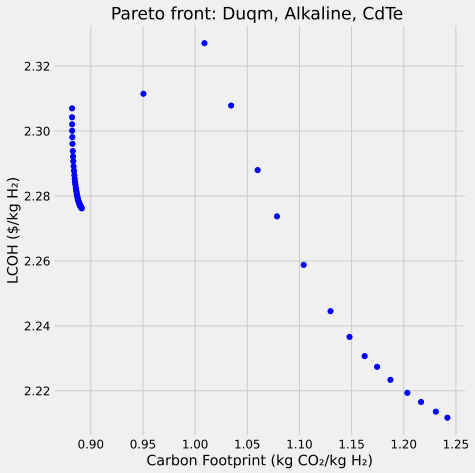

Figure C.4: Pareto front - Duqm, Alkaline, CdTe. This graph displays the LCOH and CF performance of the scenario for different weight factors.

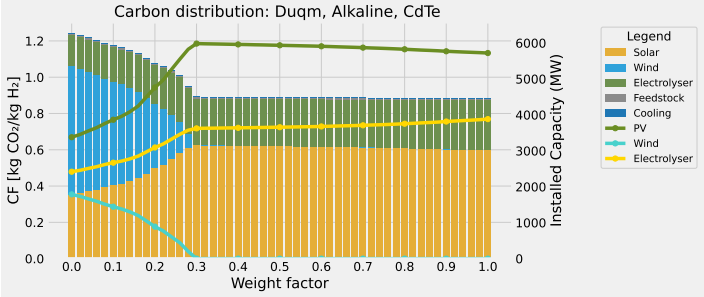

Figure C.5: Carbon Footprint - Duqm, Alkaline, CdTe. The CF (primary y-axis, stacked bar) and installed capacity (secondary y-axis, line graph) plotted against the weight factor.

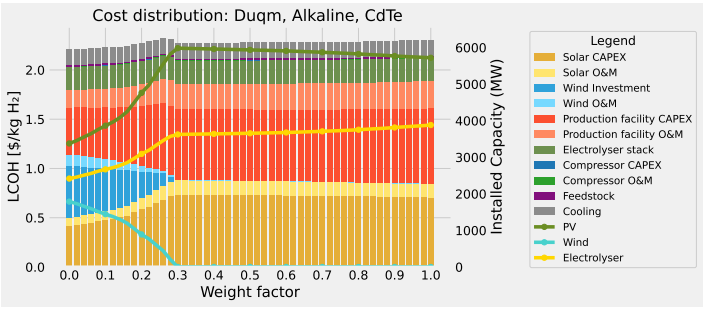

Figure C.6: Levelised Cost of Hydrogen - Duqm, Alkaline, CdTe. The LCOH (primary y-axis, stacked bar) and installed capacity (secondary y-axis, line graph) plotted against the weight factor.

Copper Indium Gallium Selenide

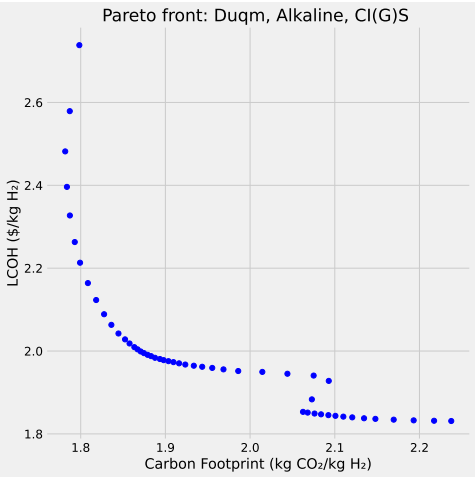

Figure C.7: Pareto front - Duqm, Alkaline, CI(G)S. This graph displays the LCOH and CF performance of the scenario for different weight factors.

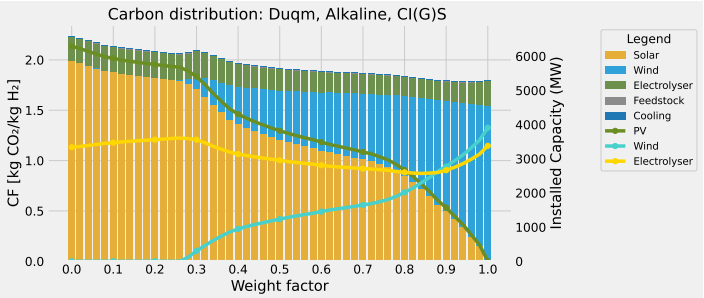

Figure C.8: Carbon Footprint - Duqm, Alkaline, CI(G)S. The CF (primary y-axis, stacked bar) and installed capacity (secondary y-axis, line graph) plotted against the weight factor.

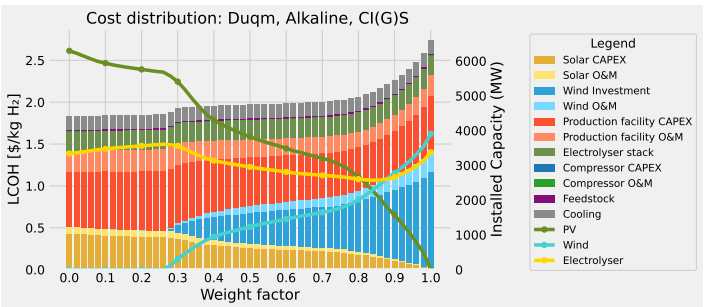

Figure C.9: Levelised Cost of Hydrogen - Duqm, Alkaline, CI(G)S. The LCOH (primary y-axis, stacked bar) and installed capacity (secondary y-axis, line graph) plotted against the weight factor.

C.1.2. Groningen - Alkaline
Mono-crystalline Silicon

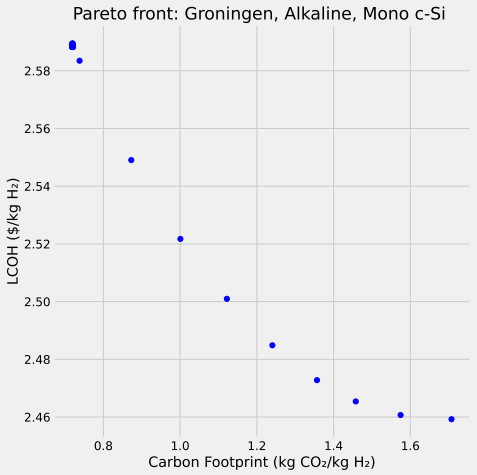

Figure C.10: Pareto front - Groningen, Alkaline, Mono c-Si. This graph displays the LCOH and CF performance of the scenario for different weight factors.

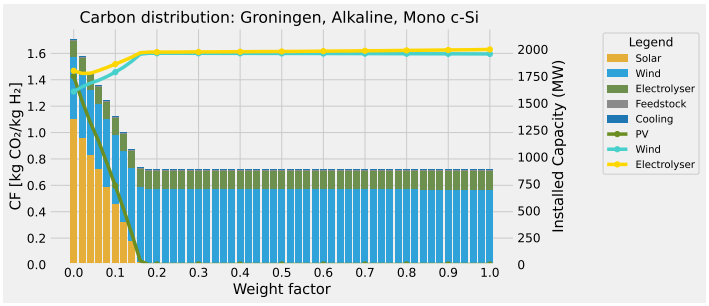

Figure C.11: Carbon Footprint - Groningen, Alkaline, Mono c-Si. The CF (primary y-axis, stacked bar) and installed capacity (secondary y-axis, line graph) plotted against the weight factor.

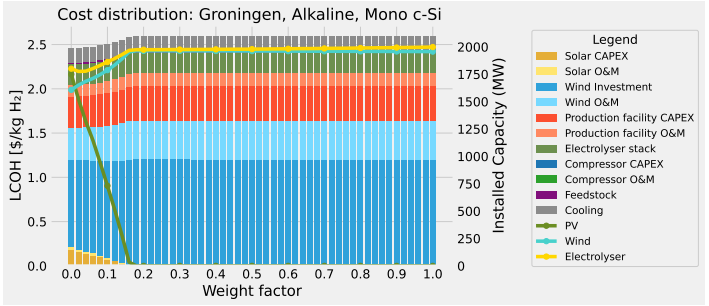

Figure C.12: Levelised Cost of Hydrogen - Groningen, Alkaline, Mono c-Si. The LCOH (primary y-axis, stacked bar) and installed capacity (secondary y-axis, line graph) plotted against the weight factor.

Cadmium Telluride

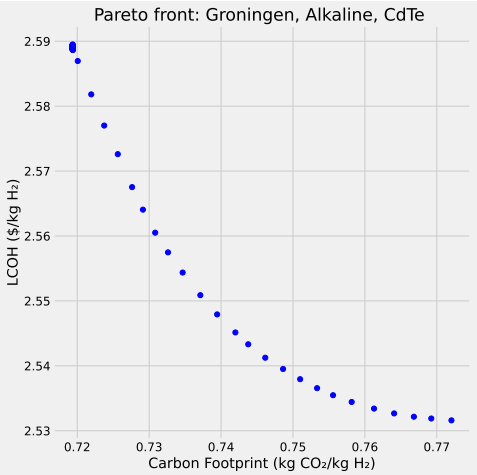

Figure C.13: Pareto front - Groningen, Alkaline, CdTe. This graph displays the LCOH and CF performance of the scenario for different weight factors.

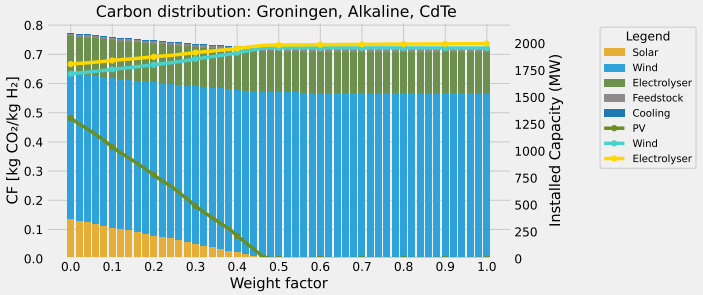

Figure C.14: Carbon Footprint - Groningen, Alkaline, CdTe. The CF (primary y-axis, stacked bar) and installed capacity (secondary y-axis, line graph) plotted against the weight factor.

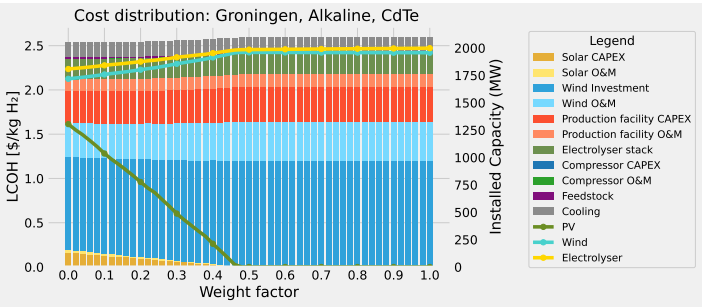

Figure C.15: Levelised Cost of Hydrogen - Groningen, Alkaline, CdTe. The LCOH (primary y-axis, stacked bar) and installed capacity (secondary y-axis, line graph) plotted against the weight factor.

Copper Indium Gallium Selenide

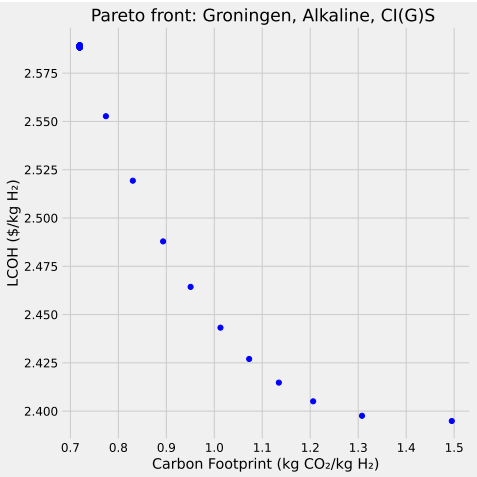

Figure C.16: Pareto front - Groningen, Alkaline, CI(G)S. This graph displays the LCOH and CF performance of the scenario for different weight factors.

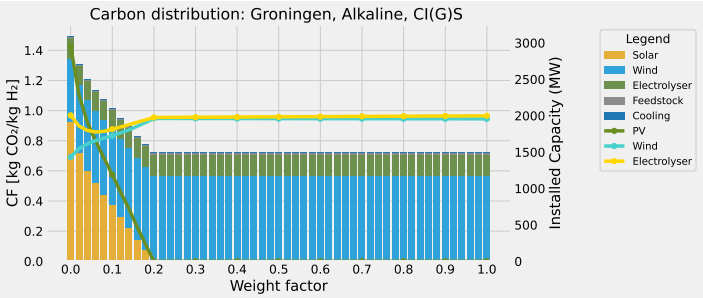

Figure C.17: Carbon Footprint - Groningen, Alkaline, CI(G)S. The CF (primary y-axis, stacked bar) and installed capacity (secondary y-axis, line graph) plotted against the weight factor.

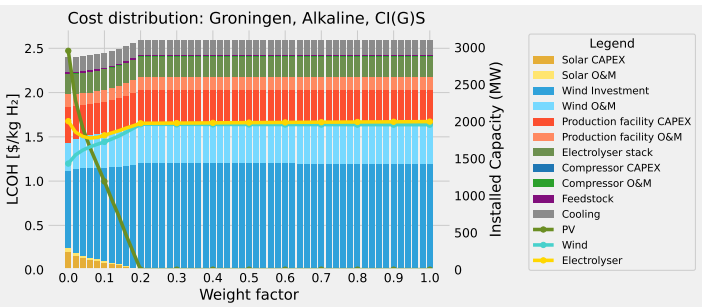

Figure C.18: Levelised Cost of Hydrogen - Groningen, Alkaline, CI(G)S. The LCOH (primary y-axis, stacked bar) and installed capacity (secondary y-axis, line graph) plotted against the weight factor.

C.1.3. Dakhla - Alkaline

Mono-crystalline Silicon

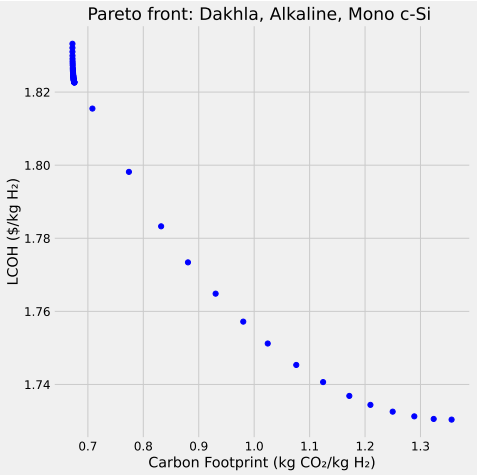

Figure C.19: Pareto front - Dakhla, Alkaline, Mono c-Si. This graph displays the LCOH and CF performance of the scenario for different weight factors.

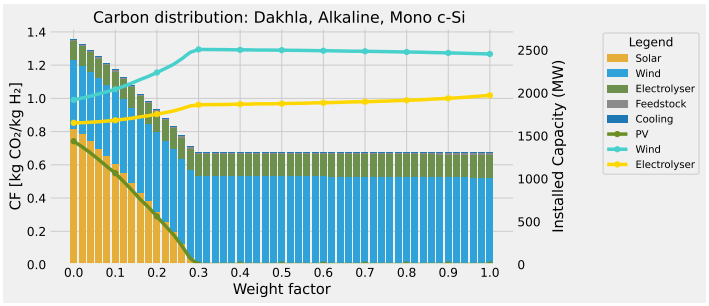

Figure C.20: Carbon Footprint - Dakhla, Alkaline, Mono c-Si. The CF (primary y-axis, stacked bar) and installed capacity (secondary y-axis, line graph) plotted against the weight factor.

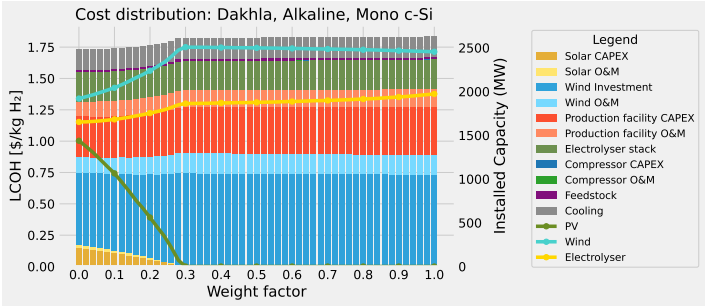

Figure C.21: Levelised Cost of Hydrogen - Dakhla, Alkaline, Mono c-Si. The LCOH (primary y-axis, stacked bar) and installed capacity (secondary y-axis, line graph) plotted against the weight factor.

Cadmium Telluride

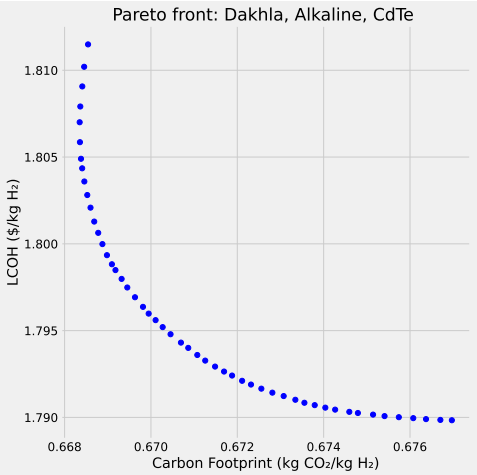

Figure C.22: Pareto front - Dakhla, Alkaline, CdTe. This graph displays the LCOH and CF performance of the scenario for different weight factors.

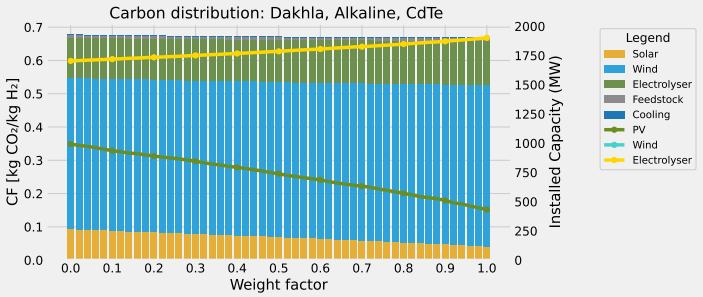

Figure C.23: Carbon Footprint - Dakhla, Alkaline, CdTe. The CF (primary y-axis, stacked bar) and installed capacity (secondary y-axis, line graph) plotted against the weight factor.

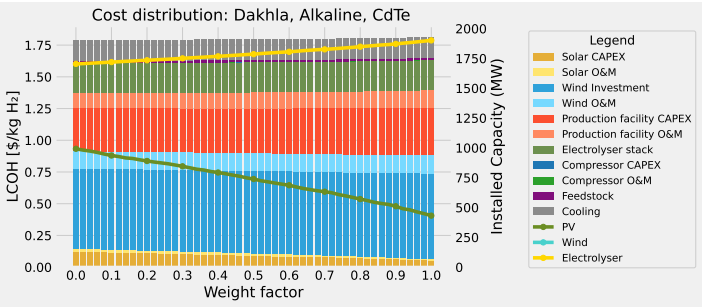

Figure C.24: Levelised Cost of Hydrogen - Dakhla, Alkaline, CdTe. The LCOH (primary y-axis, stacked bar) and installed capacity (secondary y-axis, line graph) plotted against the weight factor.

Copper Indium Gallium Selenide

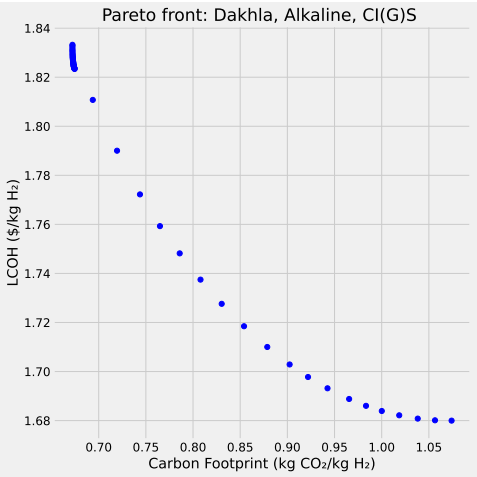

Figure C.25: Pareto front - Dakhla, Alkaline, CI(G)S. This graph displays the LCOH and CF performance of the scenario for different weight factors.

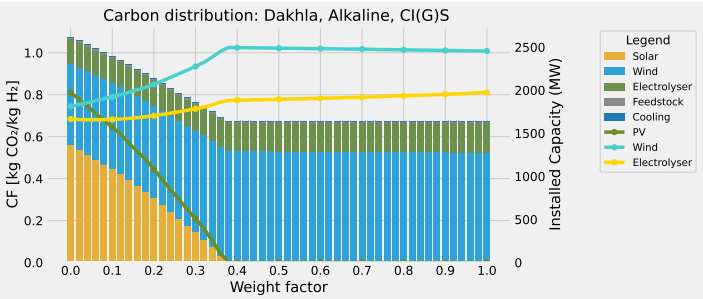

Figure C.26: Carbon Footprint - Dakhla, Alkaline, CI(G)S. The CF (primary y-axis, stacked bar) and installed capacity (secondary y-axis, line graph) plotted against the weight factor.

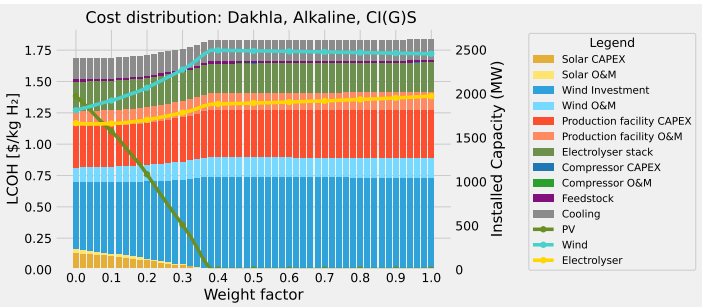

Figure C.27: Levelised Cost of Hydrogen - Dakhla, Alkaline, CI(G)S. The LCOH (primary y-axis, stacked bar) and installed capacity (secondary y-axis, line graph) plotted against the weight factor.

C.1.4. PEM

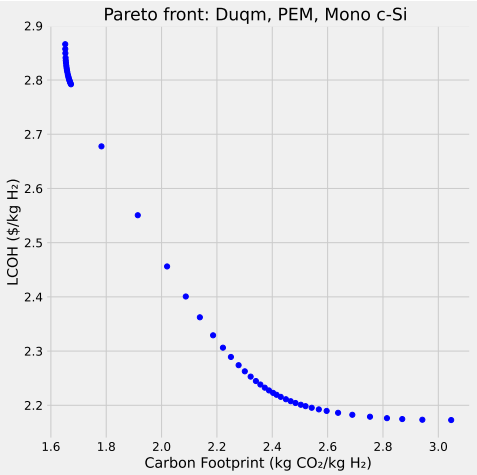

Figure C.28: Pareto front - Duqm, PEM, Mono c-Si. This graph displays the LCOH and CF performance of the scenario for different weight factors.

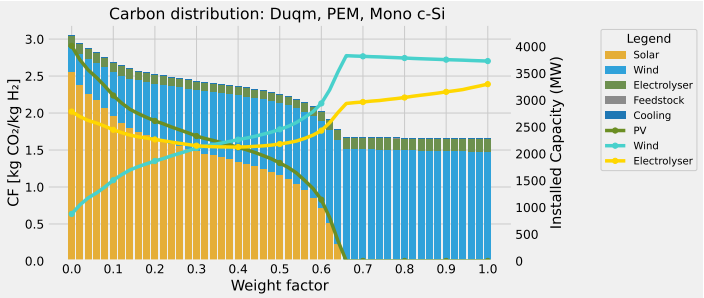

Figure C.29: Carbon Footprint - Duqm, PEM, Mono c-Si. The CF (primary y-axis, stacked bar) and installed capacity (secondary y-axis, line graph) plotted against the weight factor.

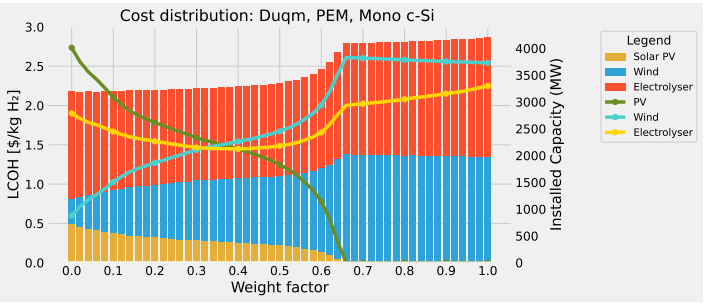

Figure C.30: Levelised Cost of Hydrogen - Duqm, PEM, Mono c-Si. The LCOH (primary y-axis, stacked bar) and installed capacity (secondary y-axis, line graph) plotted against the weight factor.

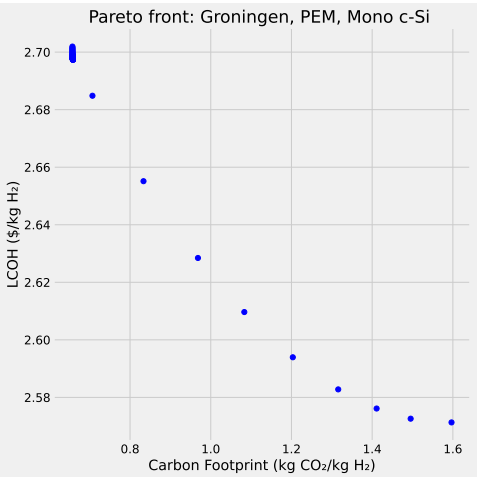

Figure C.31: Pareto front - Groningen, PEM, Mono c-Si. This graph displays the LCOH and CF performance of the scenario for different weight factors.

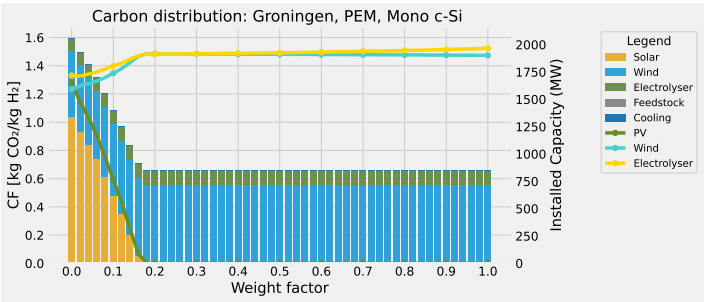

Figure C.32: Carbon Footprint - Groningen, PEM, Mono c-Si. The CF (primary y-axis, stacked bar) and installed capacity (secondary y-axis, line graph) plotted against the weight factor.

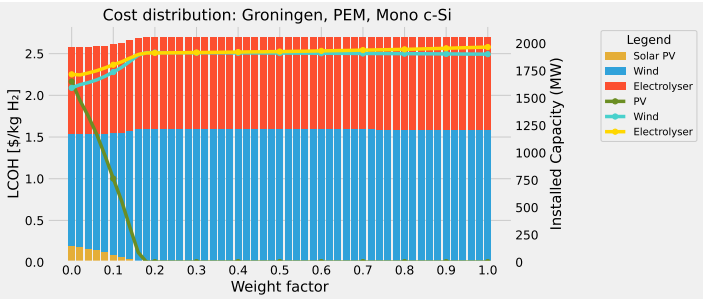

Figure C.33: Levelised Cost of Hydrogen - Groningen, PEM, Mono c-Si. The LCOH (primary y-axis, stacked bar) and installed capacity (secondary y-axis, line graph) plotted against the weight factor.

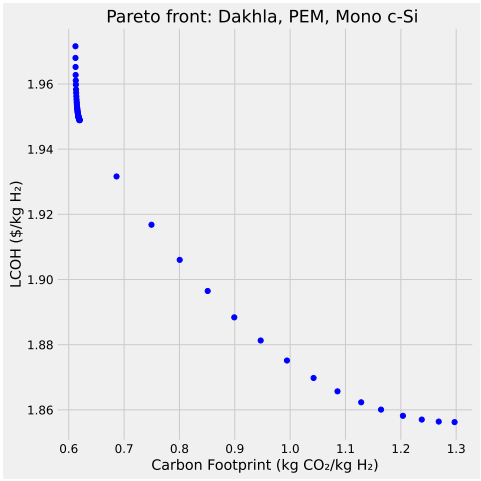

Figure C.34: Pareto front - Dakhla, PEM, Mono c-Si. This graph displays the LCOH and CF performance of the scenario for different weight factors.

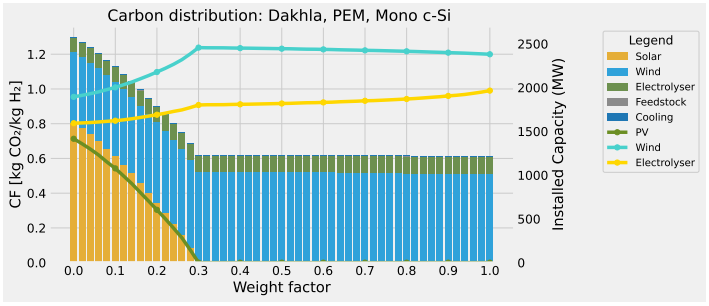

Figure C.35: Carbon Footprint - Dakhla, PEM, Mono c-Si. The CF (primary y-axis, stacked bar) and installed capacity (secondary y-axis, line graph) plotted against the weight factor.

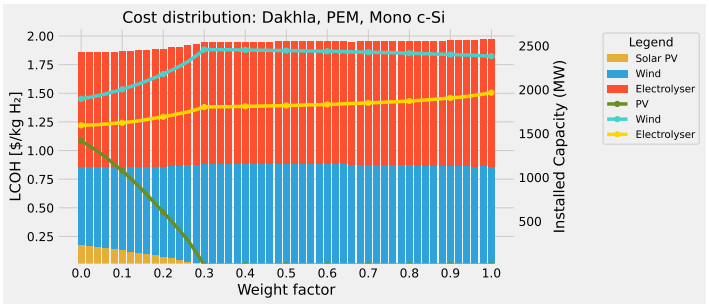

Figure C.36: Levelised Cost of Hydrogen - Dakhla, PEM, Mono c-Si. The LCOH (primary y-axis, stacked bar) and installed capacity (secondary y-axis, line graph) plotted against the weight factor.

C.1.5. Carbon price

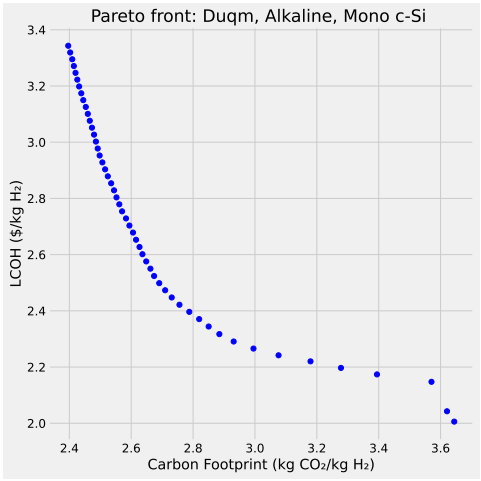

Figure C.37: Pareto front - Duqm, Alkaline, Mono c-Si with a carbon price. This graph displays the LCOH and CF performance of the scenario for different weight factors.

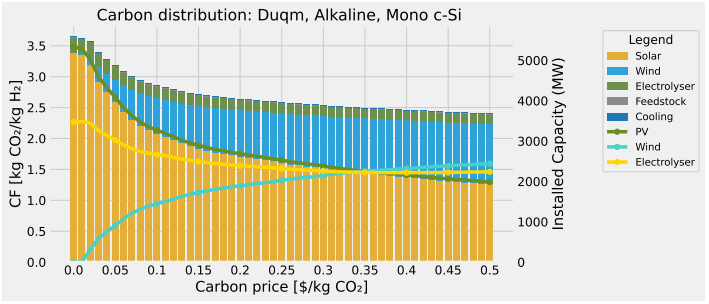

Figure C.38: Carbon Footprint - Duqm, Alkaline, Mono c-Si with a carbon price. The CF (primary y-axis, stacked bar) and installed capacity (secondary y-axis, line graph) plotted against the weight factor.

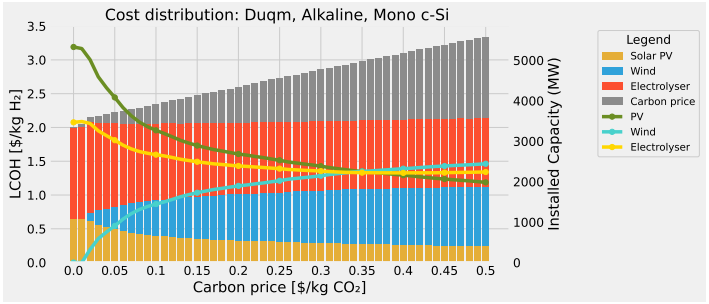

Figure C.39: Levelised Cost of Hydrogen - Duqm, Alkaline, Mono c-Si with a carbon price. The LCOH (primary y-axis, stacked bar) and installed capacity (secondary y-axis, line graph) plotted against the weight factor.